The feasibility of the manufacturing of a printed circuit type heat exchanger produced from graphite

I.J.V. DE KOCK

12691798

Dissertation submitted in partial fulfillment of the requirements for the degree Master of Engineering at the Potchefstroom Campus of the North-West University

Supervisor: Prof. J. Markgraaff

November 2009

Acknowledgements

I would like to thank my parents, Danie and Venita de Kock, who always supported me, not only in my formal education, but in all the various aspects of my life. Thank you for always standing behind me with encouragement and love.

Thank you also to all my friends, family and colleagues for words of encouragement and understanding during the course of this study.

Thank you to my supervisor, Prof. Markgraaff for his guidance and teachings that came from his wide experience and knowledge in the worlds of science and engineering.

But certainly, I would not have arrived here if it were not for the constant guidance of my Heavenly Father. Were it not that he lit up the way in front of me and provided the means and the time, this study would never have been completed. All praise be to God Almighty!

Abstract

The development of high temperature heat exchangers will play a vital part in the success of High Temperature Nuclear Reactors (HTRs). Manufacturing such heat exchangers from metals is becoming increasingly difficult as the operating temperatures keep rising. Above 1000°C most metals loose their strength and have high creep rates, while certain ceramic materials (including graphite, in the absence of oxygen) are able to operate at these temperatures.

A literature study was done in order to identify the major problems regarding the use of graphite for heat exchanger construction as well as to investigate to what extent graphite has been used for heat exchanger construction in the past. Following from the literature survey, it was decided to design and manufacture a Printed Circuit Heat Exchanger (PCHE) from isotropic graphite to gain experience regarding the use of graphite as a heat exchanger material. This heat exchanger was then tested in order to learn about the operation of a graphite heat exchanger and to determine its effectiveness. A model of the heat exchanger was also constructed in order to determine what the performance of such a heat exchanger should theoretically be.

It was found that the single greatest hurdle standing in the way of graphite being used as a heat exchanger material is its high gas permeability. This causes mixing between the two fluid streams as well as leakages to the environment, which have a negative effect on the heat exchanger's heat transfer capability. The methods used to establish a seal between the consecutive plates of the PCHE are also affected by the permeability of the graphite. Coatings on the surface of the graphite might be able to reduce its permeability and can also inhibit the high temperature degradation of graphite in the presence of oxygen.

Manufacturing very small flow channels for the PCHE is limited by the availability of small enough end mills. Alternative manufacturing techniques is needed to economically construct a graphite PCHE. It was also found that the heat transfer effectiveness of the heat exchanger is influenced negatively by heat losses to the environment through the outer surface of the heat exchanger. Effective insulation around the heat exchanger or a graphite material with higher heat conductivity perpendicular to the flow direction might solve this problem.

This study concluded that if diffusion bonding techniques, effective coatings and a graphite material with increased heat conductivity perpendicular to the flow direction are used, manufacturing a printed circuit heat exchanger from graphite is feasible.

Keywords: Graphite; Printed Circuit; Heat Exchanger; Manufacturing; IHX; HTR

Uittreksel

Die ontwikkeling van hoë temperatuur hitteruilers is van uiterste belang vir die suksesvolle implementering van Hoë-temperatuur Kernreaktors (HTR's). Aangesien die verwagte werkstemperature van hierdie tipe hitteruilers aanhoudend hoër raak, word dit al hoe moeiliker om dit uit metale te vervaardig. Meeste metale verloor hul sterkte by temeperature hoër as 1000°C en het 'n hoë kruiptempo, terwyl sekere keramieke (insluitend grafiet, in die afwesigheid van suurstof) by hierdie temeperature kan funksioneer.

'n Literatuurstudie is gedoen met die doel om die grootste probleme met betrekking tot die gebruik van grafiet as 'n hitteruilermateriaal te identifiseer, asook om te bepaal tot watter mate grafiet al in die verlede gebruik is om hitteruilers te vervaardig. Na aanleiding hiervan is besluit om 'n Geëtste-baan Hitteruiler (GBH) to ontwerp en uit isotropiese grafiet te vervaardig met die doel om ondervinding op te doen aangaande die gebruik van grafiet as 'n hitteruiler material. Daarna is hierdie hitteruiler getoets om die werking van 'n grafiet hitteruiler te ondersoek. 'n Model is ook opgestel sodat 'n vergelyking gemaak kan word tussen die teoretiese resultate vanuit die model en die werklike resultate vanuit die toetse.

Die gasdeurlaatbaarheid van grafiet is geïdentifiseer as die grootste struikelblok in die gebruik van grafiet as 'n hitteruilermateriaal. As gevolg hiervan vind vermenging van die twee vloeiers plaas en is lekkasies na die omgewing ondervind wat 'n negatiewe effek het op die effektiwitiet van die hitteruiler. Ook die metodes wat gebruik kan word om 'n seël tussen die onderskeie hitteruiler plate te bewerkstellig word deur die deurlaatbaarheid van die grafiet beïnvloed. Hierdie probleem kan moontlik opgelos word deur 'n geskikte dun lagie op die oppervlak van die grafiet aan te bring. So 'n dun lagie kan ook gebruik word om die degradasie van grafiet by hoë temperature in die teenwoordigheid van suurstof te verminder.

Die vervaardiging van die baie klein vloei kanaaltjies van 'n GBH word by grafiet beperk deur die beskikbaarheid van klein genoeg snybeitels. Alternatiewe vervaardigingsmetodes word benodig om 'n grafiet GBH ekonomies te vervaardig. Hierdie studie het ook bevind dat baie hitte na die omgewing verlore gaan deur die buitewande van die hitteruiler. Genoegsame isolasie of 'n grafiet met 'n verhoogde hittegeleidingsvermoë loodreg op die vloeirigting mag moontlik hierdie probleem oplos.

Hierdie studie het tot die gevolgtrekking gekom dat indien diffusiehegtingsmetodes, effektiewe dun lagies en 'n grafiet met 'n verhoogde hittegeleidingsvermoë loodreg op die vloeirigting gebruik word, die vervaardiging van 'n GBH uit grafiet moontlik is.

Sleutelwoorde: Grafiet; Geëtste-baan; Hitteruiler; Vervaardiging; IHX; HTR

Table of Contents

Acknowledgements III
Abstract V
Uittreksel VII
Table of Contents IX
List of Figures XI
List of Tables XIII
List of Symbols XV
Abbreviations XVII

Chapter 1: Introduction 2
1.1 Background and Objective 3

Chapter 2: Literature Survey 8
2.1 Graphite as a Heat Exchanger Material 9
2.2 The Permeability problem 9
2.3 Degradation of Graphite at High Temperature 12
2.4 Shaping of Graphite 13
2.5 Graphite heat exchanger designs 16
2.5.1 Current Graphite Heat Exchanger Types 16
2.5.1.1 Block Type Graphite Heat Exchangers 16
2.5.1.2 Plate Type Graphite Heat Exchangers 17
2.5.2 Printed Circuit Heat exchanger 19
2.6 Conclusion 21
2.7 Aim of this study 21

Chapter 3: Laboratory Scale Heat Exchanger Design, Manufacturing and Testing 22
3.1 Introduction 23
3.2 Heat Exchanger Design 23
3.2.1 PCHE Flow Channel Configuration 23
3.2.2 Laboratory Scale Graphite Printed Circuit Heat Exchanger Design 24
3.2.2.1 Material chosen for the design of the heat exchanger 25
3.2.2.2 Chosen heat exchanger size and flow geometry 25
3.2.2.3 Discussion on the heat exchanger design 27
3.3 Heat Exchanger Manufacturing 32
3.3.1 Graphite material used for manufacturing 32

3.3.2 Creating the machining tool path 33
3.3.3 Machining of individual plates 34
3.3.3.1 The choice of cutting tool 34
3.3.3.2 Clamping of graphite to the table of a milling machine 36
3.3.3.3 Milling of the heat exchanger flow channels 39
3.3.4 Heat exchanger assembly 42
3.4 Heat Exchanger Testing 45
3.4.1 Test description 45
3.4.1.1 Heat transfer test requirements 45
3.4.1.2 Pressure drop test requirements 47
3.4.2 Test setup 49
3.4.2.1 Heat transfer test setup 49
3.4.2.2 Pressure drop test setup 60
3.4.3 Testing procedures 60
3.4.4 Test Results 61
3.4.5 Discussion of results 63

Chapter 4: Heat Exchanger Theoretical Model 66
4.1 Introduction 67
4.2 Flow configuration analysis 67
4.3 Construction of the heat exchanger model 70
4.4 Results from the model 78

Chapter 5: Comparison of Results 82
5.1 Introduction 83
5.2 Heat transfer results 83
5.3 Pressure drop results 85

Chapter 6: Conclusions and Recommendations 86
6.1 Background 87
6.2 Practical Experiences Gained 87
6.3 Conclusions 88

Appendix A: Graphite Material Specifications 90
Appendix B: Programme Code for Mathematical Analysis 94
Appendix C: Heat Exchanger Manufacturing Drawings 100
Appendix D: Flow Metre Calibration Curve 106
Bibliography 110

List of Figures

Figure 1: Uses of high temperature nuclear heat 3
Figure 2: Direct Cycle vs. Indirect Cycle 4
Figure 3: Placement of an intermediate heat exchanger 5
Figure 4: Percentage elongation and yield strength vs. temperature for high temperature alloys (Hechanova, 2006) 6
Figure 5: Copper - Titanium phase diagram (Saito *et al.*, 1976:267) 11
Figure 6: Crucibles made from glassy carbon SIGRADUR® 12
Figure 7: Block type heat exchanger segments (from SGL Block Heat Exchanger Brochure (2008)) and a schematic representation of a block type heat exchanger in operation. 17
Figure 8: Plate type graphite heat exchanger (modified after SGL Plate Heat Exchanger Brochure (2008)) 18
Figure 9: Simple schematic representation of a typical printed circuit heat exchanger 19
Figure 10: Zigzag flow configuration for a PCHE 23
Figure 11: Discontinuous sine wave shaped flow configuration. (Tsuzuki *et al.*, 2007:1704) 24
Figure 12: Overall dimensions of heat exchanger core (dimensions in mm) 25
Figure 13: Section view of a segment of two stacked heat exchanger plates (dimensions in mm) 26
Figure 14: Fin shape deduced from the sine wave (dimensions in mm) 26
Figure 15: Sine wave shaped fins relative positions (dimensions in mm) 27
Figure 16: Isometric view of a single HX plate design model (view of plate underside in background) 27
Figure 17: Exploded view of two stacked HX plates 28
Figure 18: Pressure plate used for top and bottom (dimensions in mm) 30
Figure 19: Model of assembled heat exchanger 31
Figure 20: Completed HX plates 32
Figure 21: Graphite stock material 33
Figure 22: Some factors influencing tool diameter 34
Figure 23: Tool used for machining the HX plates (pen included for scale) 35
Figure 24: Machining tool two-fluted cutting tip 36
Figure 25: Vacuum clamp box clamped to the table 37
Figure 26: Cutting grooves into the top of the vacuum clamp box 37
Figure 27: Vacuum clamp groove network with holes 37
Figure 28: Damaged graphite due to failing of the vacuum clamp 38
Figure 29: Fixing the graphite to the milling machine using the corner clamp method 39
Figure 30: Milling machine used to machine the HX plates 40
Figure 31: Breaking of the graphite at thin sections (< 1mm) 40
Figure 32: Start of a HX plate milling operation 41
Figure 33: End of a HX plate milling operation 41
Figure 34: Assembled heat exchanger core showing o-rings 42

Figure 35: Bottom pressure plate with tensioning rods 43
Figure 36: Heat exchanger core on the bottom pressure plate 43
Figure 37: Assembled heat exchanger 44
Figure 38: Schematic representation of a manometer 47
Figure 39: Schematic representation of the test setup used for the heat transfer tests 49
Figure 40: Heat transfer test setup. 1: Gas cylinder with reducing valve; 2: Flow meters; 3: Heater; 50
Figure 41: Heater element 51
Figure 42: Installed heater with insulation 51
Figure 43: Schematic representation of the hot gas duct insulation 52
Figure 44: Equivalent thermal circuit of heat loss through hot gas duct 52
Figure 45: Uninsulated hot gas pipe 58
Figure 46: Hot gas pipe insulation 59
Figure 47: Insulated hot gas pipe 59
Figure 48: Pressure drop test setup 60
Figure 49: Graphical representation of the heat exchanger inlets and outlets at a mass flow of 2.6×10^{-4} kg/s 62
Figure 50: Pressure drop test data 63
Figure 51: A schematic representation of the heat exchanger, showing the known parameters 67
Figure 52: Flow configuration with approximated continuous channels (dashed) 68
Figure 53: Structure of EES heat exchanger model 75
Figure 54: Structure of EES pressure drop model 78
Figure 55: Heat exchanger model results for effectiveness 79
Figure 56: Heat exchanger model results for inlet and outlet temperatures 80
Figure 57: Analysis results for pressure drop 81
Figure 58: Heat transfer test results 83
Figure 59: Analysis results of the heat transfer 84
Figure 60: Comparison of the pressure drop test data with that from the analysis 85

List of Tables

Table 1: Machining parameters used in different studies 15
Table 2: O-ring seal and groove geometry 29
Table 3: Geometrical parameters used in the choice of tool diameter 35
Table 4: Heat transfer test fixed parameters 46
Table 5: Testing fluid data 50
Table 6: Reducing valve data 50
Table 7: Flow meter data (calibration curve presented in Appendix D) 51
Table 8: Parameters for the calculation of Ra 57
Table 9: Heat transfer coefficients for pipe insulation calculation 58
Table 10: Temperature test data for a mass flow of 2.6×10^{-4} kg/s 61
Table 11: Pressure drop test data 62
Table 12: Heat exchanger geometrical parameters 69
Table 13: List of assumptions made during the heat exchanger analysis 78

List of Symbols

A	:	Area (m^2)
A_c	:	Cross sectional flow area of a channel (m^2)
A_f	:	Surface area of a single fin (m^2)
$A_{f,top}$	:	Area of the top of a single fin (m^2)
A_{ff}	:	Total free flow area (m^2)
$A_{f,total}$	:	Total surface area of all fins (m^2)
A_H	:	Heat transfer area (m^2)
$A_{H,cond}$	:	Conduction heat transfer area (m^2)
°C	:	Degrees Celsius
C	:	Product of mass flow and specific heat at constant pressure (W/K)
C	:	Constant
C_{max}	:	Larger of the two values of C for the hot and cold stream (W/K)
C_{min}	:	Smaller of the two values of C for the hot and cold stream (W/K)
c_p	:	Specific heat at constant pressure (J/kg.K)
C_r	:	Ratio of C_{min} to C_{max}
D	:	Tool Diameter (m)
D_H	:	Hydraulic diameter of the channels (m)
F	:	Feed per tooth (mm/tooth)
f	:	Darcy-Weisbach friction factor (m)
g	:	Gravitational acceleration (m/s^2)
H	:	Height (m)
ΔH	:	Height difference (m)
h	:	Convection heat transfer coefficient ($W/m^2.K$)
K	:	Kelvin
K	:	Pipe loss factor
k	:	Conduction heat transfer coefficient (W/m.K)
L	:	Length (m)
L_{ch}	:	Channel length (m)
L_f	:	Fin length (m)
L_w	:	Length heat has to be transferred through a plane wall (wall thickness) (m)
$\dot{m}$	:	Mass flow [kg/s]
m	:	Meter
mm	:	Millimetre
N	:	Rotational speed of tool (rev/min)
N_{ch}	:	Number of channels/plate

N_f	:	Number of fins/plate
N_{pl}	:	Number of plates in the heat exchanger
n	:	Number of teeth on tool
n	:	Constant
NTU	:	Number of transfer units
Nu	:	Nusselt number
P	:	Wetted perimeter (m)
P_f	:	Fin Perimeter (m)
p	:	Pressure (Pa)
Δp	:	Pressure difference (Pa)
Q_{Max}	:	Maximum possible heat transferable from the hot to the cold stream (W),
Q	:	Heat transferred (W)
R_f''	:	Fouling factor (m^2.K/W)
R_w	:	Wall conduction resistance (K/W)
R	:	Thermal Resistance (K/W)
T	:	Temperature (°C or K)
T_s	:	Surface temperature (°C or K)
T_∞	:	Environmental temperature (°C or K)
ΔT	:	Temperature Difference (°C or K)
t	:	Thickness of a fin (m)
UA	:	Overall heat transfer coefficient (W/K)
V	:	Fluid velocity (m/s)
V_{cutter}	:	Surface speed of cutter or cutting speed (m/min)
W	:	Watt (W)
W_{ch}	:	Width of a single channel (m)

Greek Letters

α	:	Thermal diffusivity (m^2/s)
β	:	Volumetric thermal expansion coefficient (K^{-1})
ε	:	effectiveness
η_o	:	Overall surface efficiency of a finned surface
η_f	:	Surface efficiency of a single fin (W/m.K)
ρ	:	Density (kg/m^3)
υ	:	Linear speed of work piece or feed rate (mm/tooth)
ν	:	Kinematic viscosity (m^2/s)
Δ	:	Difference

Abbreviations

C/C	:	Carbon-Carbon Composites
CAD	:	Computer Aided Design
CTE	:	Coefficient of Thermal Expansion
CVD	:	Chemical Vapour Deposition
CNC	:	Computer Numerically Controlled
EDM	:	Electron Discharge Machining
EES	:	Engineering Equation Solver
HX	:	Heat Exchanger
IHX	:	Intermediate Heat Exchanger
HTR	:	High Temperature nuclear Reactor
NTU	:	Number of Transfer Units
PBMR	:	Pebble Bed Modular Reactor
PCHE	:	Printed Circuit Heat Exchanger
PTFE	:	Poly-tetrafluoroethylene
NGNP	:	Next Generation Nuclear Plant

Chapter 1

Introduction

1.1 Background and Objective

The concept of the High Temperature nuclear Reactor (HTR) has enjoyed much attention in the energy production industry in recent years. There are many reasons for this, including its improved safety characteristics, high energy efficiencies, its ability to produce energy with zero CO_2 emissions and because it can deliver very high temperature process heat (around 1000°C).

There are many commercial applications for the high temperature heat produced by HTRs. Figure 1 shows a schematic representation of some of these applications:

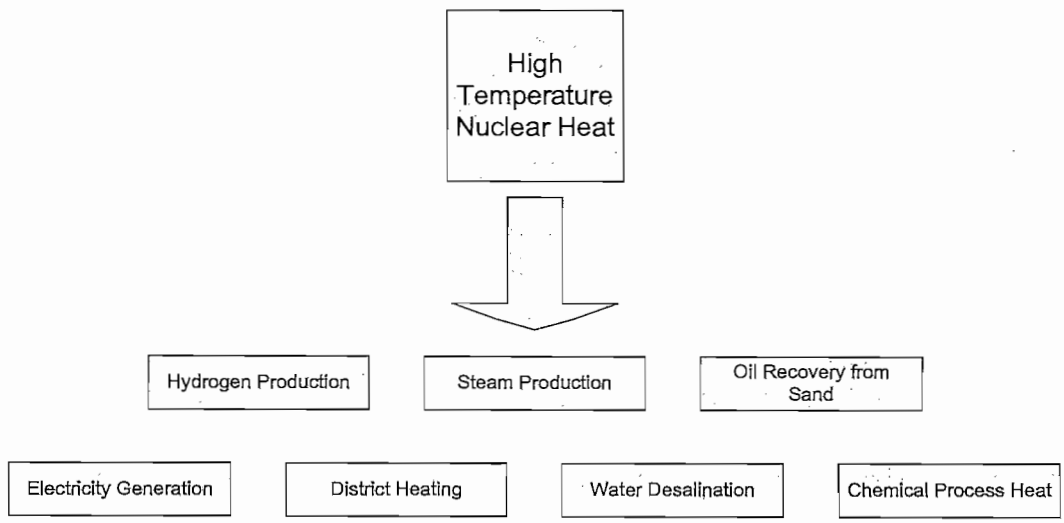

Figure 1: Uses of high temperature nuclear heat

To use nuclear heat for these and other applications, one has to be able to transfer the heat generated in the core of the nuclear reactor to the application. There are two proven methods to achieve this, namely a direct or an indirect cycle[1]. The difference between the two methods is shown schematically in Figure 2:

[1] There are also systems that combine these two methods, called combined cycles.

In the case of a direct cycle, the fluid flowing through the nuclear reactor is the same fluid that drives the application. An indirect cycle transfers the heat from the primary loop (flowing through the nuclear reactor) to the secondary loop (driving the application)[2]:

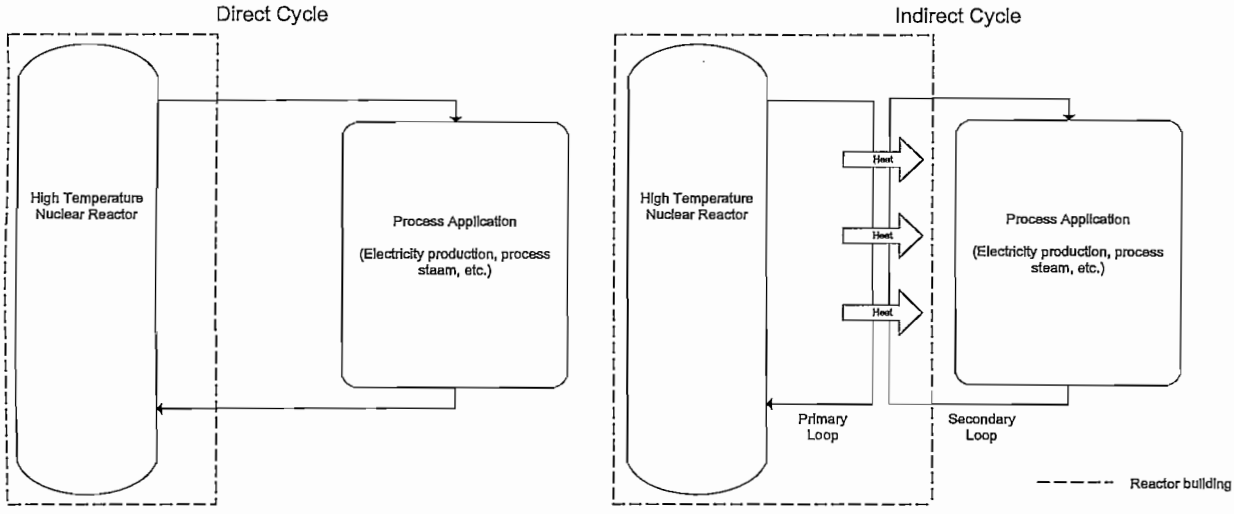

Figure 2: Direct Cycle vs. Indirect Cycle

Heat transfer from the primary to the secondary loop is achieved by using an Intermediate Heat Exchanger[3] (IHX) placed as shown in Figure 3.

[2] The use of the second loop in the indirect cycle becomes obvious when one considers the safety implications of directly coupling the primary loop with a process application. The primary loop of a nuclear reactor might contain some radioactive contaminants picked up in the reactor core. If these contaminants were to escape from the reactor building, it may cause catastrophic radioactive pollution. By using a primary loop that never leaves the reactor building, the chances of contaminants escaping are reduced greatly. Also, the loss of the core coolant (the fluid in the primary loop) due to a breach of the primary loop is regarded as a very serious accident scenario in the nuclear industry. If the heat generated in the core is not sufficiently removed, the reactor may experience a meltdown. This problem is mitigated by reducing the risk of damage to the coolant loop by not exposing it to the environment outside of the reactor building. Because of these reasons, it is better to use the primary loop only to remove the heat from the core and to use a secondary loop to deliver the heat to the application.

[3] Since IHXs for HTRs transfer heat at very high temperatures, they will be treated as synonymous to high temperature heat exchangers throughout this dissertation.

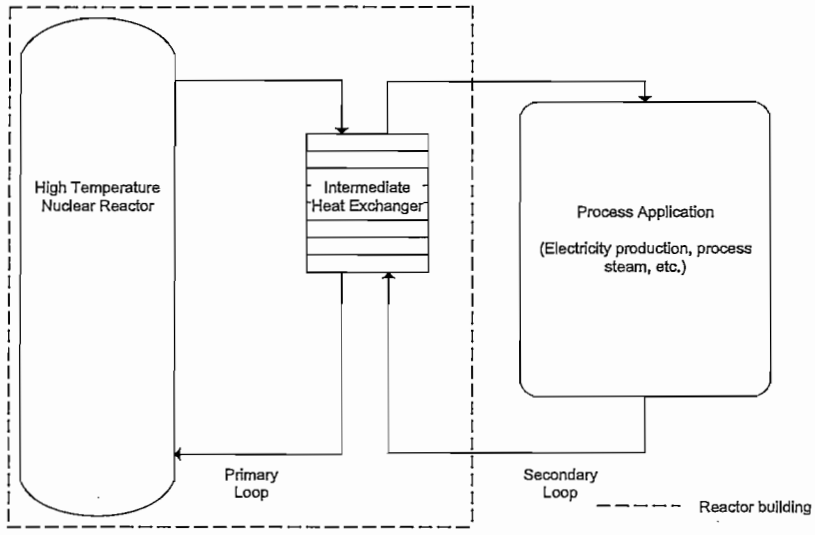

Figure 3: Placement of an intermediate heat exchanger

IHXs used in HTRs will operate at temperatures in the range of 700°C - 1000°C and even slightly higher (McDonald, 1996:31). This makes the choice of heat exchanger material very important and problematic, since a material is needed that can withstand these high temperatures. The use of metals for this type of heat exchanger has been proven in the past. A helical tube bundle heat exchanger, produced from Inconel 617, was tested up to 950°C in a 10MW, electrically heated circuit by the Germans in the 1980's, using helium as both the primary and the secondary fluid (McDonald, 1996:12). The heat exchanger performed well during these tests and the Inconel material provided satisfactory high temperature strength. However, due to certain manufacturing, maintenance and operational issues, tubes with large diameters (15mm – 30mm), spaced relatively far from each other had to be used in this design. This resulted in the heat exchanger having a moderate surface compactness (heat transfer area per unit volume) of $50m^2/m^3$ and a thermal density of $4.5MW/m^3$. According to McDonald (1996:13), a surface compactness of above $1000m^2/m^3$ with a power density of about $15MW/m^2$ is needed to construct an economically viable IHX for an HTR. Achieving these values was proven impractical for metal helical bundle heat exchangers by the cited experiment. This highlights the first hurdle when considering metals for high temperature heat exchanger manufacturing, namely that, even though a few metals is able to withstand temperatures higher than 1000°C, a commercial heat exchanger designed using them will have to be extremely large due to its power density being limited by maintenance and operational issues. Also, the cost of such a large heat exchanger, manufactured from expensive nickel based alloys, will be too high to be economically viable.

Another problem when considering metals for manufacturing a high temperature heat exchanger is the fact that all metals exhibit a decrease in strength with increasing temperature. This is evident from Figure 4, which shows the results of tensile tests performed on four high

temperature alloys at different temperatures (Hechanova, 2006:17). These tests show that all four of the alloys exhibit a large decrease in yield strength at about 800°C. This decrease in strength means that metals will display increasingly high creep rates and lower structural integrity at high temperatures which is unacceptable in heat exchanger design.

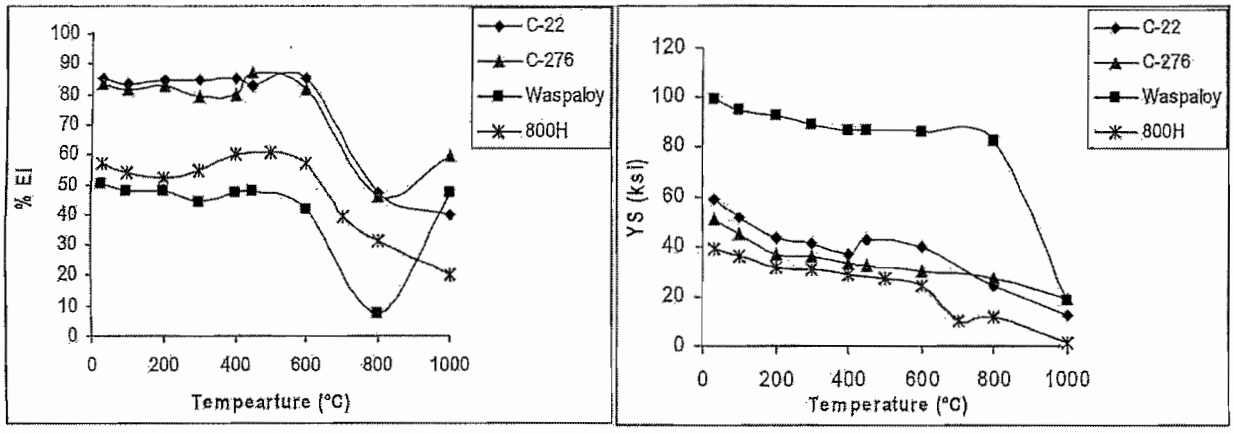

Figure 4: Percentage elongation and yield strength vs. temperature for high temperature alloys (Hechanova, 2006)

A further issue regarding metals is the fact that most metals are very susceptible to oxidation in air at high temperatures. To render them more resistant to oxidation, expensive alloying elements such as molybdenum and chromium have to be added to the alloy, which increases the overall cost of the material (Budinski & Budinski, 2002:424).

Due to the problems cited and since reliability and economic viability is so important in the nuclear industry, ongoing efforts are made to explore the use of alternative materials for use in heat exchangers operating at elevated temperatures.

It has been advocated that the use of ceramic materials could provide solutions to the problems above (McDonald, 1996:22) since these materials, in general, exhibit acceptable yield strength, high creep resistance and resistance to oxidation at high temperatures.

One particular ceramic studied for use in high temperature heat exchangers is silicon carbide (SiC) (Schulte-Fischedick *et al.*, 2006:1285), mainly because of its good thermal conductivity – an important consideration in heat exchanger design due to the fact that it is needed to provide acceptable heat transfer effectiveness. Similar to most other ceramic materials, SiC is extremely hard and brittle, making it a difficult material to shape and form for manufacturing purposes. Also, its relatively large thermal expansion coefficient makes it very sensitive to temperature fluctuations.

Another group of materials that, like SiC, display good thermal conductivities is graphite materials. Although they exhibit acceptably high thermal stability in protective atmospheres, these materials may surpass SiC as a candidate material for use in high temperature heat exchangers in that they display very small thermal expansion coefficients and are, generally, much easier to shape and form.

The objective of this study is to further explore the use of graphite as a viable heat exchanger material by reviewing problems associated with its use and also the extent to which it is currently used in the heat exchanger industry. Furthermore, the associated practical problems and material issues regarding graphite are investigated hands on in order to get a feel for the use of this material for such an application. It is envisaged that the experience gained in this manner will contribute to an understanding of the manufacturing feasibility of a high temperature graphite heat exchanger.

Chapter 2

Literature Survey

2.1 Graphite as a Heat Exchanger Material

The use of graphite as a high temperature heat exchanger material introduces some problems. Firstly, graphite is known to be a porous material. If graphite were to be used for the manufacturing of a heat exchanger, this porosity would cause fluid permeation between the primary and secondary fluids, which is unacceptable in a nuclear environment.

A second problem when using graphite for high temperature heat exchanger manufacturing is the degradation that graphite undergoes when exposed to an oxidising environment at high temperatures. This degradation starts at temperatures as low as 300°C. According to Xiaowei *et al.* (2004:279), the oxidation rate is very low below 400°C, but rises sharply between 500°C and 850°C. This limits the use of graphite in air to low temperature applications and poses a risk for its use in a heat exchanger for the HTR, or any other very high temperature application (>1000°C).

A third subject that needs to be studied is the shaping of graphite. The local knowledge on this matter is limited and more information is needed before any manufacturing using graphite can be done.

Lastly, a review is done of the low temperature graphite heat exchanger designs currently in use.

2.2 The Permeability problem

The pores in graphite are a result of its manufacturing process. Budinski & Budinski (2002:296) explain this as follows: petroleum coke (from the incomplete combustion of coal or petroleum) is milled into a fine powder and mixed with a pitch binder. This paste-like material is then formed by extrusion, or other methods, to create partially completed shapes, which are then sintered at very high temperature (around 1000°C). By sintering, all of the volatiles are removed from the product as gases and a material consisting of a mixture of graphite and amorphous carbon remains. The spaces that were once filled by the gases remain as a network of open pores throughout the material. The final stage of the process consists of graphitising the product during long periods of high temperature (2500°C – 2800°C) exposure. During this stage, the carbon atoms arrange themselves into the organised hexagonal planes of the graphitic structure. The porosity of the material is reduced somewhat during graphitising, but the average completed graphite plate still has a porosity of 18% – 32% (Wang *et al.*, 2004:1027). This intrinsically porous nature of graphite is observed even in high quality, isotropic, nuclear grade graphite (Sun *et al.*, 2004:1).

The method used most often to stop gas permeation through graphite is called impregnation. During this process, a filler material is used to infiltrate the graphite and fill the pores, thereby sealing the surface and closing all gas flow paths. The choice of filler material is a very important since the properties of this material determine many of the operating boundaries of the heat exchanger. In a study by Wang *et al.* (2004:1027) poly-tetrafluoroethylene was used (PTFE) as the impregnating material, reducing the porosity of a graphite plate from 18.24% to 3.29%. This proves that a polymer filler is very effective in reducing gas permeation at low temperatures, but it cannot be used in high temperature heat exchangers because of its low softening point. Therefore, studies was undertaken to find filler materials able to withstand higher temperatures. Sogabe *et al.* (1996:70) impregnated a high density isotropic graphite with boron oxide at 1200°C and 15MPa. A decrease in nitrogen permeability at 25°C of four orders of magnitude was reported. The boron oxide has a maximum operating temperature of 400°C, which is substantially better than the polymer, but not nearly the 1000°C needed for the HTR heat exchangers. In another study, Sogabe and Matsumoto (1995:386) impregnated a high density isotropic graphite with two different borosilicate glasses at 1200°C and 15MPa. It was shown that impregnation by one of the glasses reduced the gas permeation of the graphite by as much as five orders of magnitude. These glasses have softening points of about 600°C. It was also concluded that machining of the graphite after impregnation reduces the effectiveness of the impregnating material in sealing the graphite.

From the above studies it is evident that, even though the graphite itself can withstand extremely high temperatures, the usable temperature of the material is limited by the melting or softening point of the impregnating material. Thus, impregnation by these specific materials is not suitable for sealing graphite that will be used for a high temperature IHX and more options need to be considered. One such an option is found in a study on the gas permeability of graphite impregnated with a copper-titanium alloy (Sogabe *et al.,* 1996:1154). This material showed a reduction in permeability similar to that obtained by the borosilicate glass, but the difference lies in the obtainable operating temperature. The alloy used was 99% copper with 1% titanium by weight. The purpose of the 1% titanium was to increase the wettability of the copper on graphite. Pure copper generally does not have a good wettability on carbon materials. From the phase diagram of copper and titanium, shown in Figure 5, can be seen that the liquid phase for this alloy starts at about 1050°C. This is much higher than the melting points of any of the other impregnating materials mentioned. Because of this, the impregnation of graphite with a copper-titanium alloy (1% Ti by weight) seems to be a viable option as a high temperature graphite surface sealing method.

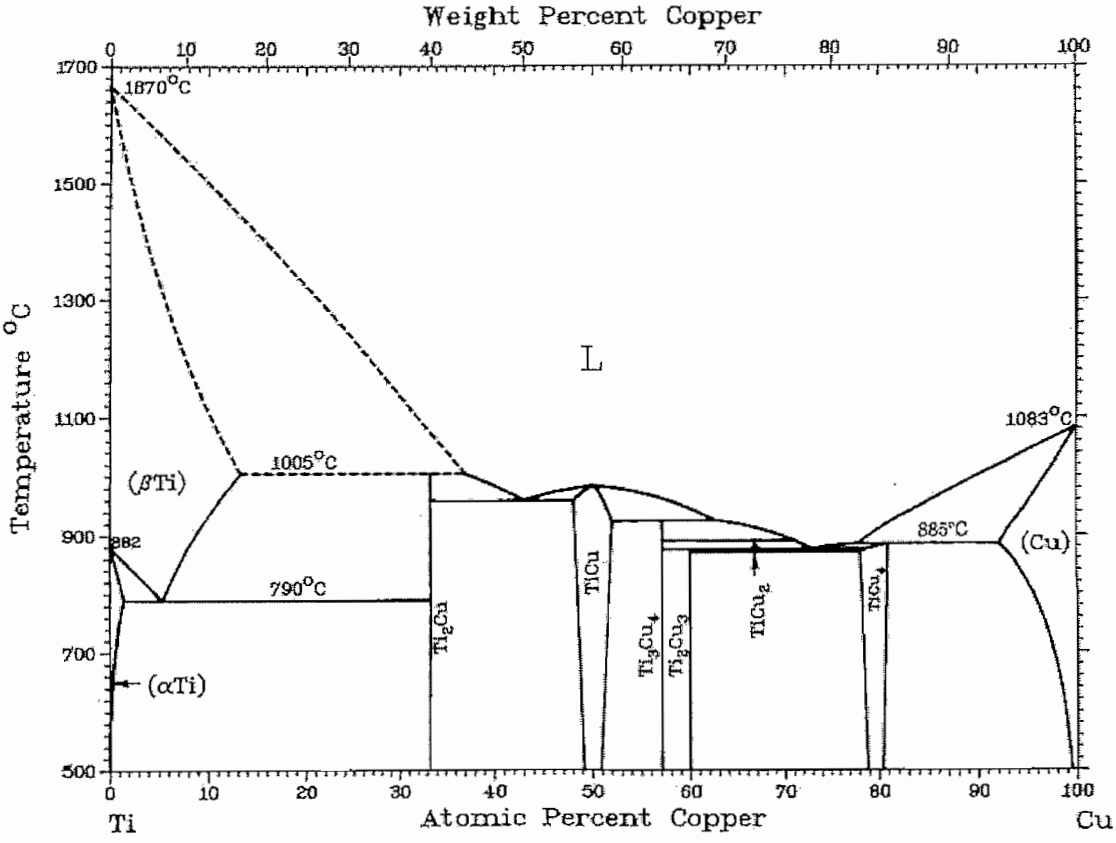

Figure 5: Copper - Titanium phase diagram (Saito *et al.*, 1976:267)

Another possible method to seal the surface of graphite and still retain its high temperature operability is to use carbon itself as the sealant. Two forms of carbon seem rather suitable.

The first is pyrolytic carbon. This form of carbon is created by a process called Chemical Vapour Deposition (CVD), in which a gaseous hydrocarbon is chemically decomposed onto a substrate at closely regulated temperatures, pressures and concentrations. Pyrolytic carbon (or pyrocarbon) is reported to have a gas permeability between 4 and 13 orders of magnitude less than the average isotropic graphite (Pierson, 1993:161).

The second form of carbon that might be suitable is known as glassy carbon (Figure 6). Glassy carbon is created by the carbonisation of specific resins, notably phenol based and furfural ones. This creates a smooth, hard, and shiny carbon that cannot be graphitised and has a closed microporous structure. Glassy carbon is reported as having a gas permeability of 10 orders of magnitude less than natural graphite (Setton, 2002:6). Thus, both of these carbon materials have the potential to decrease the permeability of graphite substantially without affecting the high temperature operability at all. However, further study is needed to prove their practical applicability.

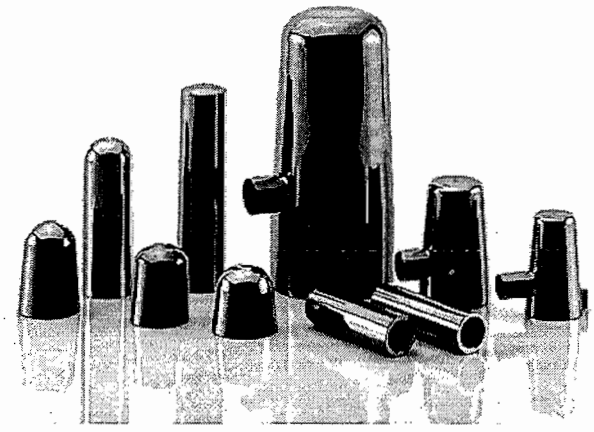

Figure 6: Crucibles made from glassy carbon SIGRADUR®

2.3 Degradation of Graphite at High Temperature

There are different approaches to stop the oxidation of graphite at high temperatures. According to McKee (1991: 174) the methods normally used can be categorized into two main groups, namely active site poisoning of the material and using oxygen barrier coatings.

The method of active site poisoning involves dipping the graphite in some aqueous solution and drying it afterwards. The deposit that is left on the graphite inhibits the reaction of oxygen with carbon and thus helps to prevent degradation. Active site poisoning has a limited effective lifetime and is usually more suited to low temperature applications (Weiming & Chung, 2002:1249). The other method, namely oxygen barrier coatings, relies on a physical coating of some material applied over the entire graphite component to keep oxygen away from the carbon. These coatings are usually in the form of either a noble metal (like iridium, platinum or rhodium (McKee (1991: 176)) or some ceramic (like SiC, TiC, $ZrSiO_4$ or glass (Weiming & Chung, 2002:1249)). The cost of noble metal coatings is, of course, exceptionally high and the wetting of graphite by metals is generally poor (Molina *et al.*, 2007:991). Ceramic coatings, on the other hand, are much cheaper and the CVD process generally used to create them is well understood. The ceramic investigated the most as an oxygen barrier is silicon carbide (SiC). It has a high thermal conductivity and is easily deposited on the graphite surface. The only trouble with silicon carbide is that its Coefficient of Thermal Expansion (CTE) is different to that of graphite. This causes the SiC coating to crack during thermal cycles, creating paths for oxygen to reach the graphite substrate. A solution put forth by Fergus & Worrell (1995:537) is to use an outer layer of SiC together with an inner layer of boron nitride or boron carbide. The boron in this inner layer reacts with silica formed on the walls of the cracks of the SiC, creating a borosilicate with low viscosity. This borosilicate then flows over the exposed graphite substrate

at the bottom of the crack, covering it and protecting it from oxidation. The study found that this double layer will protect a graphite substrate for 9 days at 1500°C and for 6 days at 1400°C. Unfortunately, lower temperatures were not included in this study and how this system will perform at 1000°C it is therefore unknown.

The degradation inhibiting coatings discussed may also, with further study, prove to be solutions to the permeability problem discussed in the previous section because they cover the entire graphite surface, inadvertently sealing all the open pores and thus stopping the flow of gas through the material. It might therefore prove useful to examine the possibility of finding a coating that is a simultaneous solution to both problems.

A question that may rightly be asked at this stage, is whether a protective barrier coating is really necessary in the inert helium environment of the HTR. There should be little or no free oxygen available to cause oxidation of the graphite. The problem is that it is very difficult to keep all oxygen out of the reactor main loop. According to Xiaowei *et al.*(2004:279), the graphite internals of the HTR-10[4] research reactor did show some degradation even in the inert helium atmosphere. The source of oxygen seemed to be a leak in the steam generator as well as air trapped in the graphite components inside the reactor. If these sources of oxygen could be removed or the helium could be cleaned continuously, the oxidation of all the graphite components inside the main loop, including the IHX, could be controlled at acceptable levels. It seems that the best solution to the high temperature graphite degradation problem would be to try and create a completely inert environment, rather than to try and protect each component individually by coatings. However, since this is an idealisation of reality, further investigation into coatings is probably needed.

2.4 Shaping of Graphite

Due to the high chemical inertness of graphite, chemical etching is usually not an option when shaping graphite. Mechanical shaping methods are more suitable to this material, with the most common process being high speed milling.

The milling of isotropic graphite has been proven successful by a number of studies, including Nieminen *et al.* (1996:32), Schroeter *et al.* (2006:128) and Yang *et al.* (2009:4395). This process is a common practice in the mould and die manufacturing industry, where graphite electrodes are manufactured for use in Electron Discharge Machining (EDM) processes.

[4] The HTR-10 is a 10MW pebble bed nuclear test reactor that is located at the Institute of Nuclear Energy Technology, Tsinghua University, Beijing, China.

According to Nieminen *et al.* (1996:25) the mechanism of the machining of graphite is very different from that of metals due to the great differences in their toughness, hardness and microstructure. Graphite is not cut by undergoing plastic deformation, removing material in the form of chips as is the case in metals. According to Schroeter *et al.* (2006:129) graphite undergoes brittle fracture at the cutting point, removing the material by creating very small dust particles. Because of this brittle nature, there are no high temperatures present in the tool and the machining forces are relatively low.

According to Kalpakjian and Schmid (2006:726), several independent parameters are used to define a normal end-milling operation. These are:

- V_{cutter} : Surface speed of the cutter or cutting speed in metres/minute.
- D : Tool diameter in metres.
- n : Number of teeth on the tool.
- F : Feed per tooth in millimetre/tooth

These parameters are then used to calculate more usable values which are actually used in the programming of a Computer Numerically Controlled (CNC) milling machine. These are:

$$N = \frac{V_{cutter}}{D} \quad [1]$$

where

N : The rotational speed of the spindle (RPM),

and

$$\upsilon = F \times N \times n \quad [2]$$

where

υ : Linear speed of the work piece or the feed rate in (mm/min)

The above mentioned studies have all used different machining parameters in their tests, as shown in Table 1.

Table 1: Machining parameters used in different studies

Study	Machining Parameters			
	V_{cutter} (m/min)	D (mm)	F (mm/tooth)	n
Nieminen *et al.* (1996:26)	424 – 1400	3 and 10	0.08 and 0.2	2
Schroeter *et al.* (2006:129)	200 – 800	8 and 16	0.05	2
Yang *et al.* (2009:4395)	160 – 240	10	0.05 and 0.1	2

Nieminen *et al.* (1996:32) concluded that the feed rate was the most important parameter influencing accuracy, whereas cutting speed influences tool life negatively. Schroeter *et al.* (2006:131) disagrees with the finding that higher cutting speeds decreases tool life, saying that "...in the case of machining graphite, in contrast to machining ferrous materials, hardened or not, an increase in cutting speed does not reduce the tool life". In fact, their studies showed an increase in tool life with higher cutting speeds. Yang *et al.* (2009:4395) agrees that the lower feed rates produce a better surface finish, but concludes that it also creates more flank wear since the tool is in contact with the work piece for a longer time.

When consulting the machining data provided by tool manufacturers (SECO Machining Navigator Catalogue: Solid End Mills, 2008:119), the following parameters are recommended for machining graphite with a 1.5mm, 2 fluted end mill[5]:

- V_{cutter} = 400m/min or the maximum RPM of the milling machine
- F = 0.018 mm/tooth

These values correlate with those in the studies of Table 1.

One more thing must be noted about the machining of graphite. According to Schroeter *et al* (2006:129) the machining of graphite produces fine particles in the form of a powder. This is different from metals, which create large chips of material upon machining. These fine particles will infiltrate the motors and mechanisms of the mill and may cause fouling and even damage. Since graphite is a conductor of electricity, airborne particles may also cause damage by creating short circuits in electronic equipment. It is therefore vital to employ an effective vacuum cleaning system to remove the dust particles as they are being cut away from the work piece.

[5] This is the tool used to machine the heat exchanger plates discussed further on in this study.

2.5 Graphite heat exchanger designs

2.5.1 Current Graphite Heat Exchanger Types

For a long time graphite heat exchangers have had a fixed place in the industry as a heat management component. They are mostly used in the chemical industry, where they are utilised because of their unparalleled chemical inertness. They are usually made from a polymer impregnated graphite so as to solve the porosity problem. However, because of this, their operating temperatures are limited to about 200°C (See section 2.2). Therefore, current commercial graphite heat exchangers are not seen as a high temperature heat management solution. The two designs used most often are the block type heat exchanger and the plate type heat exchanger.

2.5.1.1 Block Type Graphite Heat Exchangers

From the SGL Block Heat Exchanger Brochure (2008), a block type graphite heat exchanger can be seen as a shell-and-tube heat exchanger where the tube-side fluid, as well as the shell-side fluid, flows through individual flow channels. They are made from solid cylindrical or cubic graphite blocks with the primary flow passages drilled through them axially. The secondary flow passages are then drilled through the block, perpendicular to the primary passages in such a manner that none of the primary and secondary passages intersect. A few of these blocks are then stacked on top of each other and the whole stack is placed inside a metal vessel acting as the pressure boundary. The primary fluid passes axially through the aligned passages from one block to the other, while the secondary fluid flows in a serpentine fashion through the perpendicular passages, guided by baffles. A graphical representation of a block type heat exchanger is shown in Figure 7:

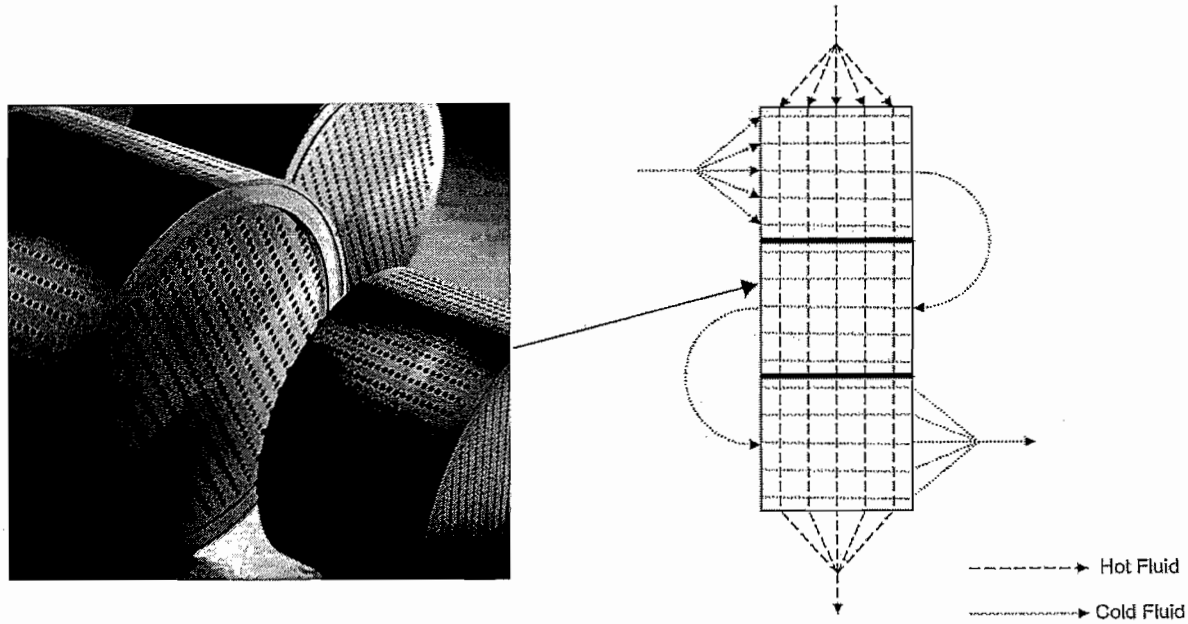

Figure 7: Block type heat exchanger segments (from SGL Block Heat Exchanger Brochure (2008)) and a schematic representation of a block type heat exchanger in operation.

2.5.1.2 Plate Type Graphite Heat Exchangers

Plate type heat exchangers have a more advanced design than block type heat exchangers based on claims that they increase the heat transfer area and effectiveness, while decreasing the bulk of the component.

From studying the SGL Plate Heat Exchanger Brochure (2008), plate type heat exchangers can be described as a stack of thin, large plates. These plates are milled or pressed to result in a corrugated surface area in the centre with either the primary or secondary flow paths on the sides. The primary and secondary fluid plates are then stacked consecutively, acting as the core of the heat exchanger. A leak tight seal is created between the plates by using a sealing mechanism like a gasket or an o-ring and applying pressure on the stack through pressure plates located at each end of the stack. Figure 8 shows a depiction of this kind of heat exchanger:

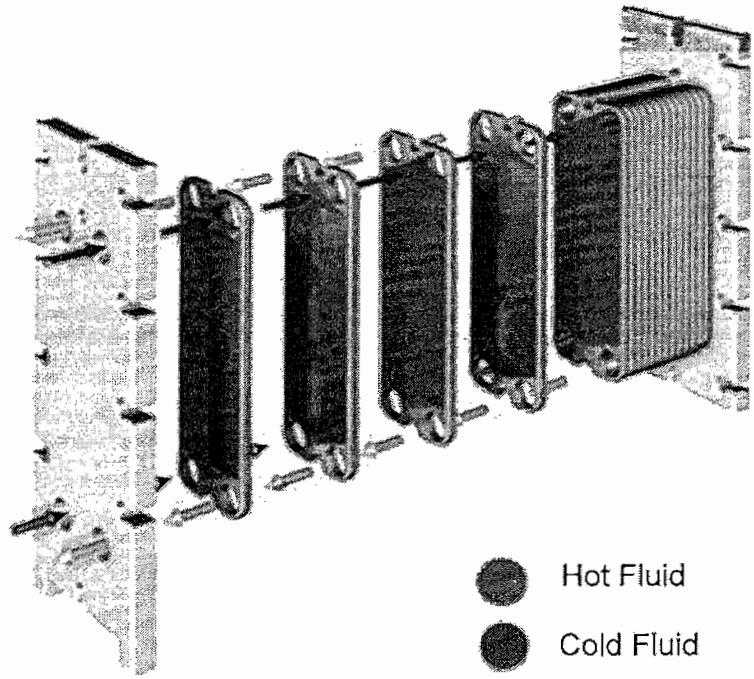

Figure 8: Plate type graphite heat exchanger (modified after SGL Plate Heat Exchanger Brochure (2008))

Plate type heat exchangers have very high heat transfer densities since the fluid is exposed to very large surface areas. They are also modular, making it easy to increase the heat transfer area by simply adding more plates. Another advantage of the plate design is ease of manufacturing. By using modern CNC milling machines, the corrugated pattern can easily be machined into the surface of the plates.

2.5.2 Printed Circuit Heat exchanger

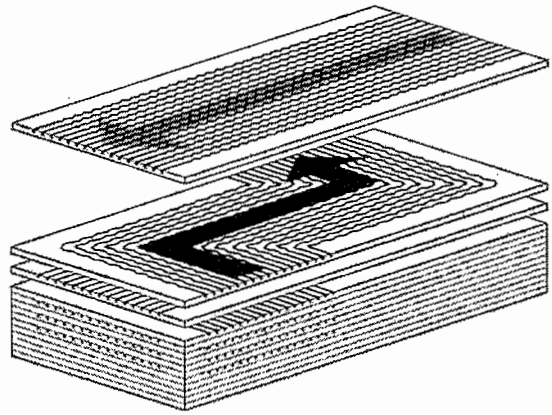

Figure 9: Simple schematic representation of a typical printed circuit heat exchanger

Another type of heat exchanger similar in construction and design to plate type heat exchangers is the Printed Circuit Heat Exchanger (PCHE) (see Figure 9). It uses the same type of alternating plate configuration as the plate type heat exchanger discussed in Section 2.5.1.2 and also have large heat transfer areas. The main difference between these two heat exchanger types lies in the shape of the flow channels formed onto the surface of individual plates. Where plate-type heat exchangers use only one large corrugated surface per plate, PCHEs have a large number of small individual flow channels etched or machined into every plate's surface. These flow channels usually have very small diameters (<1mm), and there is a high density of channels per unit area in an effort to increase the heat transfer area and the convection heat transfer coefficient. The effect of decreasing the channel diameter is evident from the standard expression for the convection heat transfer coefficient for internal flow

$$h = Nu\frac{k}{D_H} \qquad [3]$$

where:

h	:	Convection heat transfer coefficient (W/m^2.K),
Nu	:	Nusselt number,
k	:	Conduction heat transfer coefficient (W/m.K) and
D_H	:	Hydraulic diameter of the channels (m).

The hydraulic diameter is defined as

$$D_H \equiv \frac{4A_c}{P} \quad [4]$$

where:

A_c : Cross sectional flow area of a single channel (m^2) and

P : Wetted perimeter of a single channel (m).

To decrease D_H, A_c needs to be decreased. But as A_c is decreased, so is P since the area and the perimeter (or circumference) are interconnected. But still, this causes D_H to become smaller, since the area A_c is a quadratic value while P is linear. And so, as D_H is decreased, the value of h increases. This in turn increases the amount of heat transferred from the hot to the cold stream. The downside of this is the resulting increase in pressure drop according to the relationship

$$\Delta p = \left(f \frac{L_{ch}}{D_H} + \sum_{i=1,n} K_i \right) \frac{1}{2} \rho_i V^2 \quad [5]$$

where:

Δp : Pressure drop in a channel (Pa),

f : Darcy-Weisbach friction factor (m),

L_{ch} : Channel length (m),

K : Pipe loss factors,

ρ_i : Fluid density at the inlet (kg/m^3) and

V : Fluid velocity (m/s)

From Equation [5] it is found that a decrease in D_H will result in an increase in pressure drop. To counter this effect in PCHEs, the fluid velocity V is kept as low as possible, resulting in the fact that the flow in most PCHEs is laminar. Laminar flow again gives lower heat transfer rates compared to turbulent flow. Thus, the optimal design for a compact PCHE would be a balance between pressure drop and heat transfer effectiveness.

When manufacturing PCHEs from metals or ceramics, the flow channels are usually chemically etched into the individual plates. After the channels have been formed, the plates are diffusion bonded together to form one block of material containing the flow passages. If diffusion

bonding techniques are correctly applied, the joints between the individual plates can reach the same strength as that of the parent material (Li *et al.*, 2008:285).

2.6 Conclusion

The problems of graphite porosity and degradation have been studied extensively by the scientific community, and feasible solutions to both have been proposed. However, these studies were not directly related to high temperature heat exchanger design, manufacturing and construction. Also, much of the knowledge about the design, manufacture and operation of current, low temperature graphite heat exchangers are close guarded industrial secrets, and even though the printed circuit heat exchanger has all of the advantages mentioned, no record of the manufacturing of such a heat exchanger from graphite could be found in the literature.

2.7 Aim of this study

The aim of this study is to gain experience in using graphite for the manufacturing of a heat exchanger. This is accomplished by designing, manufacturing and testing a laboratory scale unit produced from isotropic graphite. It was decided to use a printed circuit type design, since it seems that very little is known about the use of graphite in this type of heat exchanger.

Even though the use of graphite calls for a protective surface coating to eliminate gas permeation and graphite degradation, and for diffusion bonding techniques to obtain a gas tight seal between the PCHE elements, a lack of funds and facilities prevent the use of these technologies in this study. However, by conducting the tests at atmospheric pressure, the permeation of gas through the graphite is minimised. Graphite degradation is eliminated by restricting gas temperatures to below 300°C and it is therefore possible to use sealing methods like o-rings or gaskets to create the seal between the heat exchanger elements.

It is also the aim of this study to construct a theoretical model of the laboratory scale unit in order to compare the results generated from the theory with that provided by the testing of the heat exchanger.

Chapter 3

Laboratory Scale Heat Exchanger Design, Manufacturing and Testing

3.1 Introduction

The purpose of this chapter is to inform the reader of how the laboratory scale printed circuit heat exchanger was designed, manufactured and tested. The results from the tests are presented at the end of the chapter.

3.2 Heat Exchanger Design

3.2.1 PCHE Flow Channel Configuration

With PCHEs, the configuration of the flow channels on the individual plates is important for a number of reasons. It impacts on the heat transfer effectiveness of the heat exchanger and has a large effect on the pressure drop across it. According to Tsuzuki *et al.* (2007:1704) the conventional design for the flow pattern configuration of a compact PCHE is a zigzag pattern of continuous channels, like that shown in Figure 10. The channels are made as small as possible in an attempt to increase the convection heat transfer coefficient as described in Section 2.5.2. It is claimed however, that this configuration creates large pressure drops between the heat exchanger inlet and outlet. It was proved from Computational Flow Dynamics (CFD) models that this was due to turbulence caused by reverse flows, swirls and eddies being created as the fluid flows around the sharp zigzag corners. This is not a favourable phenomenon, since a high energy input is needed to overcome this pressure drop, which in turn reduces the overall efficiency of the heat exchanger.

Figure 10: Zigzag flow configuration for a PCHE

In their study *Tsuzuki et al* (2007:1704) proposed a more advanced design consisting of discontinuous, sine-shaped fins claimed to resulted in a pressure drop five times smaller than that

of the traditional zigzag pattern without a reduction in heat transfer capability. Figure 11 shows a sample of this configuration. In their CFD analysis of this configuration, it was shown that the reduction in pressure drop was due to the elimination of all eddies and reverse flows by the smooth sine-shaped fins, creating a more laminar flow around the bends. Because of these advantages, it was decided that this would be a favourable configuration to use in the manufacturing of the laboratory scale graphite PCHE of this study.

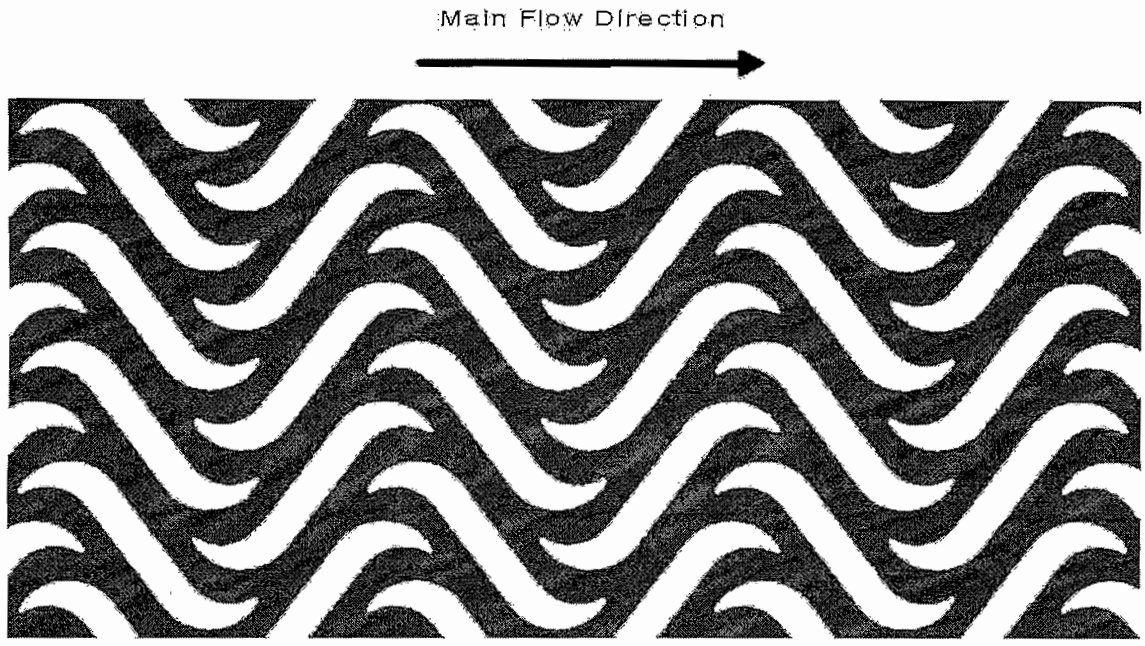

Figure 11: Discontinuous sine wave shaped flow configuration. (Tsuzuki *et al.*, 2007:1704)

3.2.2 Laboratory Scale Graphite Printed Circuit Heat Exchanger Design

As discussed in the previous section, it was decided to construct a laboratory scale printed circuit heat exchanger from graphite. The configuration of the flow channels of the individual plates has also been decided on. It was then decided to design a heat exchanger with an appropriately small size so as to suit the available manufacturing and testing facilities. This section discusses the identified material for the construction of the heat exchanger, as well as the chosen heat exchanger size and geometry. This is followed by an explanation of the design of the heat exchanger and all its features.

3.2.2.1 Material chosen for the design of the heat exchanger

Graphite, in its natural form, is an anisotropic material. This anisotropy is caused by graphite's microscopic structure, which consists of stacked layers of flat graphite sheets. These layers are usually aligned during manufacturing processes such as extrusion. Because of this, the material properties of graphite differ with respect to the orientation of the layers. In order to find a more isotropic graphite, manufacturers have developed manufacturing processes that do not cause the graphite layers to align. One such process is isostatic moulding, in which graphite is shaped by moulding it at high pressure and temperature, causing the graphite layers to be randomly orientated. The result is a high density, small kernelled, isotropic graphite material in which the material properties, such as heat conductivity, is unaffected by the orientation of the material grains. Because the use of this material eliminates the need for orientation dependant design and engineering, isotropic graphite was chosen as the material for the design and manufacturing of the laboratory scale heat exchanger.

3.2.2.2 Chosen heat exchanger size and flow geometry

The heat exchanger core dimensions were chosen relatively small so that is could easily be manufactured on the available machinery and could be accommodated by the available testing facilities. The dimensions of the chosen core size of a single plate are shown in Figure 12. The number of plates in the heat exchanger (which designates the height of the heat exchanger) was identified as twelve.

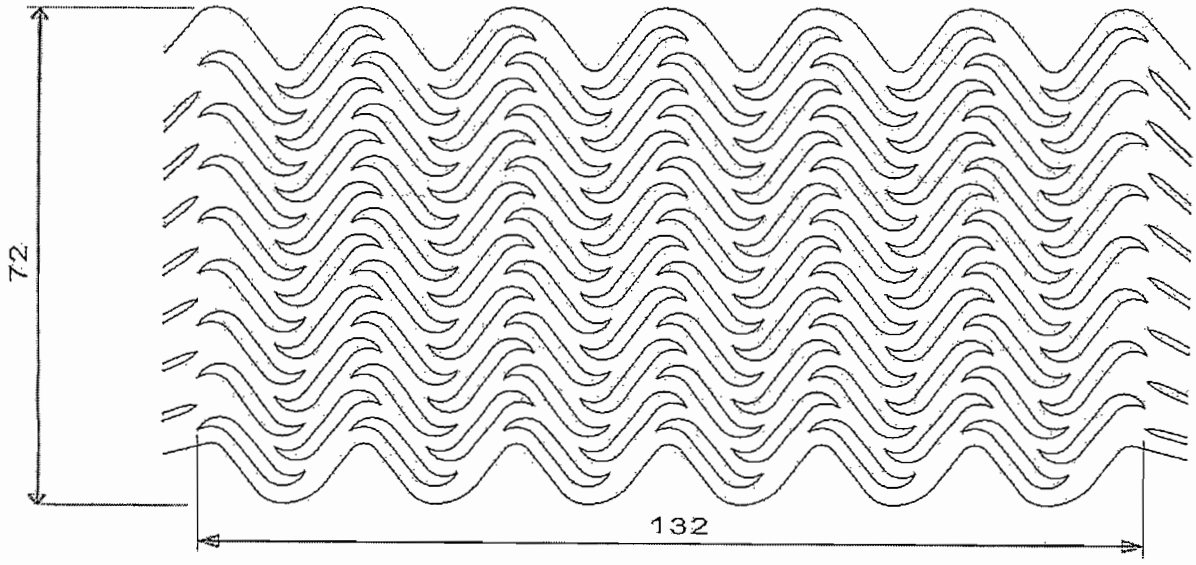

Figure 12: Overall dimensions of heat exchanger core (dimensions in mm)

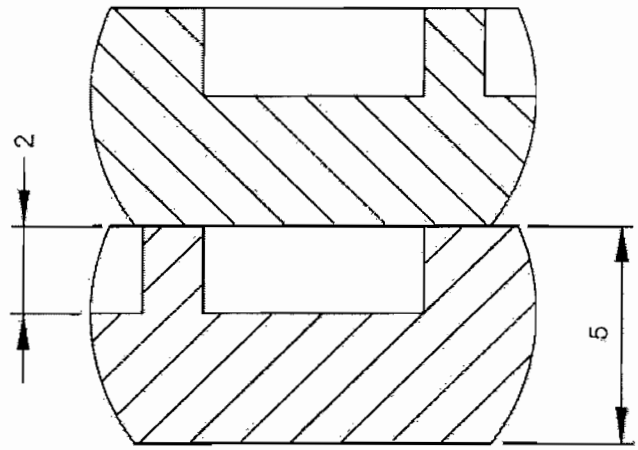

Figure 13: Section view of a segment of two stacked heat exchanger plates (dimensions in mm)

From Figure 13 the thickness of a single heat exchanger plate is shown to be 5mm. This value was constrained by the dimensions of the available material. Since it was unknown at the time what the magnitude of the forces on the end mill used for the machining of the channels would be, the channel depth (or fin height) was chosen conservatively shallow (2mm) in an effort to minimise these forces.

The design of the flow configuration is based on the discontinuous sine wave configuration proposed by *Tsuzuki et al.* (2007:1704). The shape of the fin was created by fitting smooth curves through specific points around a sine form with the help of CAD software (Figure 14). This single fin shape was then replicated, as shown in Figure 15, to cover the entire core surface of the heat exchanger plate (Figure 12).

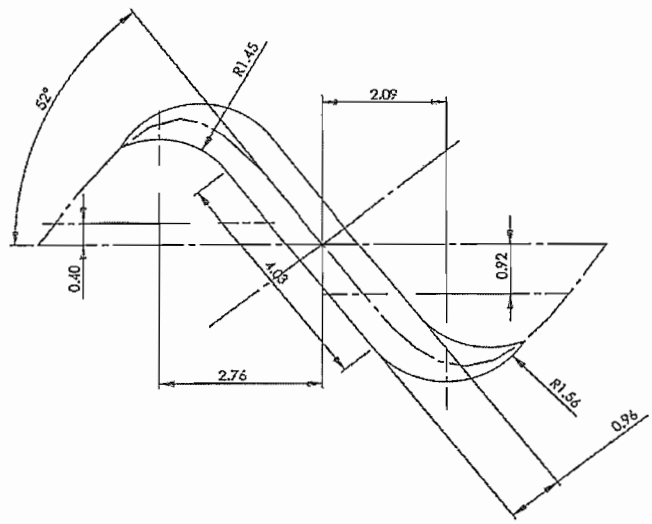

Figure 14: Fin shape deduced from the sine wave (dimensions in mm)

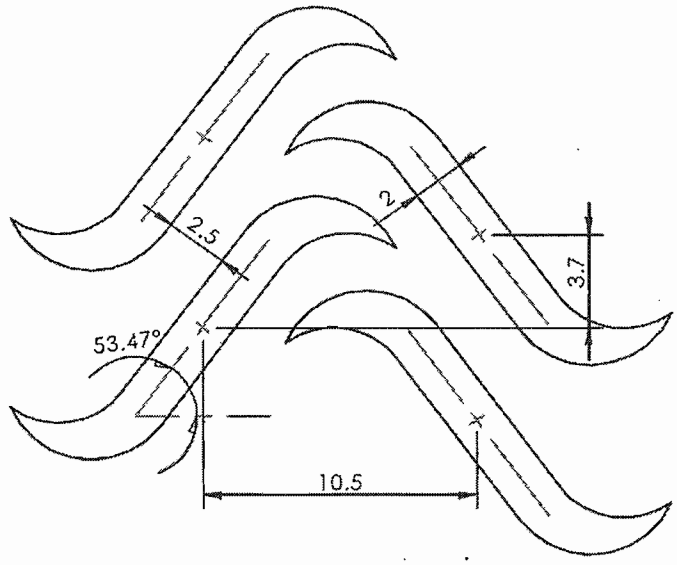

Figure 15: Sine wave shaped fins relative positions (dimensions in mm)

The choice of channel width (2.5mm) is a compromise between increasing the heat transfer area (according to Equations [3] and [4]) and the availability of end mills small enough to machine the channels. The horizontal spacing of the fins (10.5mm) was chosen so that the leading and trailing edges of consecutive fins line up appropriately.

3.2.2.3 Discussion on the heat exchanger design

A Computer Aided Design (CAD) model of a single heat exchanger plate, with the size and flow channel configuration as discussed in the previous section, is shown in Figure 16. This single plate consists of a graphite slab, 250mm long, 100mm wide and 5mm thick with the flow patterns machined onto one side.

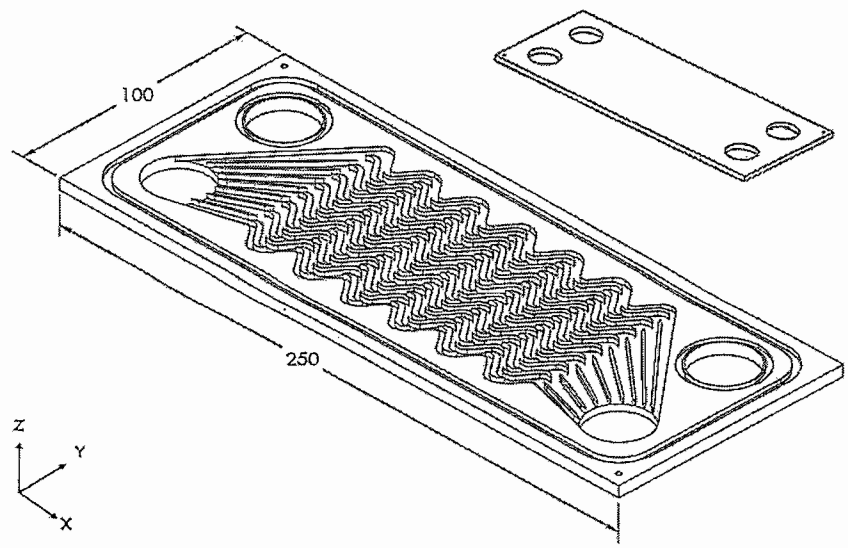

Figure 16: Isometric view of a single HX plate design model (view of plate underside in background)

To provide the heat transfer fluid to the core of the heat exchanger, four gas ducts situated at the corners of the heat exchanger core are used. These ducts are formed by the four large borings on each individual plate lined up when more than one plate is stacked on top of each other. Each duct is coupled to one of the inlets or outlets of the heat exchanger and is designed to act as a manifold for the heat exchanger core, distributing and accumulating the heat transfer fluid to and from the core.

Normally, PCHEs would need differing designs for consecutive plates to allow for separate flow paths for the hot and the cold streams respectively. The current design eliminates this need by using a single, symmetrical plate design for both fluid paths. By simply rotating consecutive plates 180° around their Z-axis, the hot and cold fluid paths are separated from each other (Figure 17). Also, the use of a single plate design increases the efficiency of manufacturing because a single machining setup can be used to machine all of the plates for the entire heat exchanger core.

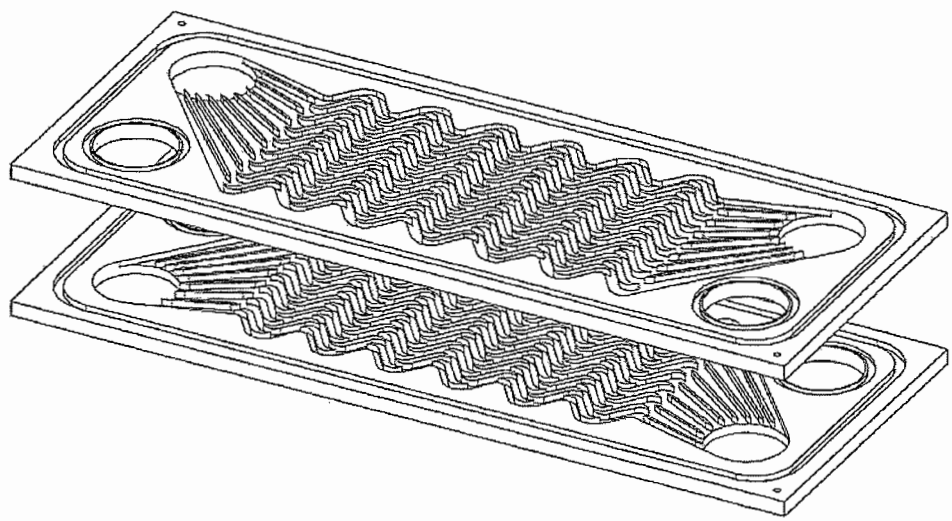

Figure 17: Exploded view of two stacked HX plates

To align the plates to each other as they are stacked, each plate is designed with two alignment holes situated at diagonal corners. When stacking the plates, guide pins can be used to align these holes for consecutive plates, ensuring that the core and gas ducts are well aligned.

All the fins in the core are designed to have sharp leading and trailing edges. This is done in order to minimise the pressure drop between the heat exchanger inlets and outlets. By making these edges sharp, eddy currents and reverse flows are minimised, thus reducing drag and ultimately the pressure drop across the heat exchanger.

To keep the two fluid streams from mixing, some form of seal between the plates is needed. The sealing method of choice would be to use diffusion bonding methods to permanently join consecutive plates to each other, thereby creating a robust seal between the fluid streams. However, due to a lack of funds and facilities this technology could not be used in this study. Thus, it was decided to use o-ring seals to establish the seal. To keep the fluid streams from mixing, seals are placed around two of the borings on each plate. The seal between the streams and the environment is established by placing another seal around the perimeter of each plate. Even though the shape of the perimeter seal is a rounded rectangle, a circular seal with equivalent circumference is fitted. It is possible to do this if the inside corner radii of the groove is designed to be no less than three times the width of the seal (Parker O-ring Handbook, 2001:4-3). The diameters of the two different o-rings used in the design are small enough to fit in the available space on the face of the heat exchanger plate. After the seal diameters was chosen, the groove dimensions were identified by consulting the seal manufacturer Parker Seals' o-ring catalogue (Parker O-ring Handbook, 2001:4-14). The groove dimensions recommended by them for a given seal width are shown in Table 2. O-ring compression is provided by the flat underside of the next plate in the stack placed on top of the o-ring when the core is assembled.

Table 2: O-ring seal and groove geometry

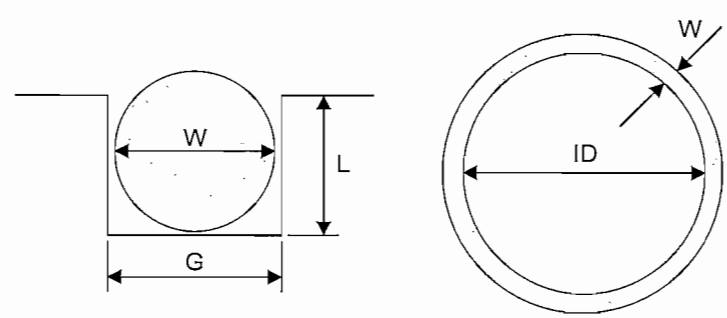

Seal Description	Seal Width (W)	Inside Diameter (ID)	Groove Depth (L)	Groove Width (G)
Gas duct seal	1.78mm	26.7mm	1.32mm	2.18mm
Perimeter seal	2.62mm	195.7mm	1.96mm	3.11mm

The o-ring material VITON™ was chosen as the seal material. This material is a fluoroelastomer dipolymer manufactured by DuPont Performance Elastomers. It is claimed that this material can withstand temperatures in the region of 200°C (DuPont Website, 2009), which explains why it was chosen.

To create the heat exchanger core, twelve individual plates are stacked on top of each other, rotating every second plate 180° around its Z axis.

To keep the heat exchanger plates together, two pressure plates were designed to be added on the top and bottom of the stack. These pressure plates (shown in Figure 18) also serve the purpose of compressing the o-ring seals between the heat exchanger plates, allowing them to create a proper seal. To provide the tension between the two pressure plates, twelve threaded rods, with washers and nuts at either end, are used. During the assembly, these bolts are tightened until consecutive graphite plates touch each other. Doing so ensures that the o-rings are compressed well while still not over tightening the nuts. Over tightening would cause damage to the graphite plates. The twelve holes for the tensioning rods are located along the edge of the plate, while the other four holes are used for the gas inlets and outlets on the bottom plate. On the top plate, these holes are used to provide an interface for instrumentation such as temperature and pressure sensing equipment. A model of the assembled heat exchanger is shown in Figure 19.

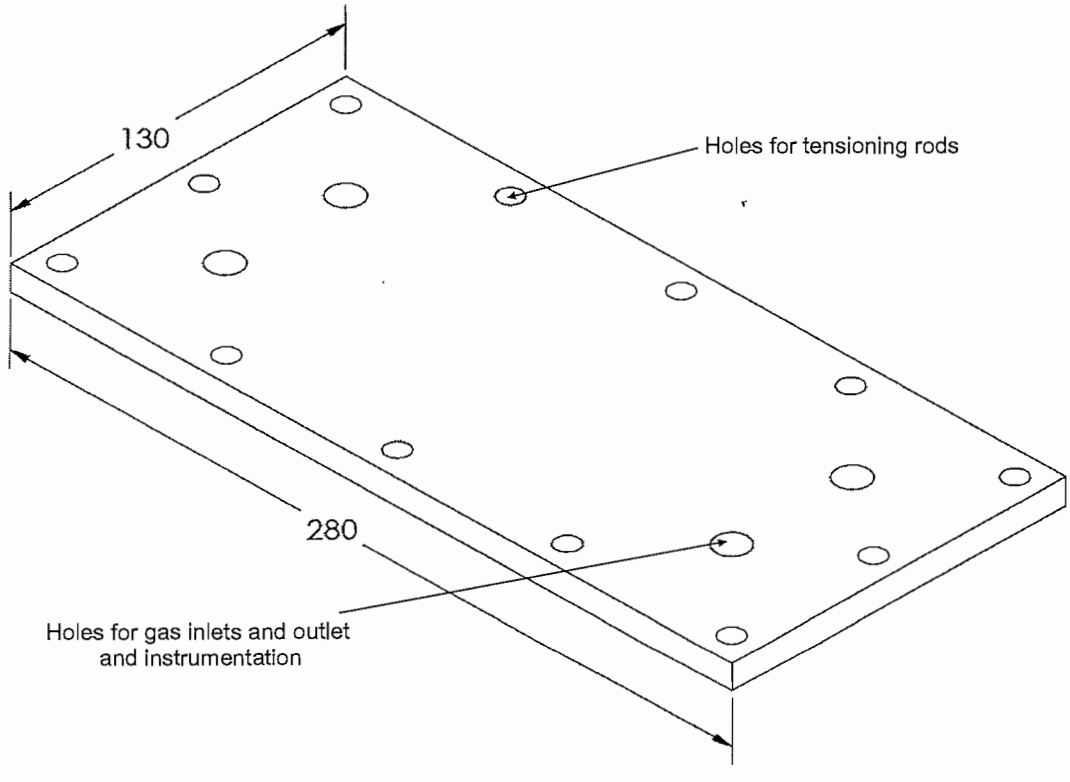

Figure 18: Pressure plate used for top and bottom (dimensions in mm)

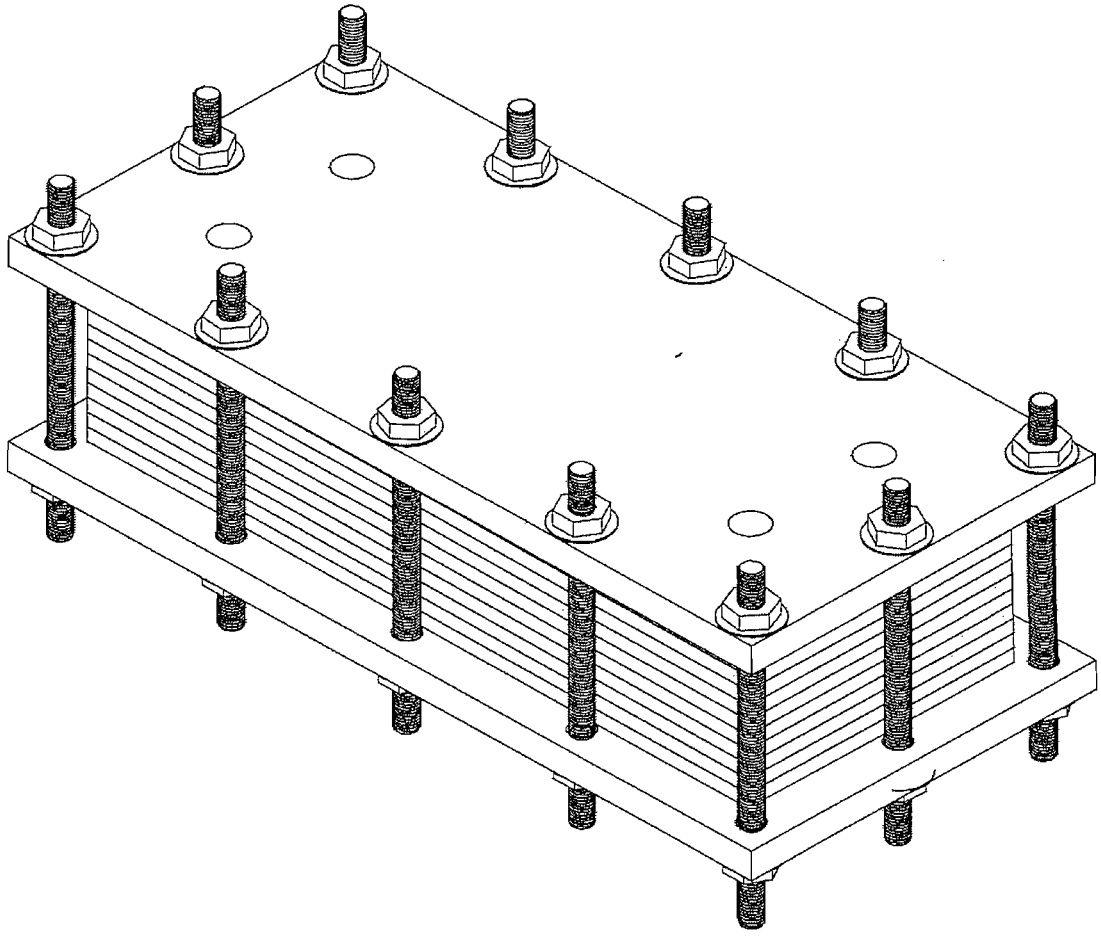

Figure 19: Model of assembled heat exchanger

3.3 Heat Exchanger Manufacturing

As mentioned in the previous section, PCHEs are usually manufactured by etching the flow channels into the surface of each plate using chemicals to remove the unwanted material. When using graphite, however, its high chemical inertness makes the use of chemical etching unfeasible. Fortunately, as discussed in Section 2.4, graphite can be machined using conventional milling methods. A few of the completed heat exchanger plates are shown in Figure 20:

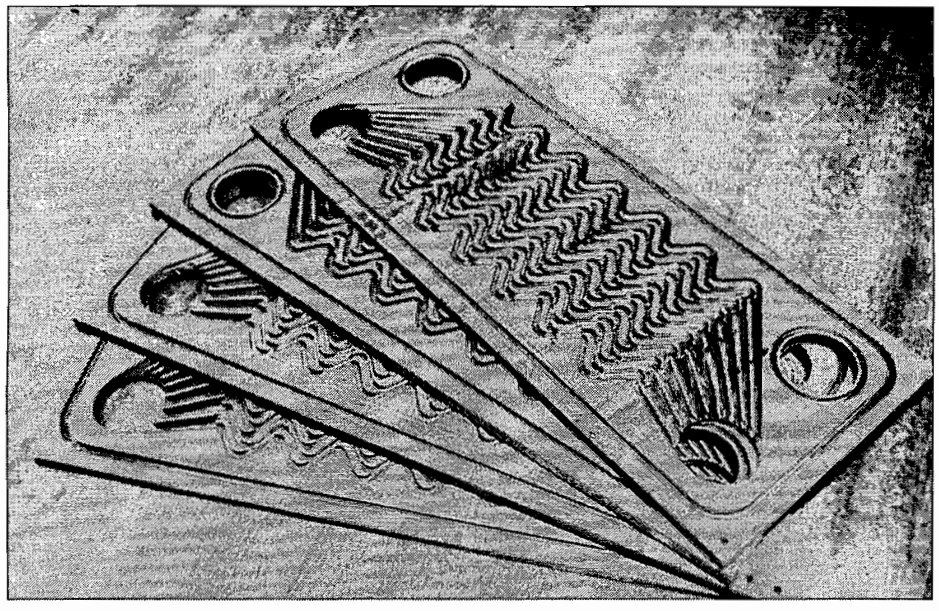

Figure 20: Completed HX plates

The remainder of this chapter discusses the manufacturing of these heat exchanger plates in detail.

3.3.1 Graphite material used for manufacturing

Many different grades of isotropic graphite are manufactured by different graphite specialist companies around the globe. However, only one supplier of this type of material could be found locally, namely Graftech International. The material supplied by them is called GRADE ATJ GRAPHITE. The properties of this material are shown in Appendix A. Even though this material is an isostatically moulded graphite, there seems to be a small amount of anisotropy present in the structure. This can be seen from the fact that the material properties are given for the "With grain" direction. However, when the material was inspected, no grain direction could be identified and the material seemed isotropic in all directions. Because of this fact, and because this was the only isostatically moulded graphite available locally, GRADE ATJ GRAPHITE from Graftech

was chosen as the material to use in the design and manufacturing of the laboratory scale heat exchanger. Figure 21 shows this material as it was received from the supplier. It has a bulk density of 1.76g/cm^3 and a heat conduction of 110 W/m.K.

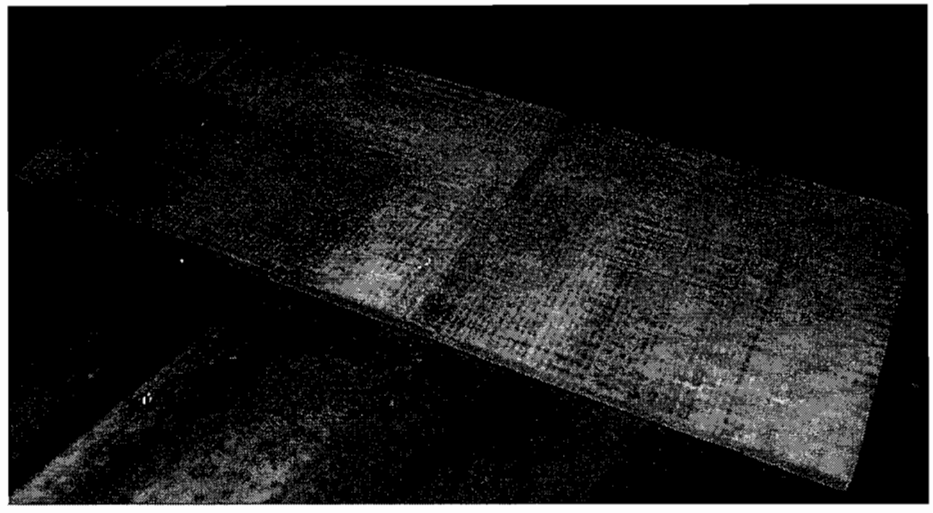

Figure 21: Graphite stock material

The flatness of the slabs was specified to the supplier as 0.5mm, as shown in the drawings. When the material was supplied, the flatness of the material was assumed to be within the specified tolerance.

3.3.2 Creating the machining tool path

The intricate and complex flow patterns used in this design could not be machined by hand. The help of a Computer Numerically Controlled (CNC) milling machine was therefore needed. These machines operate by following a set of pre-programmed commands directing a cutting tool to remove the unwanted material within the boundaries of a coordinate system. The pre-programmed commands for a CNC machine are called a tool path.

To create the machining tool path, a software package called *VISI 15.0 Student Version* from Vero Software was used. The three dimensional CAD model of a single heat exchanger plate was imported into *VISI* as a parasolid file after which the machining parameters were fed into the programme. These parameters included the spindle speed, feed rate and tool diameter. The choice of the spindle speed and feed rate was discussed in Section 2.4, while the choice of cutting tool is discussed in the next section.

3.3.3 Machining of individual plates

For the manufacturing drawings of the heat exchanger plates, see Appendix C.

3.3.3.1 The choice of cutting tool

The cutting tool chosen to machine the flow patterns into the graphite slabs was a solid carbide end mill with a diamond coating. The cutting tool manufacturer SECO recommended the diamond coated tool because of its excellent resistance to abrasion. The milling of high density isotropic graphite is generally considered a highly abrasive process due to the fact that when graphite is machined, the removed material takes the form of a very fine dust. This dust causes a lot of abrasive wear on the sides of the tool. SECO claims that their diamond coated tool will last up to ten times longer under such abrasive conditions than a standard carbide end mill.

To decide the diameter of the tool, the following were considered:

- The narrowest gap that needs to be machined. Obviously, the tool diameter must be smaller or equal to the width of this gap. See Figure 22a.
- The widest gap that needs to be machined. If this gap is much wider than the diameter of the tool, many cutting passes will be needed to remove all the material. Thus, for a small diameter tool, the time of machining becomes very long. See Figure 22b.
- The farthest that the tool have to reach down into the work piece. This determines the length of the shank that is needed. The smaller the tool diameter, the shorter are the available shank lengths. See Figure 22c.

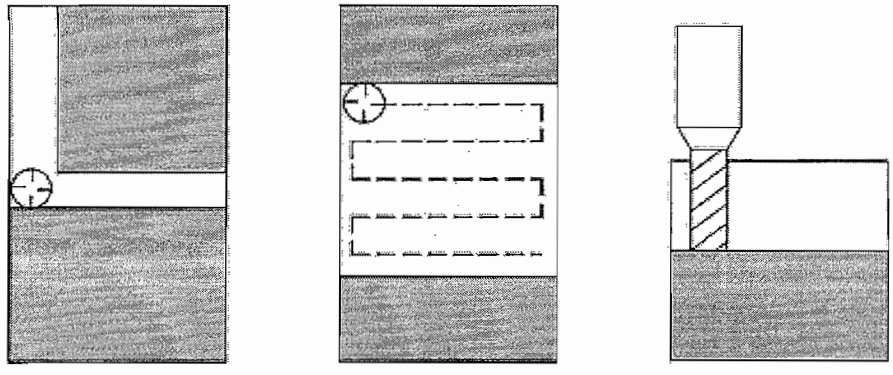

a) Tool diameter too large

b) Tool diameter too small

c) Tool shank needs to be long enough

Figure 22: Some factors influencing tool diameter

For the given case of the laboratory scale heat exchanger plate, the three parameters mentioned above are shown in Table 3:

Table 3: Geometrical parameters used in the choice of tool diameter

Geometrical Parameter	Value
Narrowest gap to be machined	1.8mm
Widest gap to be machined (excluding gas duct holes)	6.87mm
Deepest cut to be machined	2mm

From these parameters, the tool selected for the machining of the flow channels, was the SECO 600L015-DIAMOND (Figure 23 and Figure 24), a two fluted, solid carbide end mill with a diamond coating. It had a diameter of 1.5mm and a shank length of 7.5mm (SECO Machining Navigator Catalogue: Solid End Mills, 2008:119).

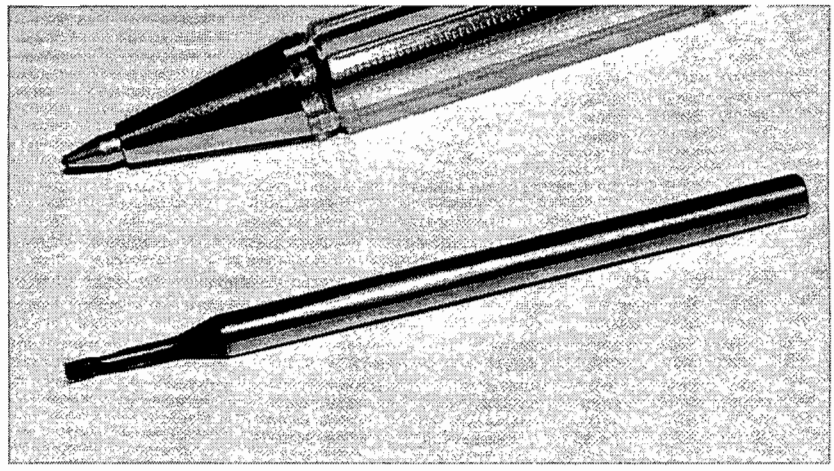

Figure 23: Tool used for machining the HX plates (pen included for scale)

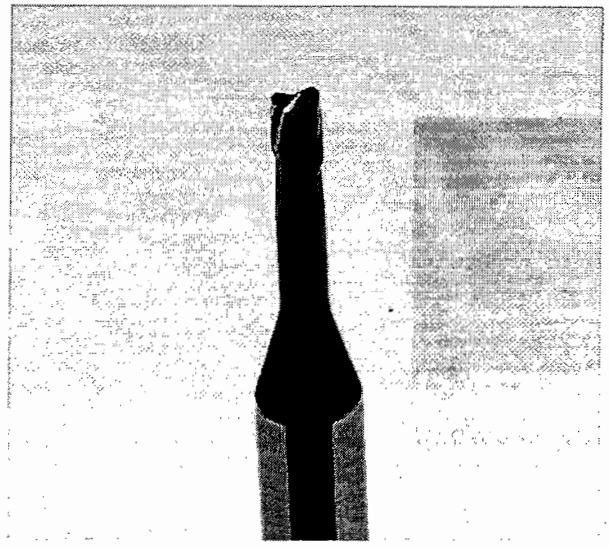

Figure 24: Machining tool two-fluted cutting tip

Another end mill with a diameter of 12.5mm was used to machine the large gas duct holes.

3.3.3.2 Clamping of graphite to the table of a milling machine

The clamping of the graphite slabs to the table of the milling machine posed a problem. The usual way of clamping a work piece to the table of a milling machine involves bolts and metal clamps. This method would certainly damage the brittle and thin graphite slabs. Thus, a different approach was needed.

The first method attempted is called a vacuum clamp. This method uses a vacuum under the work piece to pull it tightly against the table. To create the vacuum, a wooden box was constructed and clamped securely to the milling machine's table (Figure 25). A network of grooves was then cut into the top plank of the box (Figure 26). The size of the groove network was made to be just smaller than the size of the graphite slab. If the groove network was larger than the slab, air would have leaked into the vacuum and the clamp would have failed. The grooves were connected with the box's cavity by means of a number of small holes at the bottom of the grooves (Figure 27). A vacuum cleaner was then connected to the box to provide the sucking power. To keep the top plank from bending downwards due to the vacuum under it, support beams were added on the inside of the box.

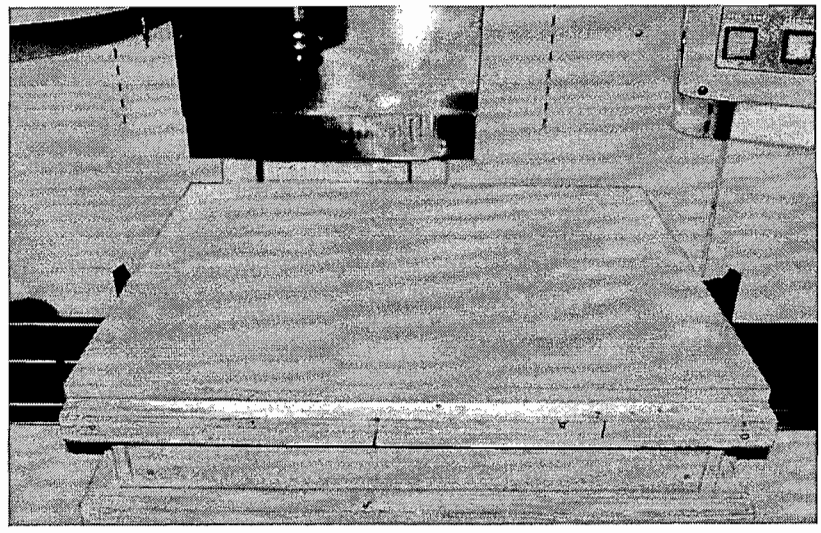

Figure 25: Vacuum clamp box clamped to the table

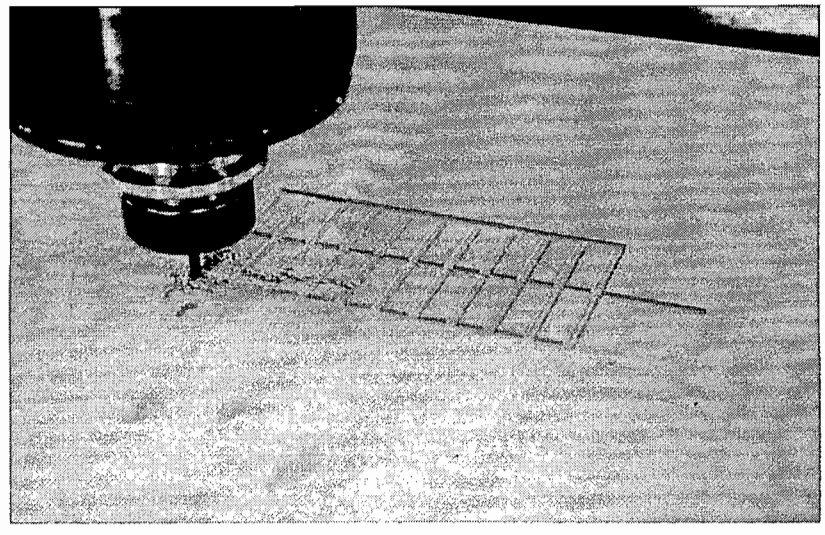

Figure 26: Cutting grooves into the top of the vacuum clamp box

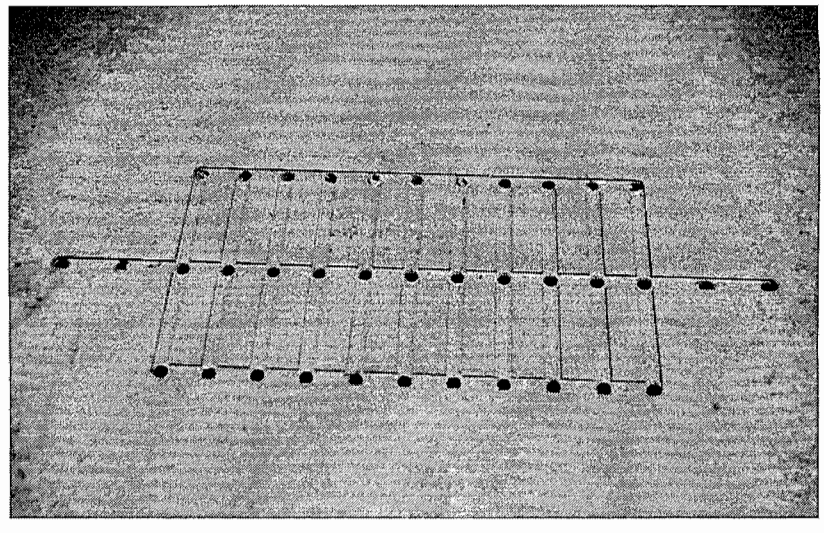

Figure 27: Vacuum clamp groove network with holes

With this vacuum clamping method, the graphite slab was clamped by placing it over the network of grooves and switching the vacuum cleaner on. As the air was removed from the box and the groove network, the work piece was pressed firmly unto the surface of the wooden box by the atmospheric pressure. Machining could then continue as normal. However, because it was not possible to create a leak tight seal between the vacuum box and the loose graphite slab placed on it, the vacuum cleaner had to remain on during the entire machining operation. This proved to be the problem with this method for this specific case. Because of the long time it took to machine one plate (± 2h) the vacuum cleaner started to overheat. This caused the sucking power to decline and the clamping power was reduced. In turn, the work piece started to move around and the graphite was damaged beyond use (See Figure 28). This problem could have been solved by using a vacuum pump instead of a vacuum cleaner. However, for this specific application, this method proved unsuccessful and another method was investigated.

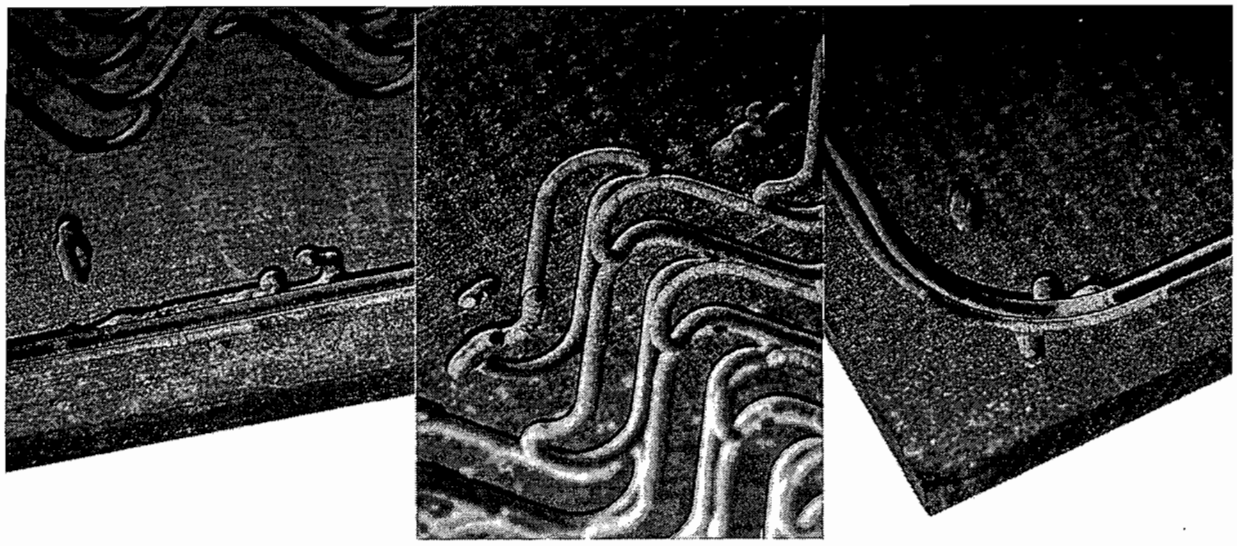

Figure 28: Damaged graphite due to failing of the vacuum clamp

The second method attempted to clamp the graphite slabs to the milling machine's table was much more successful. This method involved clamping a piece of wood securely to the machining table and attaching the graphite to it using corner brackets and woodscrews on opposite corners of the slab. This method is shown in Figure 29.

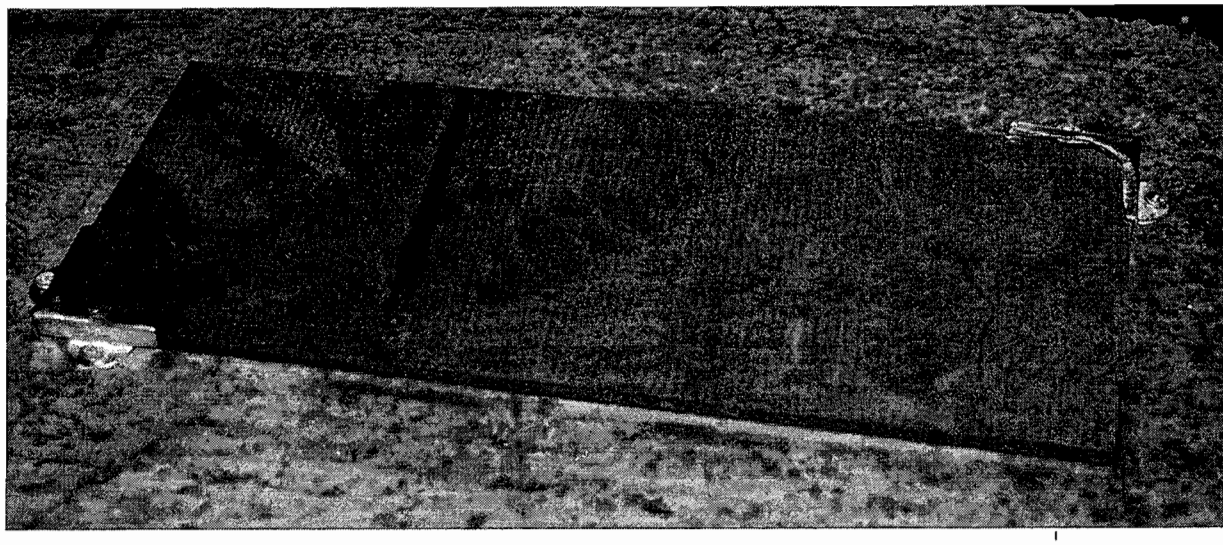

Figure 29: Fixing the graphite to the milling machine using the corner clamp method

The corner clamp method proved very efficient for this application because of its simplicity and because of the low volume of plates that were machined. However, if this method is used in high volume manufacturing, the holes into which the screws fit may start to wear out, leading to inaccurate machining. Thus, for high volume manufacturing, this method might prove unsuccessful.

3.3.3.3 Milling of the heat exchanger flow channels

The milling machine used to machine the heat exchanger plates was a HAAS TM2 Tool Room Mill, shown in Figure 30. It had a maximum spindle rotational speed of 6000rpm. As discussed in section 2.4, the speed that is recommended for graphite milling is much faster than that available with this machine (when using a 1.5mm diameter cutting tool). Thus, even though the milling machine ran at its maximum speed, the feed rate had to be kept relatively low, resulting in the time of machining being rather long. The milling of the channels of a single plate took about one and a half hour and the time necessary to machine all twelve plates was about thirty hours, including machine setups. Due to the large amount of detail incorporated into the HX plate design, the machining program was too large to fit into the internal memory of the milling machine. This problem was solved by coupling a desktop computer to the milling machine and using a trickle feeding system to supply the program to the milling machine in small sections.

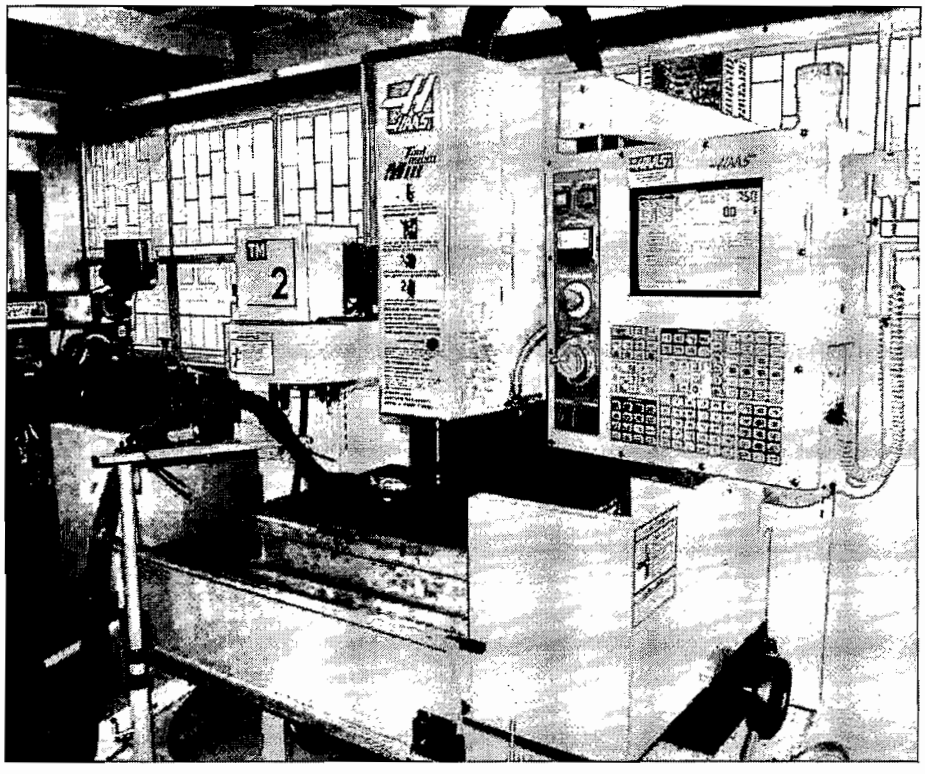

Figure 30: Milling machine used to machine the HX plates

All of the plates were machined using the same cutting tool. Some of the last plates machined showed some breaking of the graphite at some of the very thin sections (less than 1mm thick). An example of this is shown in Figure 31. The reason for this may be that the tool was starting to blunt, causing the cutting pressures on the graphite to become larger. These larger pressures may have caused the breaking seen at the very thin sections.

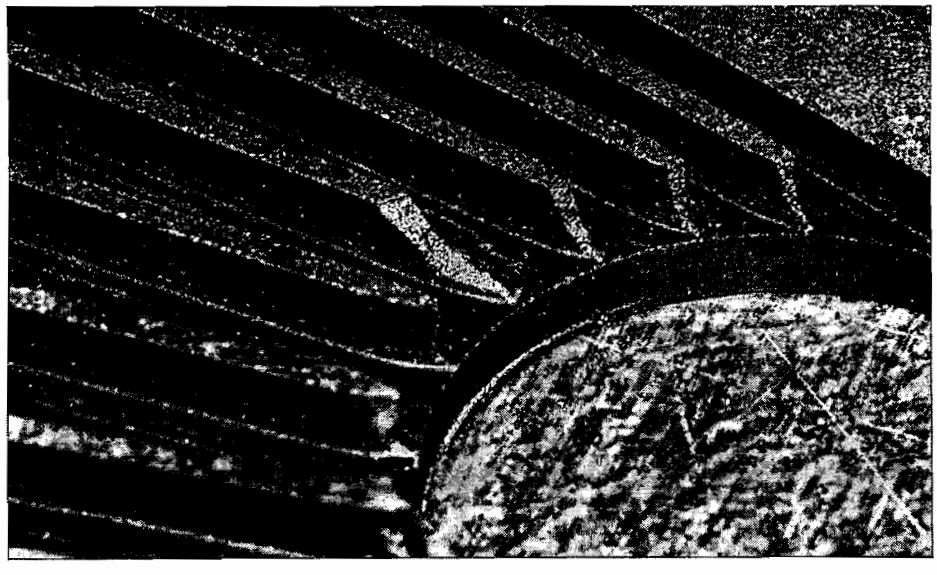

Figure 31: Breaking of the graphite at thin sections (< 1mm)

Figure 32 shows the start of the milling of one of the plates while Figure 33 shows the end. The white object in the left of these figures is the nozzle of a vacuum cleaner used to suck up the graphite dust as it was removed from the slab.

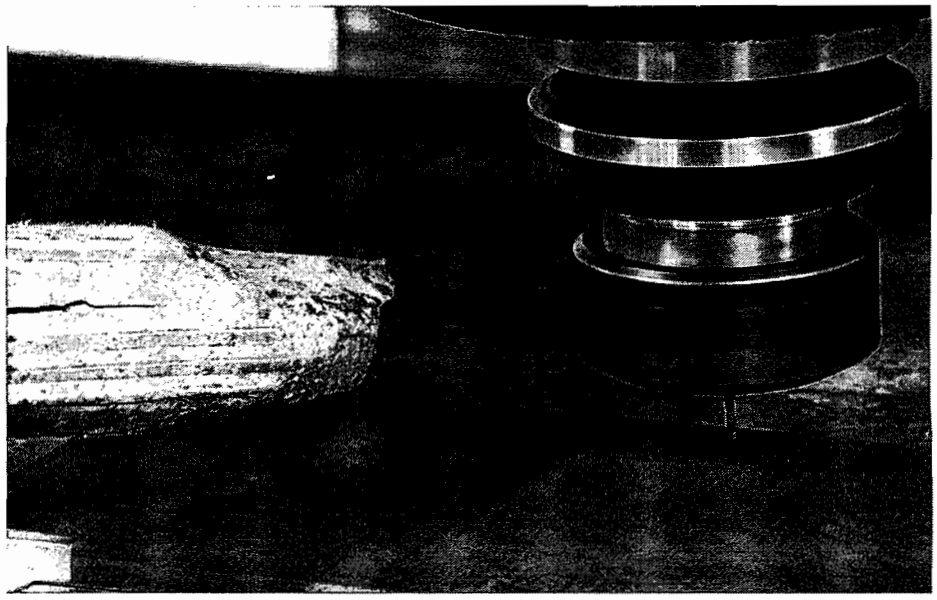

Figure 32: Start of a HX plate milling operation

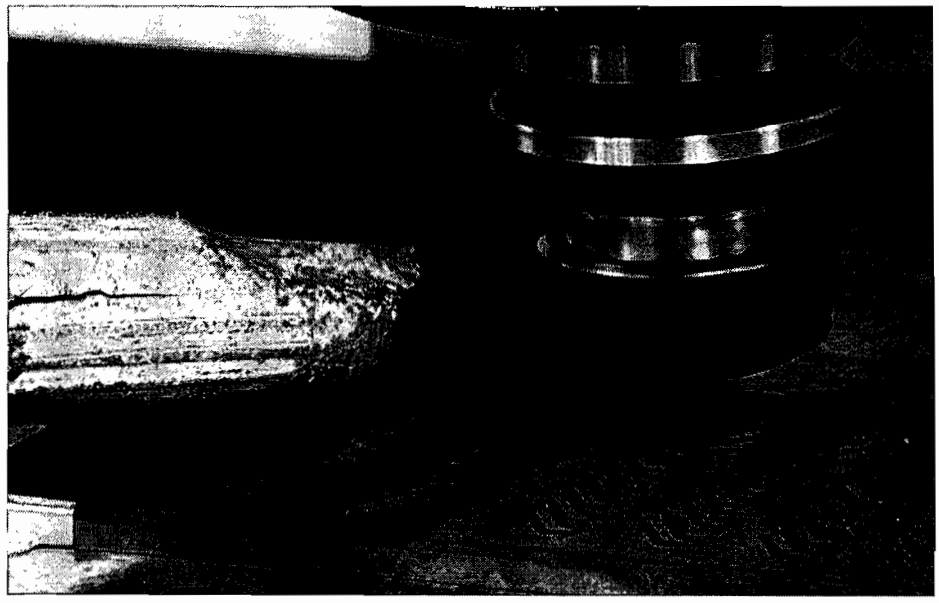

Figure 33: End of a HX plate milling operation

3.3.4 Heat exchanger assembly

The last step in the manufacturing of the graphite PCHE was the assembly of the heat exchanger. This is explained with the help of a few figures.

The first image, Figure 34 , shows the assembled heat exchanger core. The three o-ring seals are seen in their positions, one around the perimeter and two at the gas duct holes.

Figure 34: Assembled heat exchanger core showing o-rings

The bottom pressure plate is shown in Figure 35 along with the tensioning rods used to pull the pressure plates towards each other. Figure 36 shows the heat exchanger core placed onto the bottom pressure plate, while Figure 37 shows the completed assembly including the top pressure plate and tensioning nuts. The threaded holes seen on the top and bottom pressure plates were later used to connect the heat exchanger to the gas supply as well as for instrumentation.

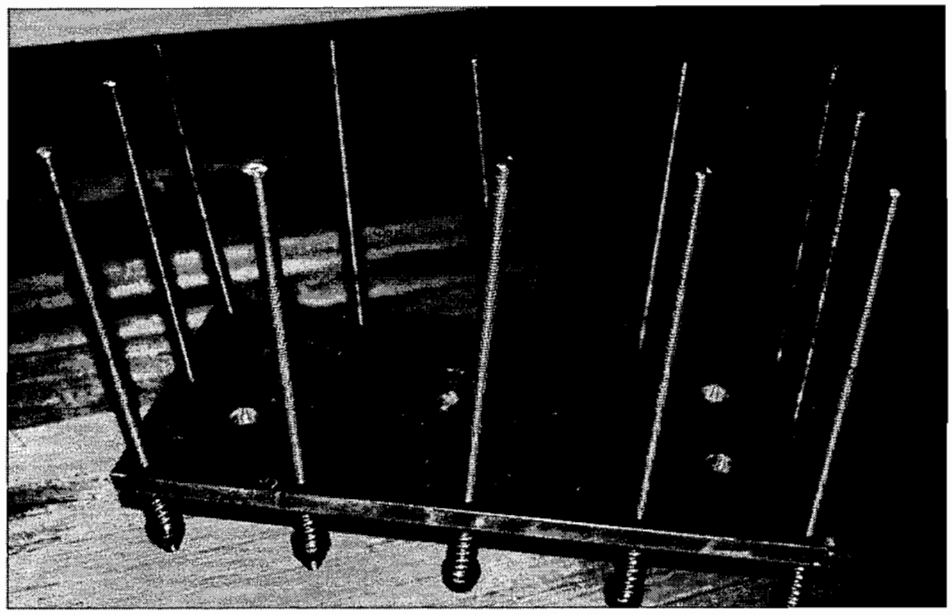

Figure 35: Bottom pressure plate with tensioning rods

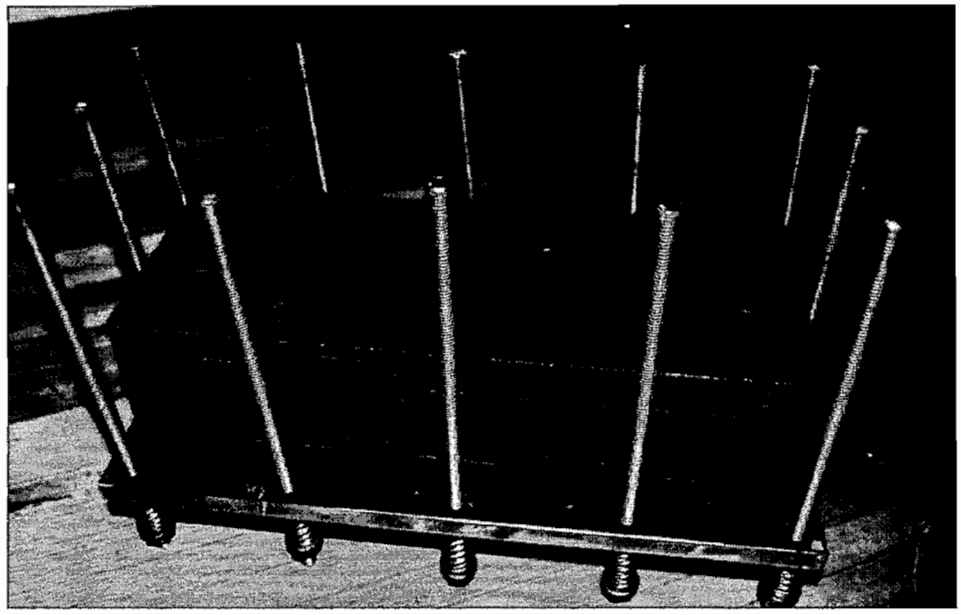

Figure 36: Heat exchanger core on the bottom pressure plate

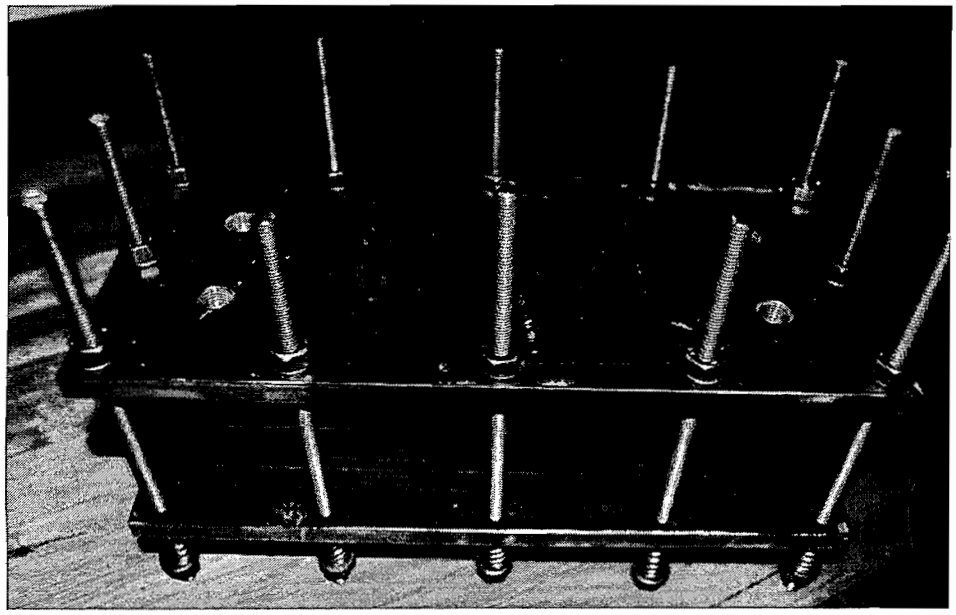

Figure 37: Assembled heat exchanger

The coil springs seen at the bottoms of Figure 35 to Figure 37 were included to provide for the thermal expansion of the graphite and pressure plates in that direction. The bolts on the tensioning rods were tightened until the consecutive graphite plates touched each other. At this point, the o-ring seals had been compressed to a satisfactory degree.

3.4 Heat Exchanger Testing

3.4.1 Test description

Two types of tests were conducted, namely a heat transfer test and a pressure drop test.

3.4.1.1 Heat transfer test requirements

The purpose of the heat transfer test was to gain experience regarding the operation of a graphite PCHE and also to determine the achievable effectiveness of the heat exchanger at a given mass flow rate.

From Incropera & DeWitt (2002:660), the heat exchanger effectiveness can be determined from test data using the following expression:

$$\varepsilon = \frac{Q}{Q_{Max}} \quad [6]$$

where

ε : Heat exchanger effectiveness,

$\dot{Q}_{Max}$: Maximum possible heat transferable from the hot to the cold stream (W),

$\dot{Q}$: Actual heat transferred from the hot to the cold stream (W).

To determine the effectiveness of the heat exchanger at heating the cold stream, Equation [6] can be written as:

$$\varepsilon = \frac{(\dot{m}c_p)_{cold}\Delta T_{cold}}{(\dot{m}c_p)_{\min}\Delta T_{Max}} \quad [7]$$

where

$\dot{m}$: Mass flow of the fluid stream (kg/s),

c_p : Specific heat capacity of the fluid (J/kg.K),

ΔT : Temperature difference (K)

which, if the same fluid is used on both sides and the mass flows are equal, reduces to

$$\varepsilon = \frac{\Delta T_{cold}}{\Delta T_{Max}} \quad [8]$$

The effectiveness of the heat exchanger at cooling the hot stream can also be calculated from Equation [8] by substituting ΔT_{cold} with ΔT_{hot}.

Equation [8], written in terms of in and outlet temperatures for the heating of the cold stream is:

$$\varepsilon = \frac{T_{cold,out} - T_{cold,in}}{T_{hot,in} - T_{cold,in}} \quad [9]$$

From the arguments above, it was found that to determine the effectiveness of a heat exchanger from test data the temperature values at the inlets and outlets to the heat exchanger, as well as mass flow measurements of the hot and the cold streams (to verify that they are equal) are needed. From this, it was decided to use the fixed parameters presented in Table 4 in conducting the tests.

Table 4: Heat transfer test fixed parameters

Test Parameter	Value
Hot side inlet temperature	200°C
Cold side inlet temperature	25°C
Hot side mass flow	2.6×10^{-4} kg/s
Cold side mass flow	2.6×10^{-4} kg/s
Outlet pressures	Atmospheric (87 kPa abs.)

As seen in Table 4, the temperature difference between the hot and cold inlets was chosen at a rather large value. This was done in an effort to make the possible heat exchange through the heat exchanger as large as possible so that the changes in outlet temperatures could be seen and measured more easily.

As can be seen from Table 4, the mass flow rates were kept relatively low. The reason for this is three fold. Firstly, as will be explained further on in this chapter, the gas for the tests was supplied from a gas cylinder. Thus, the gas supply was limited and the mass flow had to be kept low so as to have sufficient testing time before the gas ran out. Secondly, as explained in Section 2.5.2, PCHEs usually operate in the laminar region. Thus, to keep this true, the mass flow rate had to be kept low. Thirdly, the heat exchanger effectiveness is a function of the mass flow. Thus, to deliver an acceptable effectiveness, the mass flow was restricted to a relatively low value.

3.4.1.2 Pressure drop test requirements

The second test performed was the pressure drop test. The pressure drop over a heat exchanger is a very important parameter, since it directly influences the heat exchanger's overall effectiveness. The purpose of this test was to determine the pressure drop generated across the heat exchanger.

The pressure drop over the heat exchanger was calculated by using the following expression:

$$\Delta p = p_{in} - p_{out} \quad [10]$$

where:

p_{in} : Inlet pressure (Pa),

p_{out} : Outlet pressure (Pa),

Δp : Pressure difference (Pa).

Since the heat exchanger outlets were at atmospheric pressure, the value of p_{out} was already known. Thus, the only unknown parameter was the inlet pressure. This pressure was measured by placing a water manometer at the inlet to the heat exchanger. A schematic representation of such a manometer is shown in Figure 38. To find the pressure with the help of a manometer, the following expression was used:

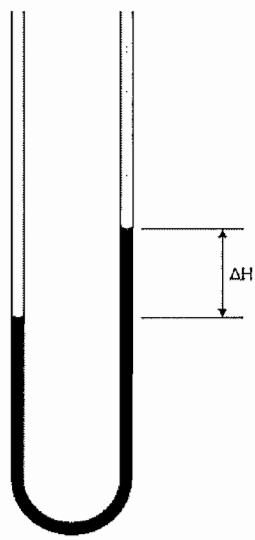

Figure 38: Schematic representation of a manometer

$$p = \rho g \Delta H \quad [11]$$

where:

ρ : Fluid density (kg/m^3),

g : Gravitational acceleration (m/s^2),

ΔH : Height difference between the two columns (m).

Thus, to determine the pressure drop across the heat exchanger using a manometer the atmospheric pressure, the height difference between the two columns of the manometer and the density of the fluid in the manometer are needed.

3.4.2 Test setup

3.4.2.1 Heat transfer test setup

For the heat transfer tests, an open loop test setup was utilized. This setup is shown schematically in Figure 39:

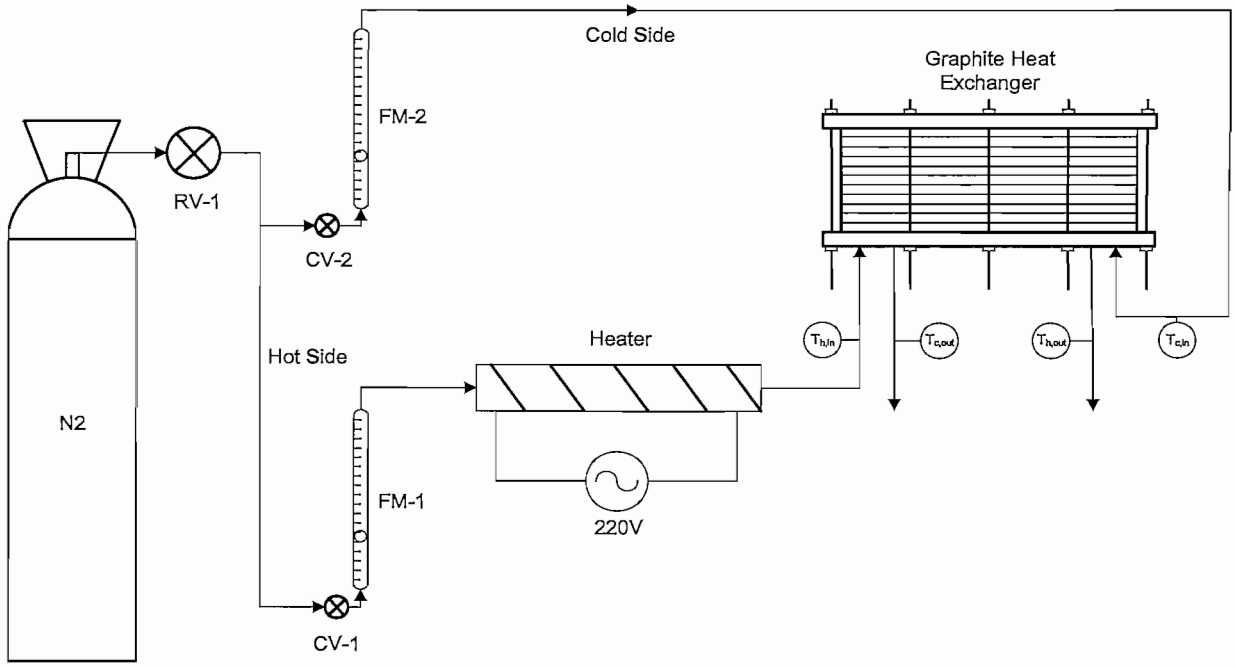

Figure 39: Schematic representation of the test setup used for the heat transfer tests

A gas cylinder was used to provide the fluid and the flow through the test setup. The gas line was split into two separate lines just after the reducing valve (RV-1). These two lines were the hot and cold gas lines respectively, with the cold line going directly to the heat exchanger, while the hot side only arrives at the heat exchanger after passing through an electrical heater. Figure 40 shows a photo of the test setup. In the following paragraphs, each of the components in Figure 39 is discussed.

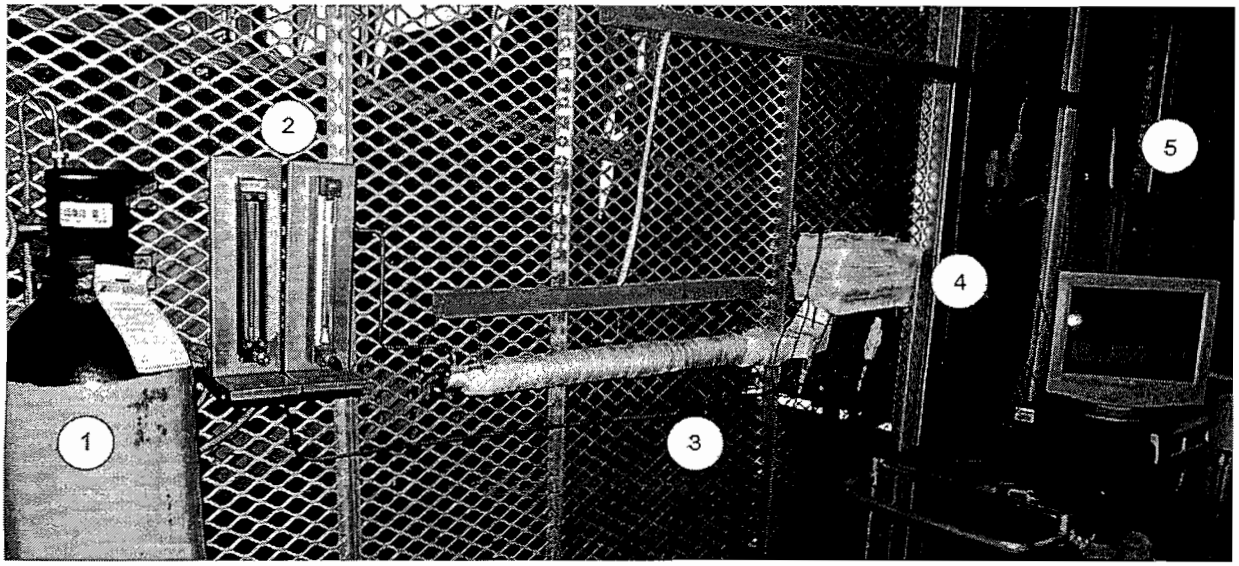

Figure 40: Heat transfer test setup. 1: Gas cylinder with reducing valve; 2: Flow meters; 3: Heater; 4: Insulated heat exchanger; 5: Data acquisition system and heater controller

The information on some of the general components in the setup is given in the following tables.

Table 5: Testing fluid data

Fluid	Nitrogen
Purity	99.998%
Max O_2	10ppm
Max Moisture	10ppm
Max CO	1ppm
Max Hydrocarbons	0.5ppm

Nitrogen was chosen as the heat conductive fluid because it is an inert gas which would inhibit the oxidation of graphite at elevated temperatures. It is also an inexpensive gas which is readily available.

Table 6: Reducing valve data

Make	Saffire
Model	NGM-10
Fluid	Nitrogen
High pressure range	0 – 28 000 kPa
Low pressure range	0 – 400 kPa

Table 7: Flow meter data (calibration curve presented in Appendix D)

Make	Fischer & Porter
Model	10A6132A/B10
Calibrated with:	Nitrogen (see Appendix D)
Tube designation	FP-1/4-25-G-5/81
Float	Stainless Steel
Maximum flow rate	22 l/min
Flow reference	1.013 bar (abs) and 0°C

To heat up the hot side fluid, an electrical pipe heater was used. This heater consists of a heating element coiled around a ceramic pipe. The hot gas line was passed through this ceramic pipe and in this manner the fluid was heated continuously as it flowed through the heater. The length of the heater is 0.7m and it has a power rating of 2500W. Figure 41 shows a photo of the heater:

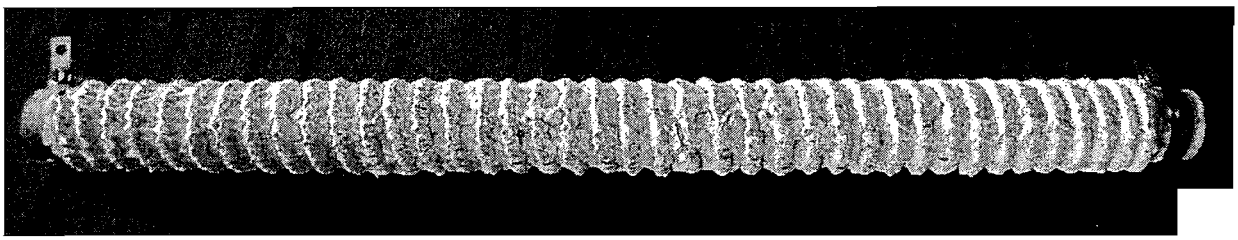

Figure 41: Heater element

To minimize the heat loss from the heater to the environment, the heater was insulated as shown in Figure 42:

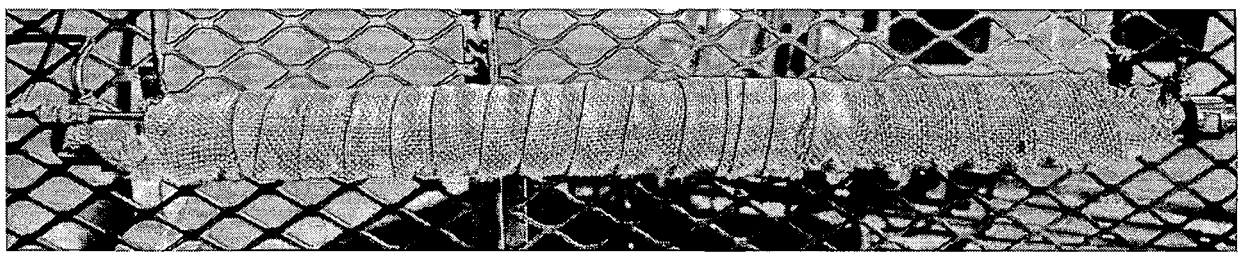

Figure 42: Installed heater with insulation

To control the heater temperature, a CN40 temperature controller was used. This controller uses a temperature input to measure the heater temperature against a given set point. It then uses a relay to switch the heater on and off as needed to maintain the temperature at the set point.

During the construction of the test setup, it was noticed that much of the heat transferred to the fluid by the heater was lost to the environment along the small pipe section between the heater

and the heat exchanger. It was then decided to insulate this pipe section using a high temperature alumina insulation. The thickness of the insulation was calculated by using a radial heat transfer model shown in Figure 43:

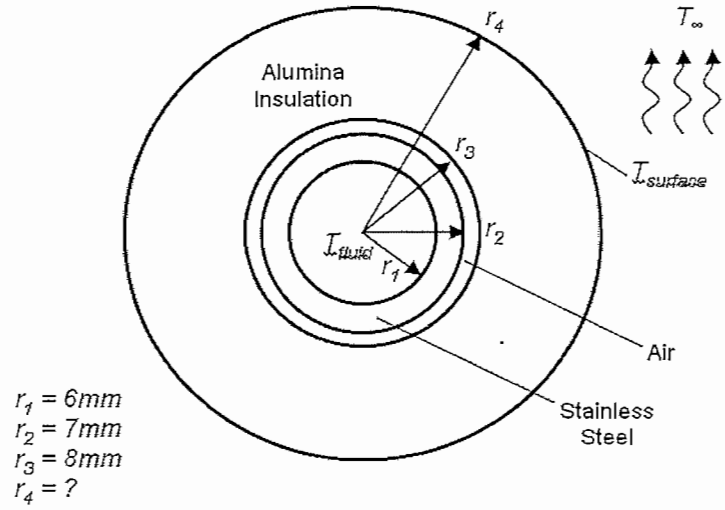

Figure 43: Schematic representation of the hot gas duct insulation

The stainless steel pipe is shown in the centre of the drawing. A layer of alumina insulation (Zircar Al30) covers the entire surface of the stainless steal pipe. Between the pipe and the insulation is a 1mm thick open space filled with air. Since the thickness of the air layer is small and the air is stagnant and inside a closed space, heat transfer through it was assumed as conduction only. The gas temperature needed inside the pipe is T_{fluid} = 200˚C while an outer insulation surface temperature, $T_{surface}$, of 45˚C would be acceptable. The temperature of the environment T_∞ = 25˚C. The equivalent thermal circuit of this system is shown in Figure 44:

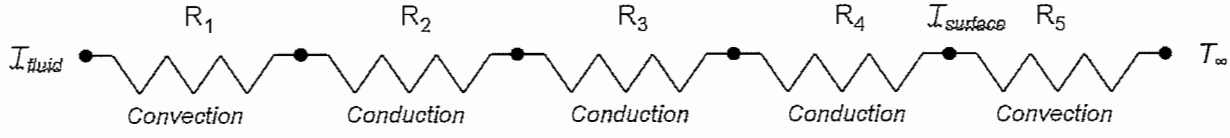

Figure 44: Equivalent thermal circuit of heat loss through hot gas duct

In order to determine the thickness of the insulation layer needed to provide the prescribed surface temperature $T_{surface}$, a heat balance was applied at this outer surface:

$$Q_{in} = Q_{out} \qquad [12]$$

where:

Q_{in} : Heat entering the surface from inside,

Q_{out} : Heat exiting the surface outwards.

Each of these was calculated by using the expression

$$Q = \frac{\Delta T}{R} \quad [13]$$

where:

ΔT : Change in temperature across the region (K)

R : Thermal resistance of the region (K/W)

Thus

$$Q_{in} = \frac{T_{fluid} - T_{surface}}{R_{in}} \quad [14]$$

where:

R_{in} : Thermal resistance between T_{fluid} and $T_{surface.}$ (K/W).

R_{in}, in turn, was calculated as

$$R_{in} = R_1 + R_2 + R_3 + R_4 \quad [15]$$

with

$$R_1 = \frac{1}{h_1 2\pi r_1 L} \quad [16]$$

where:

h_1 : Convection heat transfer coefficient at the internal wall. (W/m^2K),

L : Length of the pipe (m).

and

$$R_2 = \frac{\ln\left(\frac{r_2}{r_1}\right)}{2\pi k_1 L} \quad [17]$$

where:

k_1 : Conduction heat transfer coefficient of the stainless steel. (W/mK).

and

$$R_3 = \frac{\ln\left(\frac{r_3}{r_2}\right)}{2\pi k_2 L} \quad [18]$$

where:

k_2 : Conduction heat transfer coefficient of air. (W/mK).

and

$$R_4 = \frac{\ln\left(\frac{r_4}{r_3}\right)}{2\pi k_3 L} \quad [19]$$

where:

k_3 : Conduction heat transfer coefficient of the insulation. (W/mK).

Thus, R_{in} is given by

$$R_{in} = \frac{1}{2\pi L}\left(\frac{1}{h_1 r_1} + \frac{\ln\left(\frac{r_2}{r_1}\right)}{k_1} + \frac{\ln\left(\frac{r_3}{r_2}\right)}{k_2} + \frac{\ln\left(\frac{r_4}{r_3}\right)}{k_3}\right) \quad [20]$$

On the other side of the heat balance, the heat exiting the surface is given by

$$Q_{out} = h_2 2\pi r_3 L\left(T_{surface} - T_\infty\right) \quad [21]$$

where:

h_2 : Convection heat transfer coefficient at the outer wall. (W/m^{2}K).

Thus, by substituting Equations [14] and [21] into Equation [12], the heat balance is given by

$$\frac{T_{fluid} - T_{surface}}{\frac{1}{h_1 r_1} + \frac{\ln\left(\frac{r_2}{r_1}\right)}{k_1} + \frac{\ln\left(\frac{r_3}{r_2}\right)}{k_2} + \frac{\ln\left(\frac{r_4}{r_3}\right)}{k_3}} = h_2 r_4 \left(T_{surface} - T_{\infty}\right) \quad [22]$$

To solve this equation, the different heat transfer coefficients are needed. The convection heat transfer coefficient for the internal flow (h_1) is given by

$$h_1 = \frac{Nu.k_{N_2}}{D} \quad [23]$$

where:

Nu : Nusselt number,

k_{N_2} : Conductivity of the fluid (W/mK).

To determine the Nusselt number, it is necessary to firstly know if the flow inside the pipe is laminar or turbulent. This can be determined by calculating the Reynolds number, which is given by:

$$\mathrm{Re} = \frac{\rho V D}{\mu} \quad [24]$$

where:

ρ : Fluid density (kg/m^3),

V : Fluid Velocity (m/s),

D : Pipe Diameter (m),

μ : Fluid viscosity (kg/ms).

The density and viscosity of nitrogen at 200°C are 0.6053 kg/m^3 and 24.94x10^{-6} kg/ms (Incropera & DeWitt, 2002:920) respectively. The velocity through the pipe can be calculated using

$$V = \frac{\dot{m}}{\rho A} \quad [25]$$

where:

$\dot{m}$: Mass flow through the pipe (kg/s),

A : Pipe internal area (m^2).

With a diameter of 0.012 m and a mass flow of 2.6×10^{-4} kg/s (Table 4) the velocity in the pipe was calculated as 3.8 m/s, which gives a Reynolds number of 1106.7 from Equation [24]. Thus, the flow is well within the laminar region, since the transition to turbulent flow in pipes starts to happen only from $Re \approx 2300$ upwards (Incropera & DeWitt, 2002:467).

Since the flow inside the pipe is laminar, the Nusselt number is a constant that, for a constant surface temperature is equal to 3.66 (Incropera & DeWitt, 2002:487). Thus, using this value along with the conductivity of nitrogen at 200°C (0.0259 W/mK, Incropera & DeWitt, 2002:920), the convection heat transfer coefficient at the inner wall is:

$$h_1 = 7.9 \frac{W}{m^2 K} \quad [26]$$

According to Incropera & DeWitt (2002:545), the natural convection heat transfer coefficient at the outer surface of the insulation (h_2) can be calculated with:

$$\frac{h_2 D}{k_{air}} = C.Ra^n \quad [27]$$

where:

D : Diameter of the outer wall (m),

k_{air} : Conductivity of air (W/mK),

Ra : Rayleigh number,

C,n : Constants dependent on the Rayleigh number.

The Rayleigh number was found from the equation:

$$Ra = \frac{g\beta(T_s - T_\infty)D^3}{\nu\alpha} \quad [28]$$

where:

g : Gravitational acceleration (m/s^2),

β : Volumetric thermal expansion coefficient (K^{-1}),

ν : Kinematic viscosity (m^2/s),

α : Thermal diffusivity (m^2/s).

The values of the above mentioned parameters are given in Table 8:

Table 8: Parameters for the calculation of *Ra*

Parameter	Description	Value
α	Thermal diffusivity of air at 25°C	22.5×10^{-6} m^2/s
β	Volumetric thermal expansion coefficient. (β =1/T for ideal gasses)	0.0034 K^{-1}
g	Gravitational Acceleration	2.98 m/s^2
ν	Kinematic viscosity of air at 25°C	15.89×10^{-6} m^2/s
All parameters found from Incropera & DeWitt (2002:917)		

Using the parameters in Table 8 and Equation [28] the Rayleigh number was show to be given by

$$Ra = 566.7 \times 10^6 . D^3 \qquad [29]$$

From experience and due to space constraints, it was known that the insulation thickness ($r_4 - r_3$) would be somewhere between 3cm and 6cm thick. Thus, with D in the range of 0.008m – 0.014m, the range of the Rayleigh number was calculated as 290 – 1555. For this Reyleigh number range, the empirical constants C and n is 0.85 and 0.188 respectively (Incropera &DeWitt, 2002:554). Substituting these parameters into Equation [27] the convection coefficient on the outside of the insulation as a function of the diameter was found to be given by:

$$h_2 = \frac{k_{air}}{D} \times 0.85\left(566.7 \times 10^6 . D^3\right)^{0.188} \qquad [30]$$

The conductive heat transfer coefficients of the solid materials are given in Table 9.

Table 9: Heat transfer coefficients for pipe insulation calculation

Parameter	Description	Value
k_1	Conductive heat transfer coefficient for stainless steel	15 W/mK
k_2	Conductive heat transfer coefficient for air at 200°C	0.038 W/mK
k_3	Conductive heat transfer coefficient for alumina (Al30) insulation	0.09 W/mK
k_1 and k_2 found from Incropera & DeWitt (2002).		
k_3 for Al30 was found from the website of ZIRCAR Ceramics (www.zircarceramics.com)		

Solving Equation [22] and Equation [30] simultaneously for D, the insulation thickness ($r_4 - r_3$) required to maintain a 45°C surface temperature was calculated to be 0.035m. This insulation is shown in Figure 45 to Figure 47:

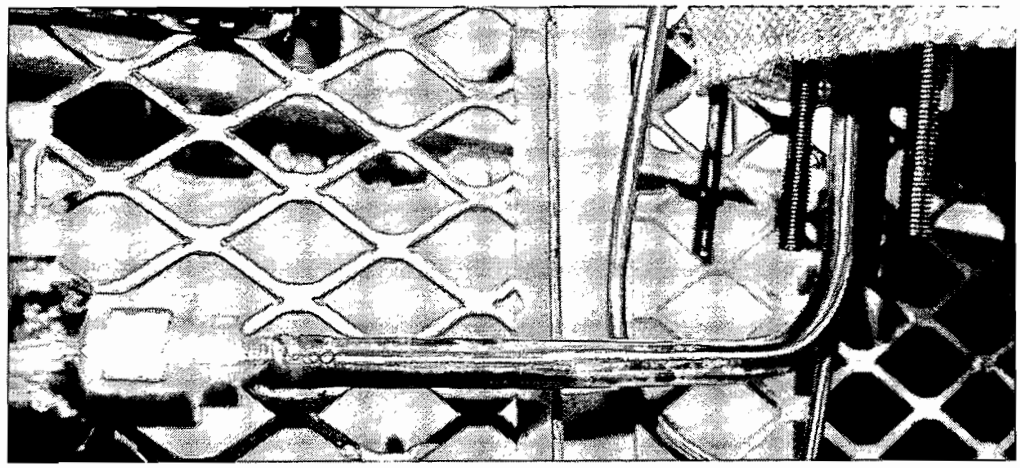

Figure 45: Uninsulated hot gas pipe

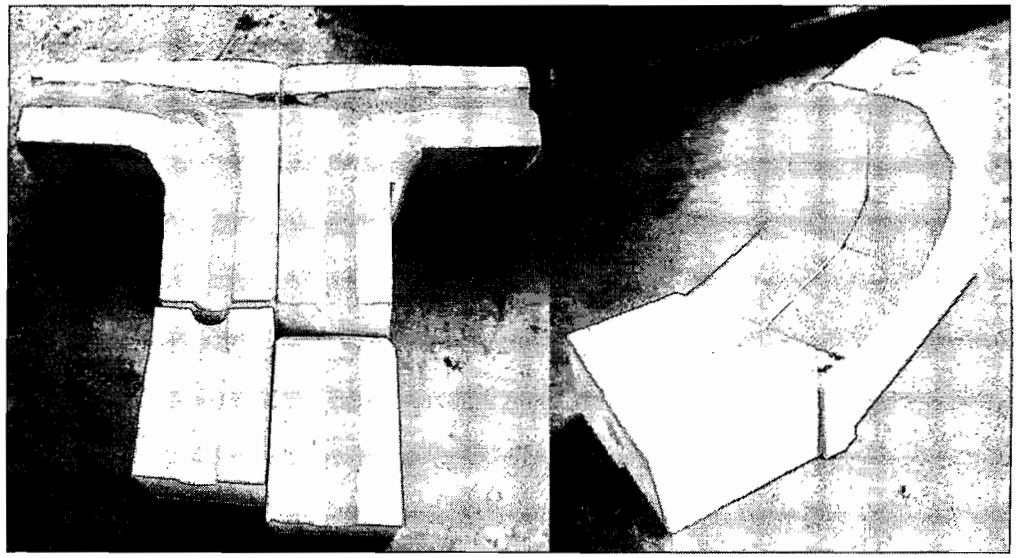

Figure 46: Hot gas pipe insulation

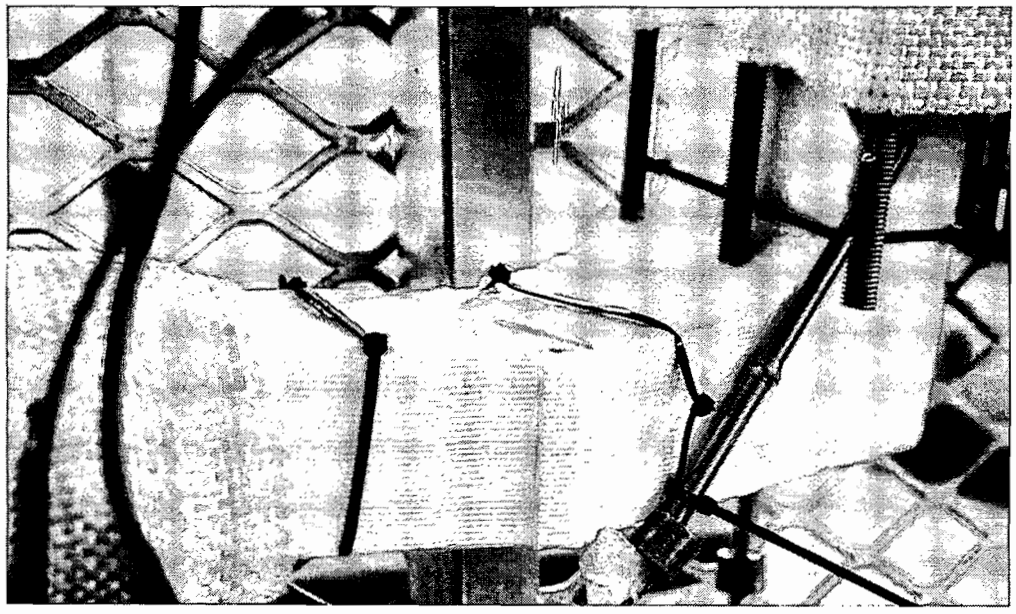

Figure 47: Insulated hot gas pipe

To gather the data generated during the tests, four thermocouples located at the heat exchanger inlets and outlets was used.

The signals from the thermocouples was passed through a 4017 ADAM™ module to a 4520 ADAM™ module which converted it to a digital serial signal. This signal was then transmitted to a desktop computer using a RS232 cable. A software package called Advantech ADAMview™ was used to capture the data, create visual outputs and log the data to a text file.

3.4.2.2 *Pressure drop test setup*

For the pressure drop test, a different test setup was used than with the heat transfer tests. This setup is shown in Figure 48:

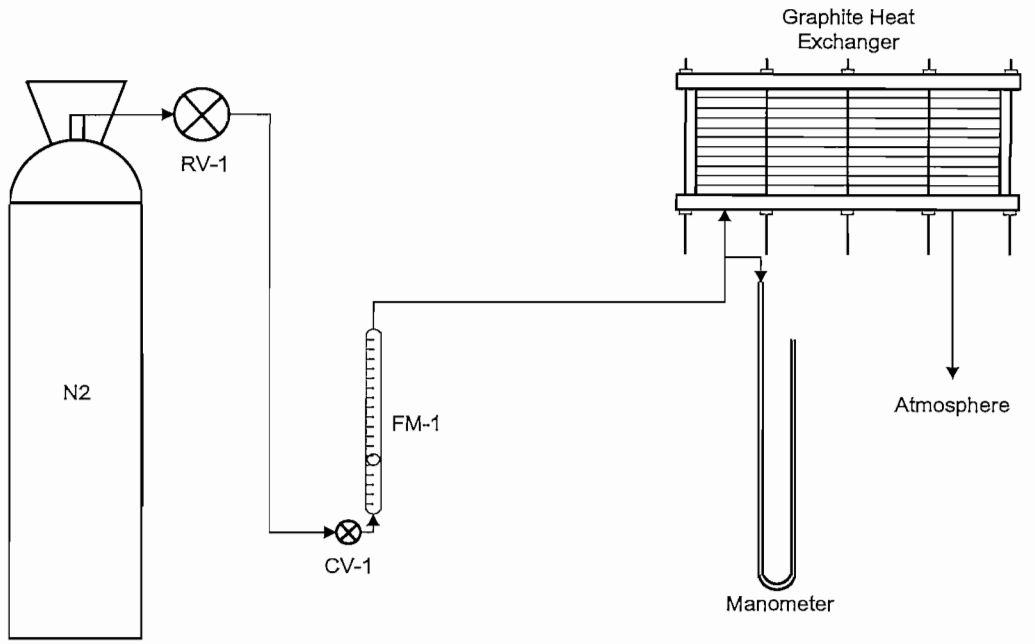

Figure 48: Pressure drop test setup

Only one gas line, and thus, only one side of the heat exchanger was used to find the pressure drop. The same flow meter was used as in the heat transfer tests. Also the reducing valve and testing fluid was the same as those used in the heat transfer tests. These components were already discussed in Section 3.4.2. A water manometer was directly connected to the setup before the heat exchanger inlet to determine the pressure at this position.

3.4.3 Testing procedures

The heat transfer test was conducted by first starting and adjusting the gas flow through the heat exchanger. The heater was started and its temperature controlled so as to achieve the desired hot inlet temperature. From this point on, the system was left unadjusted until steady state temperatures were reached. Temperature measurements were taken at appropriate intervals so as to be able to identify when the system had reached steady state. When steady state was reached, the last inlet and outlet temperature measurements were used to calculate the heat exchanger effectiveness.

The pressure drop test was conducted only through one side of the heat exchanger since the hot and cold sides of the heat exchanger are geometrically identical and no heat was added during

these tests that could influence the fluid properties. The test was conducted by increasing the mass flow through the cold side of the heat exchanger in increments of ± $6x10^{-6}$kg/s. At each increment, the height difference on the manometer was measured. This height was then converted to a pressure reading which gave the pressure drop between the heat exchanger inlet and outlet.

3.4.4 Test Results

The data gathered from the heat transfer tests, conducted at a mass flow of $2.6x10^{-4}$ kg/s, is presented in Table 10. A graphical representation of the data is presented in Figure 49.

Table 10: Temperature test data for a mass flow of $2.6x10^{-4}$ kg/s

Time (min)	Hot in	Hot out	Cold in	Cold out
0	20.2	20.2	19.5	19.5
6	84	21	19.8	20.5
10	126	21.5	20	22.8
15	147	22.8	20	25
20	162	24.8	20.1	27
25	172	26	20.2	29.2
30	179	28	20.2	31.5
35	184.5	30	20.5	34
40	188	32	20.6	35.5
45	192	33.5	20.8	37.5
50	194.5	35	21	39
55	197	37	21	40.7
60	197.5	38.8	21	42.5
65	199	40.5	21.2	44.8
70	199.8	42	21.2	45.9
75	200.8	43.5	21.4	47.5
80	202	45	21.5	49
85	202	46.3	21.5	50
90	202.5	47.5	21.5	51.5
95	202.5	49	21.7	52.5
105	203	51	21.8	55
115	203.5	53	22	56.5
125	202.8	55	22	58.5

Time (min)	Hot in	Hot out	Cold in	Cold out
135	202.5	56.5	22	60
145	202	58	22.2	61.5
155	202.2	59.5	22.5	62.7
165	202	60.5	22.5	64
165	202.2	61.8	22.8	65
185	202	62.5	23	66
195	202	64	23	66.8
205	202	64.8	23.3	67.5
215	202.5	65	23.8	68.8
235	202.2	65.5	23.8	69
250	202	66	23.8	69.8
265	201.8	67	24	70.5
280	202	67.7	24	71.2
300	202	68.5	24	72
317	202	69	24	72.8
328	202.2	69.5	24	73
342	202	70	24	73.5
362	202	70.1	24	74
385	202.5	70	24	74
395	202	70.5	24	74.2
420	201.8	71	24	74.8
450	202	71	24	74.8

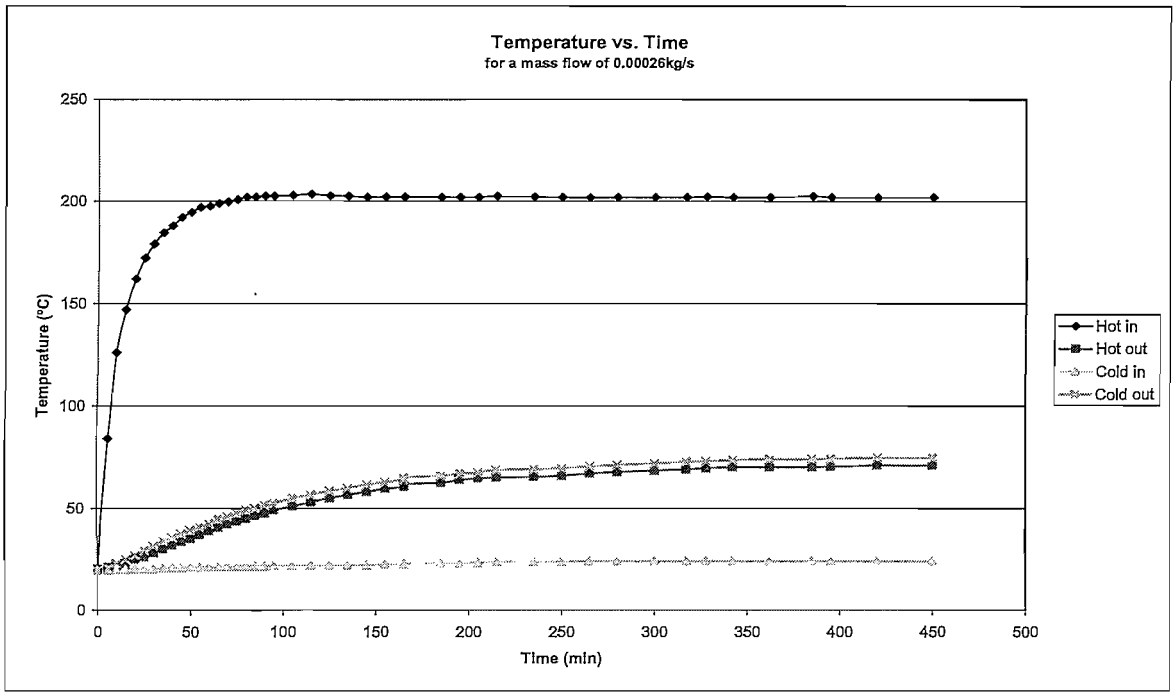

Figure 49: Graphical representation of the heat exchanger inlets and outlets at a mass flow of 2.6×10^{-4} kg/s

The data obtained from the pressure drop tests, is shown in Table 11. A graphical representation of the data is shown in Figure 50.

Table 11: Pressure drop test data

Mass Flow x 10^{-5} (kg/s)	Pressure Drop (Pa)
0	0.0
1.85	0.6
5.15	7.3
8.68	13.2
12.81	26.5
16.75	56.8
21.09	111.1
25.39	173.5
30.13	238.0
34.54	311.1
39.66	411.9

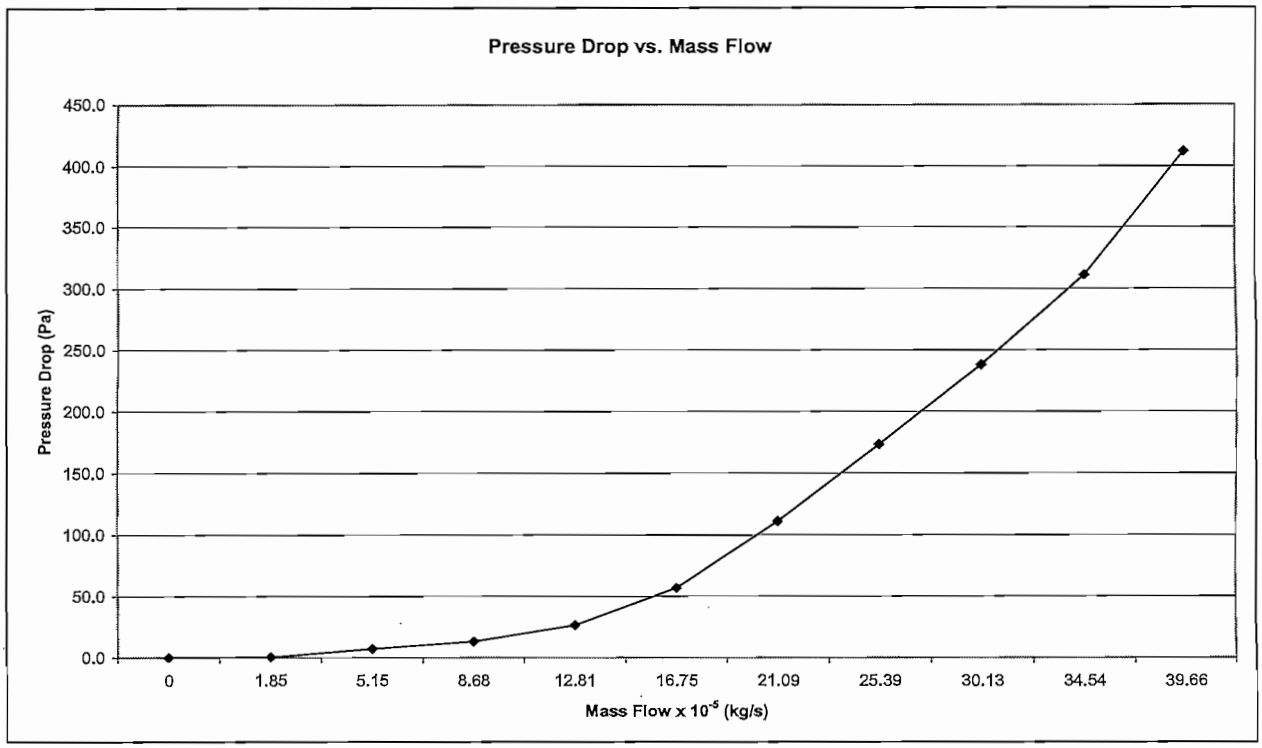

Figure 50: Pressure drop test data

3.4.5 Discussion of results

Figure 49 shows that the steady state temperature difference between the inlet and outlet is much larger for the hot stream (131°C) than the cold stream (50.8°C). The heat exchanger effectiveness calculated for the cooling of the hot stream using Equation [8] is 73.6%, while the effectiveness calculated for the heating of the cold stream is only 28.5%. It is evident from this that not all of the heat entering the heat exchanger through the hot stream is exiting it through the cold stream. Some of the heat exits the heat exchanger through other means, which might include the following:

- Small leak flows to the environment was observed during the heat exchanger tests. These flows were made visible through bubbles formed when the outside of the heat exchanger was lightly sprayed with a soap solution. Most of the bubbles originated from between adjacent plates, but some originated from the surfaces of individual graphite plates, proving the fact that the fluid travels through the porous material. The leaking from between the plates may be attributed to the o-ring seals not sealing properly on the porous graphite surface or may be due to the plates not being completely flat. Even though the manufacturer of the graphite plates was supplied with flatness tolerances, it is possible that some of the plates did not meet these tolerances since no post-

manufacturing checks was performed on the plates due to inexperience. These leak flows (to the environment as well as between the hot and the cold streams) could have influenced the heat transfer negatively and could have caused the effectiveness of heating the cold stream to drop.

- Heat losses to the environment from the surface of the heat exchanger might have reduced the amount of heat that could be transferred from the hot to the cold stream. Even though the heat exchanger was insulated, an average outer surface temperature of 40°C was measured at the time of steady state. A rough estimate of the surface heat loss was calculated using the following equation:

$$Q_{loss} = hA(T_s - T_\infty) \quad [31]$$

where:

Q_{loss}	:	Heat lost to the environment (W),
h	:	Convection heat transfer coefficient (W/m^2),
A	:	Heat exchanger surface area (m^2),
T_s	:	Surface temperature (°C),
T_∞	:	Temperature of the environment (°C).

Assuming an average convection heat transfer coefficient of 3.5W/m^2 over the whole heat exchanger surface (which is a representative value for natural convection) and an environmental temperature of 25°C, the heat loss is calculated at about 8.4W for a surface area of 0.16m^2. The heat transferred to and from the fluid streams was calculated using the standard expression

$$Q = \dot{m}.c_p.\Delta T \quad [32]$$

where:

Q	:	Heat transferred to or from the fluid stream (W),
$\dot{m}$	:	Mass flow of the fluid stream (kg/s),
c_p	:	Specific heat capacity of the fluid (J/kg.K),
ΔT	:	Temperature difference between the inlet and outlet (K)

and thus, the heat exiting through the cold stream was found to be about 12W. By adding the heat exiting through the surface and the heat exiting by means of the cold stream, the total heat leaving the heat exchanger by these means were found to be about 20.4W. On

the other hand, the heat entering the heat exchanger through the hot stream was calculated at about 31W. Thus it can be seen that the heat loss makes up a substantial amount of the heat exiting the heat exchanger. This highlights the need for very effective surface insulation, especially if the heat exchanger was to be used for heating rather than cooling.

From the results of the pressure drop tests, the pressure drop was found to increase exponentially as a function of the mass flow through the heat exchanger (Figure 50). This result was expected since the higher velocities associated with the higher mass flow will always increase the flow losses through the heat exchanger.

Chapter 4

Heat Exchanger Theoretical Model

4.1 Introduction

In Chapter 3 the testing of the laboratory scale heat exchanger was discussed. This chapter, on the other hand, explains how the theoretical model of the heat exchanger was constructed. To build such a model, it was necessary to identify all the values that are either known or that are constrained for some reason or another. A schematic representation of all the known parameters is given in Figure 51, where

T_{hi}	:	Hot side inlet temperature,
T_{ci}	:	Cold side inlet temperature,
$\dot{m}_{hi}$	:	Hot side mass flow,
$\dot{m}_{ci}$	:	Cold side mass flow,
p_{ho}	:	Hot side outlet pressure,
p_{ho}	:	Cold side outlet pressure,
B	:	Width of the heat exchanger core (Figure 12),
H	:	Height of the heat exchanger core,
L	:	Length of the heat exchanger core (Figure 12).

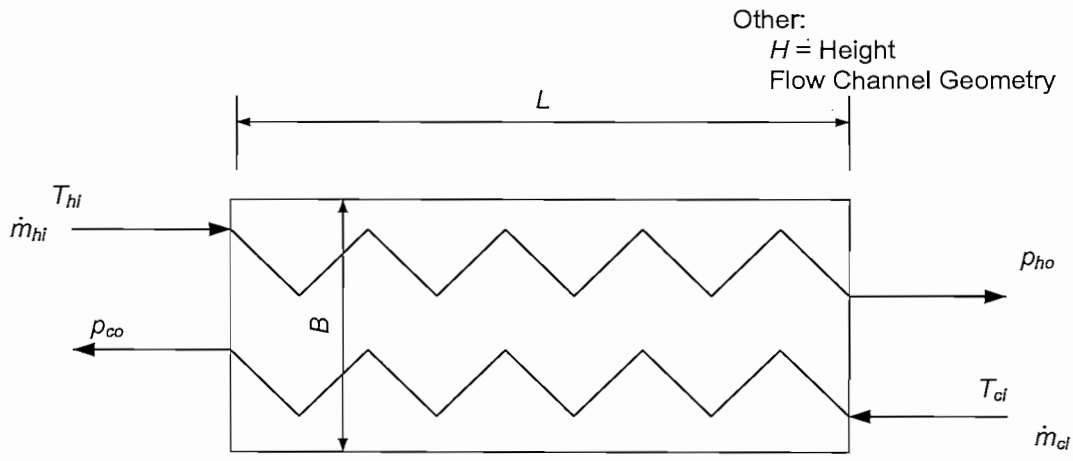

Figure 51: A schematic representation of the heat exchanger, showing the known parameters

4.2 Flow configuration analysis

To construct the model of the heat exchanger, some parameters need to be deduced from the chosen geometry of the heat exchanger and the flow configuration. For the purpose of analysing the flow configuration, it was assumed that the discontinuous sine wave pattern, shown in Figure 11, can be approximated by using continuous flow channels as those shown in dashed lines in Figure 52.

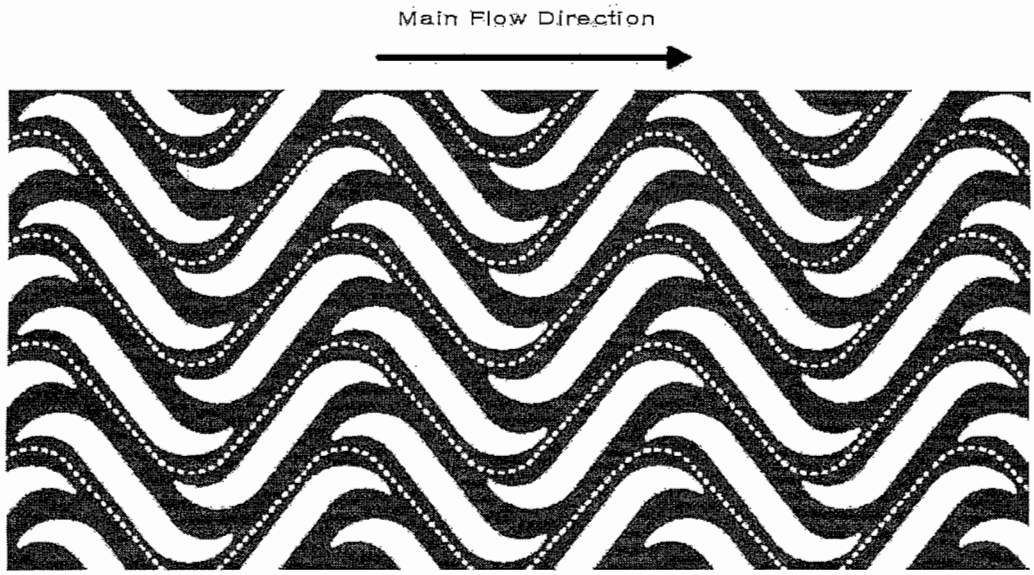

Figure 52: Flow configuration with approximated continuous channels (dashed)

By using this approximation, along with the chosen size of the heat exchanger core (see Figure 12) nine individual channels of equal length were identified on each HX plate. Since the calculation to find the length of these channels is quite cumbersome, the length of the channels was measured with the help of a CAD model by superimposing a sine wave over the channels (much as in Figure 52) and measuring the length of the wave. In this manner, the total length of each channel was found to be $L_{ch} \approx 179$mm.

The value for the channel width is shown in Figure 15 as 2.5mm. Even though there are slight variations of the channel width along its length, a good approximation can be made by taking the width $W_{ch} \approx 2.5$mm, which is the actual width for the largest part of each channel's length.

The fin height is 2mm, as shown in Figure 13. However, the active fin height used in calculations has to be half the height of the actual fin. The reason for this is that when the heat exchanger was assembled, and the seals were compressed, the top of the fins of one plate touched the bottom of the next plate. Thus, (if zero contact resistance is assumed) one half of each fin conducts heat to and from the bottom plate and half of the fin conducts heat to and from the top plate. Each actual fin can thus be seen as two fins, joined at the tips, conducting heat in different directions. For this reason, the active fin length $L_f = 1$mm.

Table 12 shows some other geometrical parameters that were deduced from the geometry:

Table 12: Heat exchanger geometrical parameters

Parameter Description	Symbol	Value	Deduced from:
Channel Length	L_{ch}	179mm	Section 4.2
Wall thickness	L_w	3mm	Figure 13
Channel width	W_{ch}	2.5mm	Figure 15
Active fin length	L_f	1mm	Figure 13
Number of fins/plate	N_f	192	Figure 12, Figure 13
Number of channels/plate	N_{ch}	9	Figure 12
Number of plates	N_{pl}	12	Chosen (Section 3.2.2.2)
Fin Perimeter	P_f	39.85mm	Figure 15, CAD
Fin top area	$A_{f,top}$	31.35mm^2	Figure 15, CAD

In order to verify the effect of the accuracy of the parameters L_w, W_{ch}, L_f, P_f and $A_{f,top}$ on the heat transferred by the heat exchanger, the calculations of this chapter was carried out with each parameter changed by 5% upwards and downwards from the values shown in this table. By doing this, it was determined that the combined effect of such changes causes the heat transferred by the heat exchanger to vary between -0.44% and +0.13% from the heat exchange calculated using the values in this table. Thus, the accuracy of the values in this table does not have a profound effect on the heat exchanging capability of this PCHE.

By using the above parameters the hydraulic diameter, fin side area, free flow area and heat transfer areas were calculated as follows:

– Hydraulic diameter D_H (using Equation [4]):

$$D_H = \frac{4A_c}{P}$$

$$D_H = \frac{4\left(2L_f \times W_{ch}\right)}{2\left(2L_f + W_{ch}\right)}$$

$$D_H = \frac{4\left(0.002 \times 0.00246\right)}{2\left(0.002 + 0.00246\right)}$$

$$D_H = 0.00206\text{m}$$

where:

A_c : Cross Sectional area of a single channel (m^2),

P : Wetted perimeter of a channel (m).

– Single Fin Side area A_f:

$$A_f = P_f \times L_f \quad [33]$$

$$A_f = 0.03985 \times 0.001$$

$$A_f = 3.985 \times 10^{-5} \text{m}^2$$

– Fin side area $A_{f,total}$:

$$A_{f,total} = N_{pl}.N_f\left(P_f \times L_f\right) \quad [34]$$

$$A_{f,total} = 12 \times 192\left(0.03985 \times 0.001\right)$$

$$A_{f,total} = 0.0918 \text{m}^2$$

– Free flow area A_{ff}:

$$A_{ff} = N_{pl}.N_{ch}\left(W_{ch} \times 2L_f\right) \quad [35]$$

$$A_{ff} = 12 \times 9\left(0.00246 \times 0.002\right)$$

$$A_{ff} = 5.3136 \times 10^{-4} \text{m}^2$$

– Heat transfer area A_H:

$$A_H = A_{f,total} + N_{pl}.N_{ch}\left(2\left(L_{ch}W_{ch}\right)\right) \quad [36]$$

$$A_H = 0.0918 + 12 \times 9\left(2\left(0.179 \times 0.00246\right)\right)$$

$$A_H = 0.1789 \text{m}^2$$

4.3 Construction of the heat exchanger model

This section explains how the heat exchanger model was constructed. The purpose of this model was to theoretically find the heat exchanger's heat transfer effectiveness as a function of the mass flowing through it[6] so as to compare this theoretical effectiveness with that of the heat exchanger tests. This was done by using the effectiveness-NTU method for the heat exchanger configuration used in the tests, namely a counter flow configuration[7], the relations of which are given by

[6] The method and equations described here can be found in, among others, Incropera and DeWitt (2002:659).

[7] The best heat transfer effectiveness is achieved with a counter flow configuration. This is because this configuration provides the largest ΔT over the whole of the heat exchanger core.

$$\varepsilon = \frac{1 - e^{(-NTU(1-C_r))}}{1 - C_r e^{(-NTU(1-C_r))}} \quad \text{if } C_r<1; \quad [37]$$

$$\varepsilon = \frac{NTU}{1+NTU} \quad \text{if } C_r=1 \quad [38]$$

where:

ε : effectiveness of the heat exchanger,

NTU : Number of transfer units.

C_r is the ratio between C_{min} and C_{max}, which are the smaller and the larger values respectively of the equation

$$C = \dot{m} \times c_p \quad [39]$$

where:

$\dot{m}$: Mass flow (kg/s),

c_p : Specific heat at constant pressure (J/kg.K).

The maximum heat transferable by the heat exchanger was calculated from

$$Q_{\max} = \dot{m} Cp (T_{hi} - T_{ci}) \quad [40]$$

where:

Q_{max} : Maximum heat transferable (W),

T_{hi} : Inlet temperature of the hot stream (°C),

T_{ci} : Inlet temperature of the cold stream (°C).

By using the heat exchanger effectiveness and the maximum transferable heat, the actual heat transferred by the heat exchanger was calculated using

$$Q = \varepsilon Q_{\max} \quad [41]$$

where:

Q : Actual heat transferred (W).

This value was then used to calculate the temperature difference between the heat exchanger inlets and outlets by using

$$\Delta T = \frac{Q}{\dot{m} Cp} \quad [42]$$

where:

ΔT : Temperature difference between heat exchanger inlet and outlet (°C).

In Equation [37] and [38], the number of transfer units (*NTU*) can be calculated from the equation

$$NTU = \frac{UA}{C_{\min}} \quad [43]$$

where:

UA : overall heat transfer coefficient (W/K).

UA, in turn, is given by the equation

$$\frac{1}{UA} = \frac{1}{(\eta_o hA)_c} + \frac{R''_{f,c}}{(\eta_o A)_c} + R_w + \frac{R''_{f,h}}{(\eta_o A)_h} + \frac{1}{(\eta_o hA)_h} \quad [44]$$

where

η_o : Overall surface efficiency of a finned surface,

h : Convection heat transfer coefficient (W/m^2.K),

A : Heat transfer area (m^2),

R''_f : Fouling factor (m^2.K/W),

R_w : Wall conduction resistance (K/W)

and *h* and *c* refer to the hot and cold streams respectively.

The fouling factor R''_f represents an additional conductive heat resistance that is created by scaling or biological growth on the heat transfer wall. This is, however, more applicable to heat exchangers using a liquid as the heat transfer fluid and that will be operated for extended time periods. Thus, in the case of a gas heat transfer fluid and a short operating time, this fouling of the wall was neglected, resulting in the simplified relation

$$\frac{1}{UA} = \frac{1}{(\eta_o hA)_c} + R_w + \frac{1}{(\eta_o hA)_h} \quad [45]$$

The parameter R_w is termed the wall conduction resistance and, for a plane wall, is given by the standard equation

$$R_w = \frac{L_w}{k.A} \quad [46]$$

where

L_w : Length over which heat has to be transferred through the wall (m),
k : Conduction heat transfer coefficient (W/m.K),
$A_{H,cond}$: Conductive heat transfer area (m^2).

The conductive heat transfer area was assumed to be the total wall area, including the base area of the fins. By measuring this area in a CAD model, $A_{H,cond} = 8.638 \times 10^{-3}$ m^2.

From Incropera and DeWitt (2002:143), the overall fin efficiency η_o was calculated as:

$$\eta_o = 1 - \frac{A_f}{A_H}(1 - \eta_f) \quad [47]$$

where

A_H : Total heat transfer area (m^2)
A_f : Surface area of one fin (m^2),
η_f : Surface efficiency of a single fin (W/m.K)

By assuming a rectangular fin with a uniform cross section from base to the tip, η_f was calculated from the equations

$$\eta_f = \frac{\tanh mL_f}{mL_f} \quad [48]$$

and

$$m = \sqrt{2h/kt} \quad [49]$$

where

L_f	:	Fin length (m),
h	:	Convection heat transfer coefficient for the unfinned base (W/m^2K),
k	:	Conduction heat transfer coefficient of the fin material (W/mK),
t	:	Thickness of the fin (m).

The only unknown parameters remaining in Equation [45] are the convection heat transfer coefficients for the hot and the cold streams. These were calculated from the standard equations

$$h_c = Nu\frac{k_c}{D_H} \quad [50]$$

$$h_h = Nu\frac{k_h}{D_H} \quad [51]$$

where *c* and *h* refer to the cold and hot stream respectively. Since the geometry of the flow configuration was known, the hydraulic diameter was calculated by using Equation [4]. Then, by using the known channel geometry and empirical data from Incropera and DeWitt (2002:496), the Nusselt number for laminar flow in a rectangular channel was found. Since the conduction heat transfer coefficient of the graphite material used is relatively low (k = 110 W/m.K), a uniform surface temperature was assumed. Then, for a channel width to channel height relation of

$$\frac{W_{ch}}{L_f} = \frac{0.00246}{0.002} = 1.23$$

the Nusselt number was calculated as Nu = 3.03.

The calculation flow sheet of the heat transfer model is shown in Figure 53. The model was constructed with the help of the software package Engineering Equation Solver (EES) (see Appendix B for the program code). To start the model, outlet temperatures were assumed. Using these temperatures, fluid properties were calculated that were in turn used to perform the rest of the calculations. At the end, new outlet temperatures were calculated that were used again to calculate new fluid properties. The model was iterated in this manner until the difference between consecutive solutions was smaller than the stop criteria of $1x10^{-9}$.

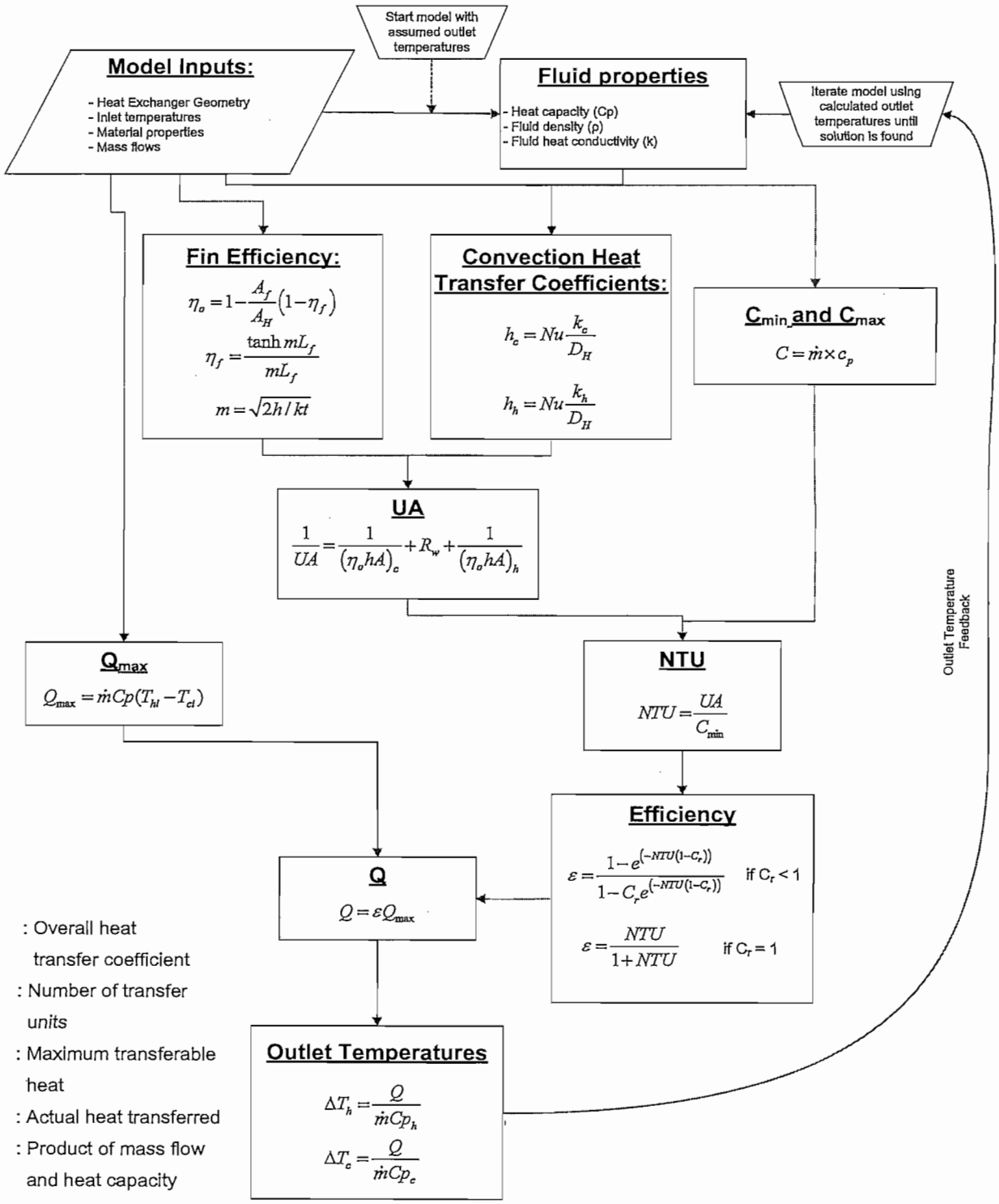

UA : Overall heat transfer coefficient

NTU : Number of transfer units

Q_{max} : Maximum transferable heat

Q : Actual heat transferred

C : Product of mass flow and heat capacity

Figure 53: Structure of EES heat exchanger model

To calculate the pressure drop, the following equation was used

$$\Delta p = \left(f\left(\frac{L_{ch}}{D_H}\right) + 0.5 + 1 \right) \frac{\rho V^2}{2} \quad [52]$$

where

Δp	:	Pressure drop (Pa),
f	:	Darcy-Weisbach friction factor,
L_{ch}	:	Channel length (m),
D_H	:	Hydraulic diameter (m),
ρ	:	Fluid density (kg/m^3),
V	:	Fluid velocity (m/s).

The factors 0.5 and 1 in the above equation represent the flow losses from the heat exchanger inlet and outlet respectively.

The fluid velocity V was calculated from the mass flow and geometrical pararneters by using the equation

$$V = \frac{\dot{m}}{\rho \times \frac{A_{ff}}{2}} \quad [53]$$

where

A_{ff}	:	Free flow area of the heat exchanger (m^2).

The free flow area is divided by two in the above equation because only the free flow area of one fluid stream is needed to calculate the fluid velocity. The parameter A_{ff} was calculated previously for both the hot and the cold side and therefore needs to be divided by two to find this free flow area.

The Darcy-Weisbach friction factor for laminar flow is given by

$$f_c = \frac{57}{\mathrm{Re}} \quad [54]$$

where

Re	:	Reynolds number.

The Reynolds number, in turn, was calculated from the expression

$$\mathrm{Re} = \frac{\rho V D_H}{\mu} \qquad [55]$$

where

μ : Fluid viscosity (kg/ms).

By substituting all the above parameters into Equation [52], the pressure drop through the heat exchanger was calculated. Also, since the outlet pressure was known to be atmospheric, the pressure drop was used to calculate the inlet pressure as follows

$$\Delta p = p_{in} - p_{out} \qquad [56]$$

The calculation flow sheet of the pressure drop model is shown in Figure 54. The model was constructed with the help of EES (see Appendix B for the program code). To start the model, an inlet pressure was assumed. The model was then iterated in the same manner as the heat transfer model and a solution was found when consecutive solutions differed less than 1×10^{-9}.

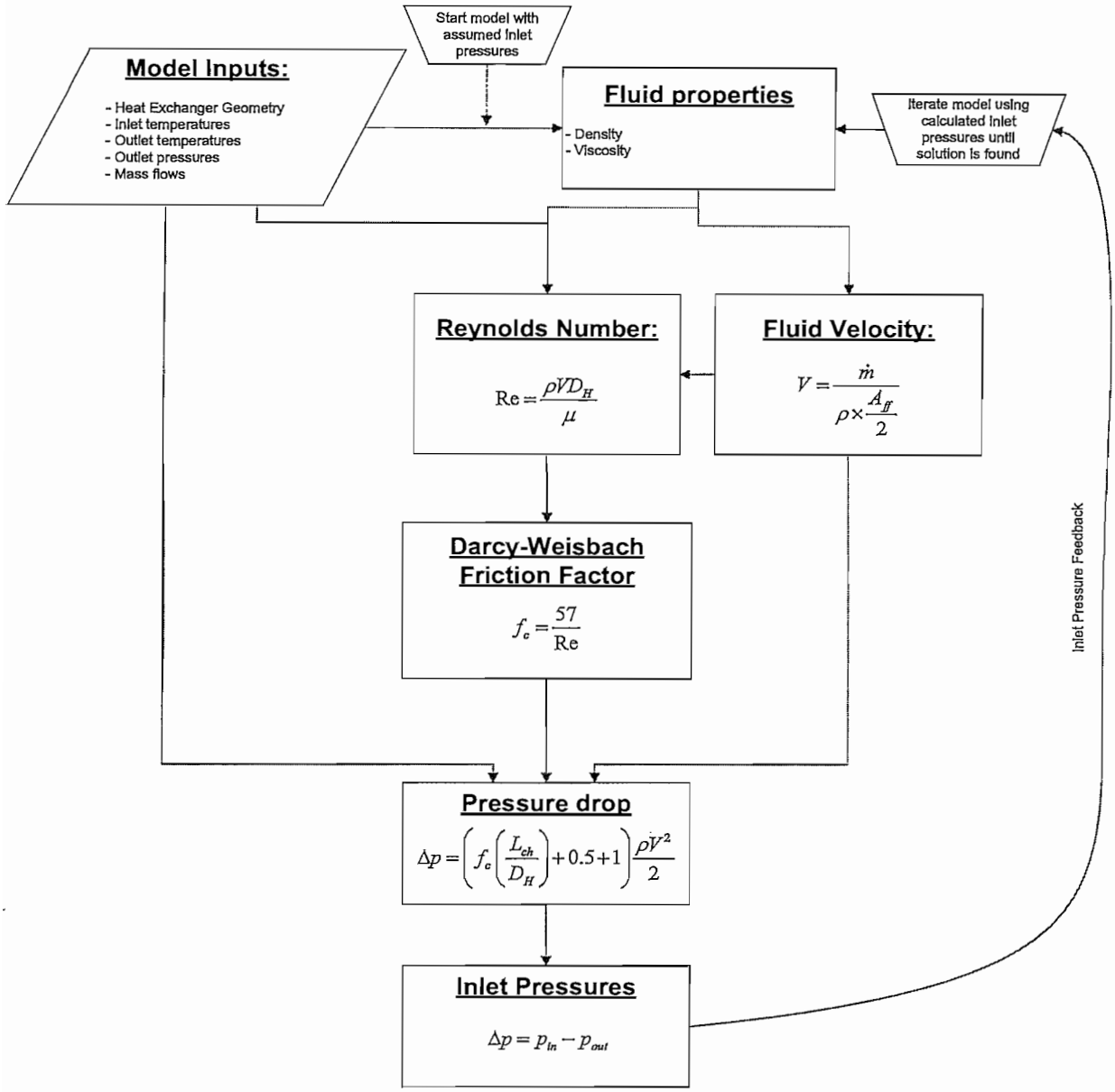

Figure 54: Structure of EES pressure drop model

4.4 Results from the model

Table 13 lists the assumptions used in the model of the heat exchanger.

Table 13: List of assumptions made during the heat exchanger analysis

Parameter	Assumption
Hot side fluid	N_2 (High Purity)
Cold side fluid	N_2 (High Purity)
Mass flow rates	Hot side = Cold side
Heat loss	None
Leak flows	None
Hot side inlet temperature	200°C
Cold side inlet temperature	25°C

Similar to the conducted tests, the hot side and cold side mass flow rates were chosen to be equal.

The results for the heat transfer analysis are shown in Figure 55 and Figure 56:

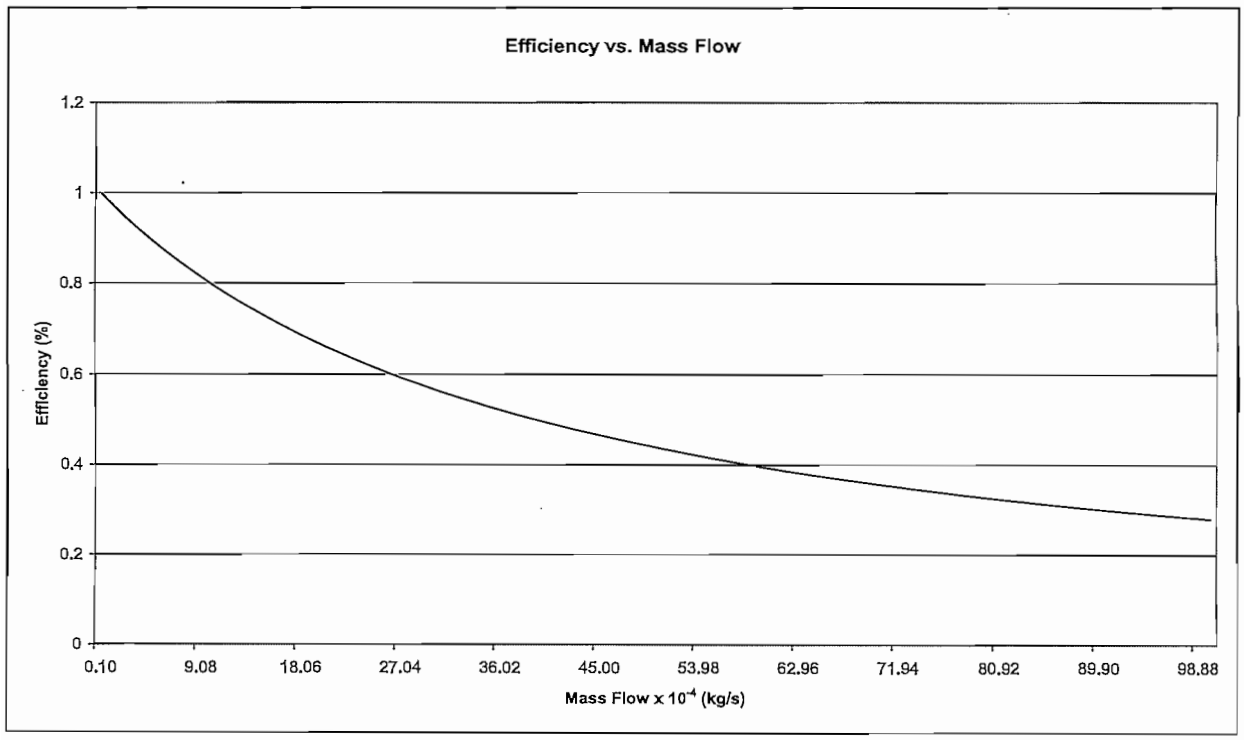

Figure 55: Heat exchanger model results for effectiveness

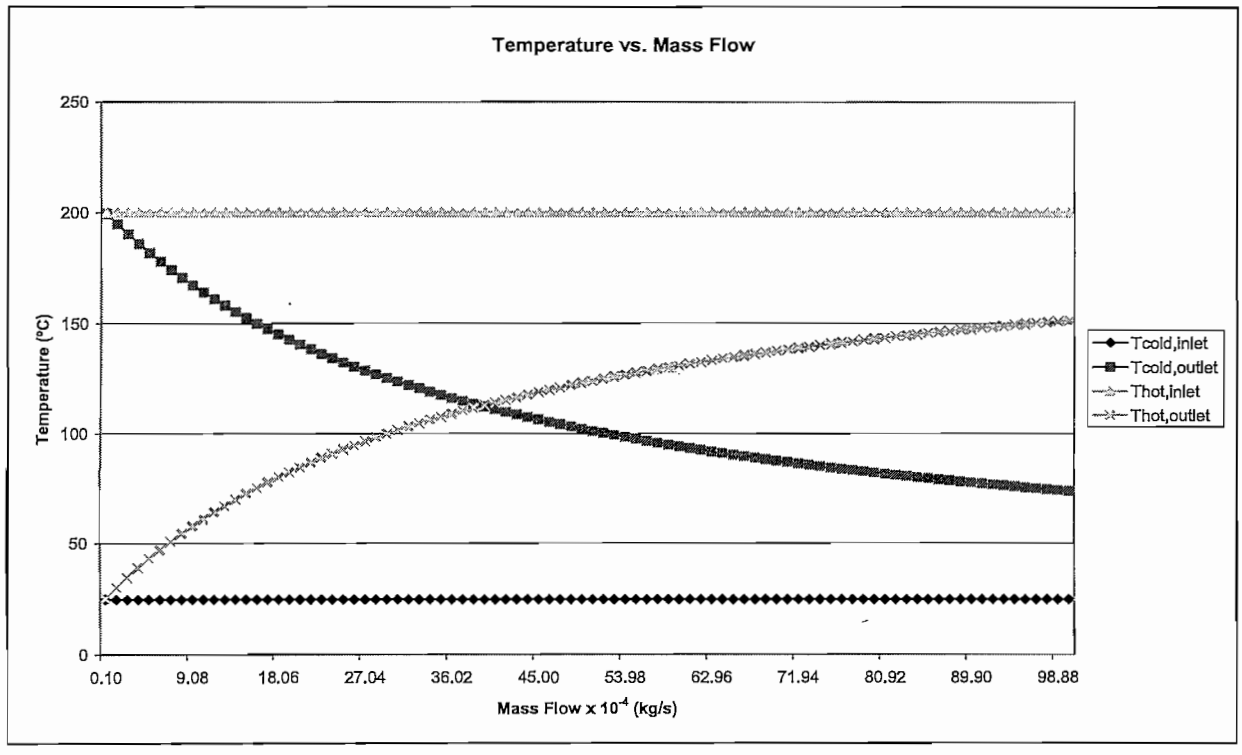

Figure 56: Heat exchanger model results for inlet and outlet temperatures

The heat transfer model shows that the heat exchanger's effectiveness drops exponentially as a function of mass flow, as is evident from Figure 55. This result is confirmed by Figure 56, where it is shown that the temperature difference between the inlets to outlets of both streams become smaller as the mass flow is increased. Thus, by controlling the mass flows to a certain level, a specific heat exchanger effectiveness is achievable. Also, it is evident from these results that, if the heat loss is assumed to be zero (as was the case for this model), the ΔT between the inlet and outlet of the hot stream should be equal to that of the cold stream.

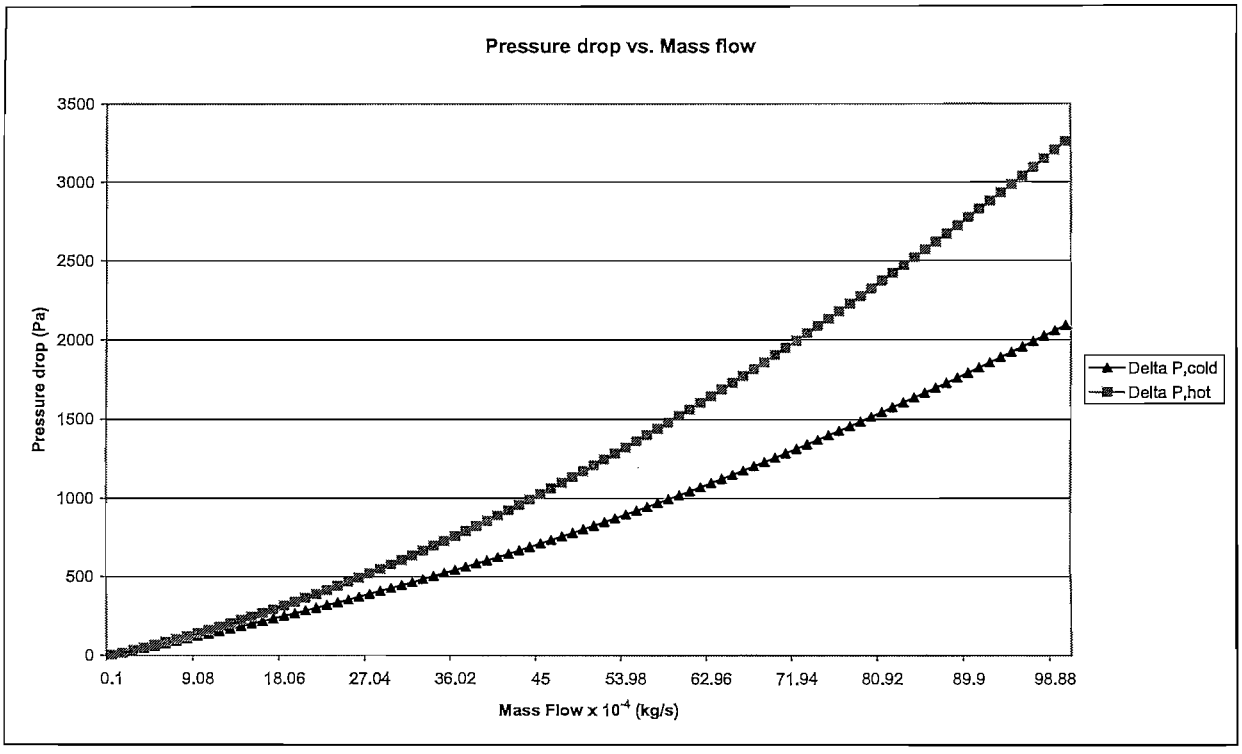

Figure 57: Analysis results for pressure drop

The results for the pressure drop model are shown in Figure 57. It was found that the pressure drop between the heat exchanger inlet and outlet increases as the mass flow is increased. This result was expected, since the higher mass flow would result in higher velocities, increasing the drag and other losses through the heat exchanger. Also, due to the difference in temperature between the hot stream and the cold stream, a larger pressure drop is shown for the hot stream.

Chapter 5

Comparison of Results

5.1 Introduction

In this chapter the results for the heat exchanger tests are compared with the results from the theoretical heat exchanger model.

5.2 Heat transfer results

Figure 58 shows the results from the heat transfer tests, while Figure 59 presents the results from the theoretical model in the region of the mass flow that was used during the heat transfer tests.

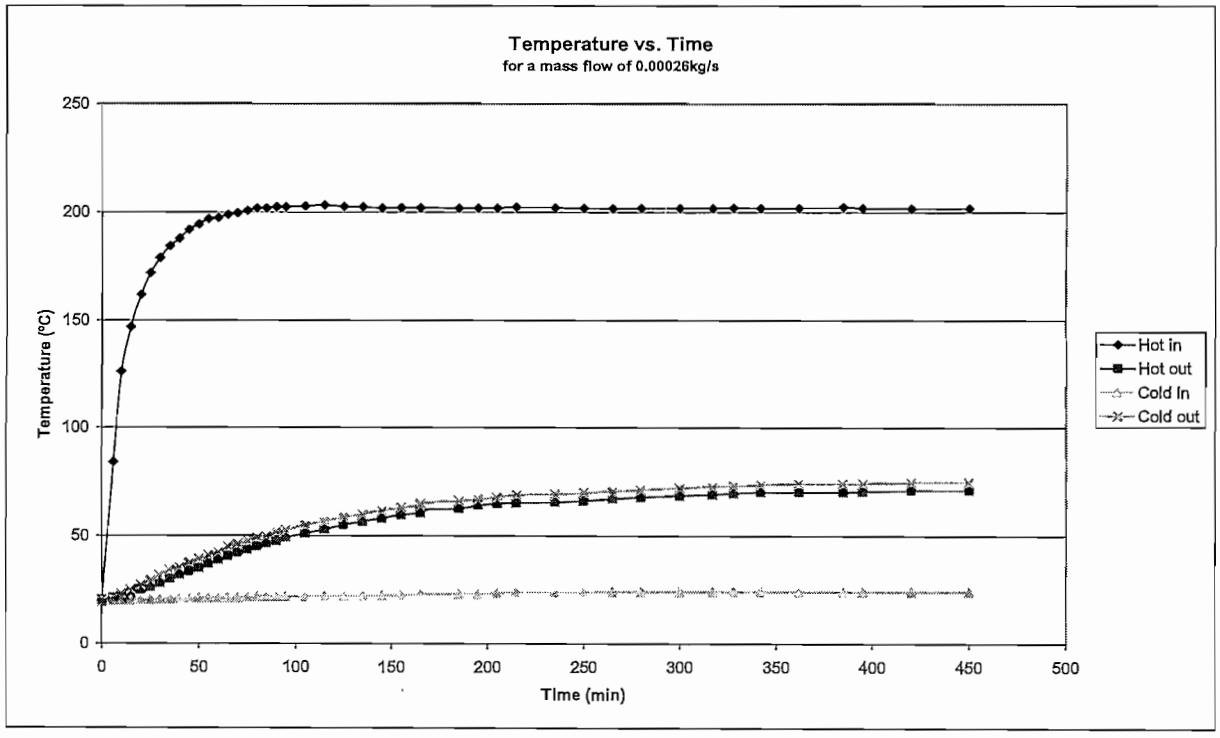

Figure 58: Heat transfer test results

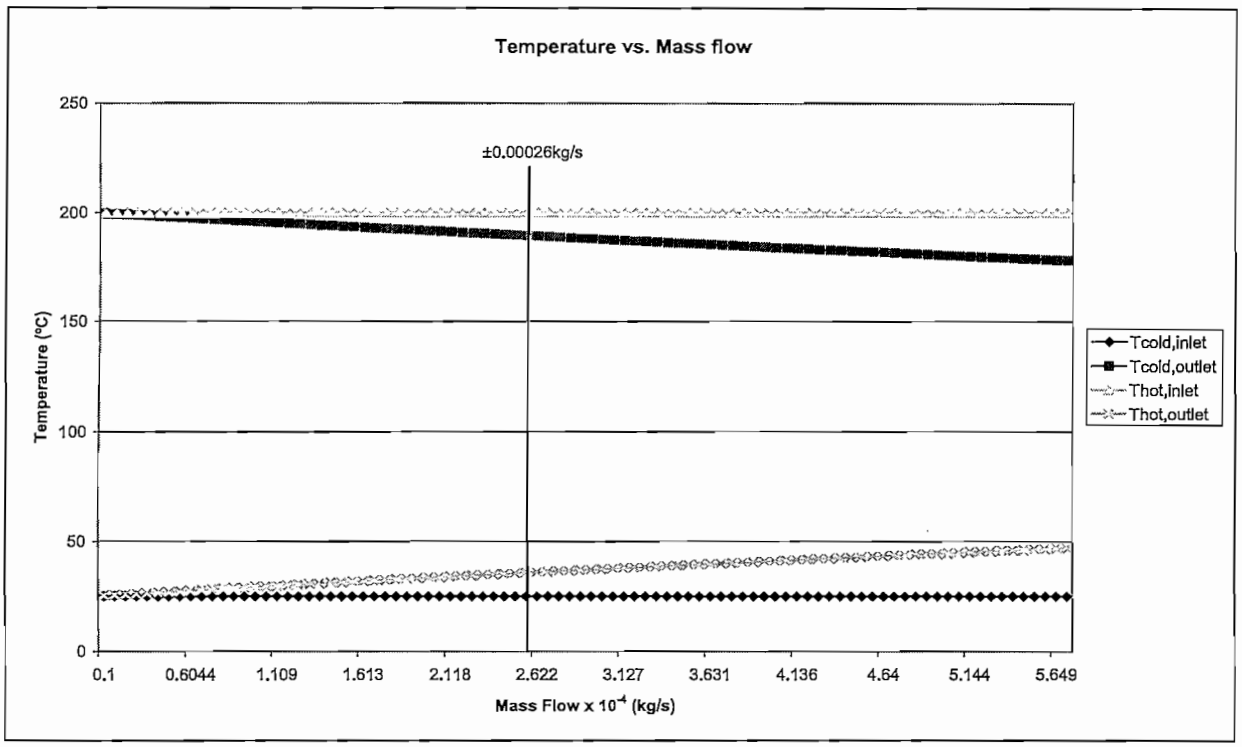

Figure 59: Analysis results of the heat transfer

At the point where the heat exchanger temperatures reached a steady state (far right on the Figure 58), the temperature difference between the hot stream inlet and outlet is 131°C with a calculated cooling effectiveness of 73.5% (Equation [8]). For the same mass flow rate of 2.6 $x10^{-4}$ kg/s in Figure 59 (indicated by the vertical line), the theoretical model calculated this temperature difference as 165.5°C with a cooling effectiveness of 94.5%. Thus, there is a 27% difference between the test results and the model results.

The steady state temperature difference between the inlet and outlet of the cold stream is 50.8°C and the heating effectiveness was calculated as 28.7% using Equation [9]. The theoretically calculated values at the same mass flow rate of $2.6x10^{-4}$ kg/s (indicated by the vertical line) give this temperature difference as 165.5°C and the effectiveness as 94.6%. Thus, there is a 70% difference between the actual values and the results from the model. This means that some of the heat leaves the heat exchanger by other means than the cold stream, the largest probably being heat loss to the environment through the surface of the heat exchanger as was shown in Section 3.4.5 where the heat loss for the specific mass flow used during the heat transfer tests was calculated. From this calculation it was shown that heat loss through the surface does contribute largely to the removal of heat from the heat exchanger. This is not visible in the theoretical results, since it was decided that, due to complications in the iterative process, heat losses would not be included in the model.

5.3 Pressure drop results

A graph showing a comparison between the pressure drop test results and the results calculated from the theoretical model is shown in Figure 60.

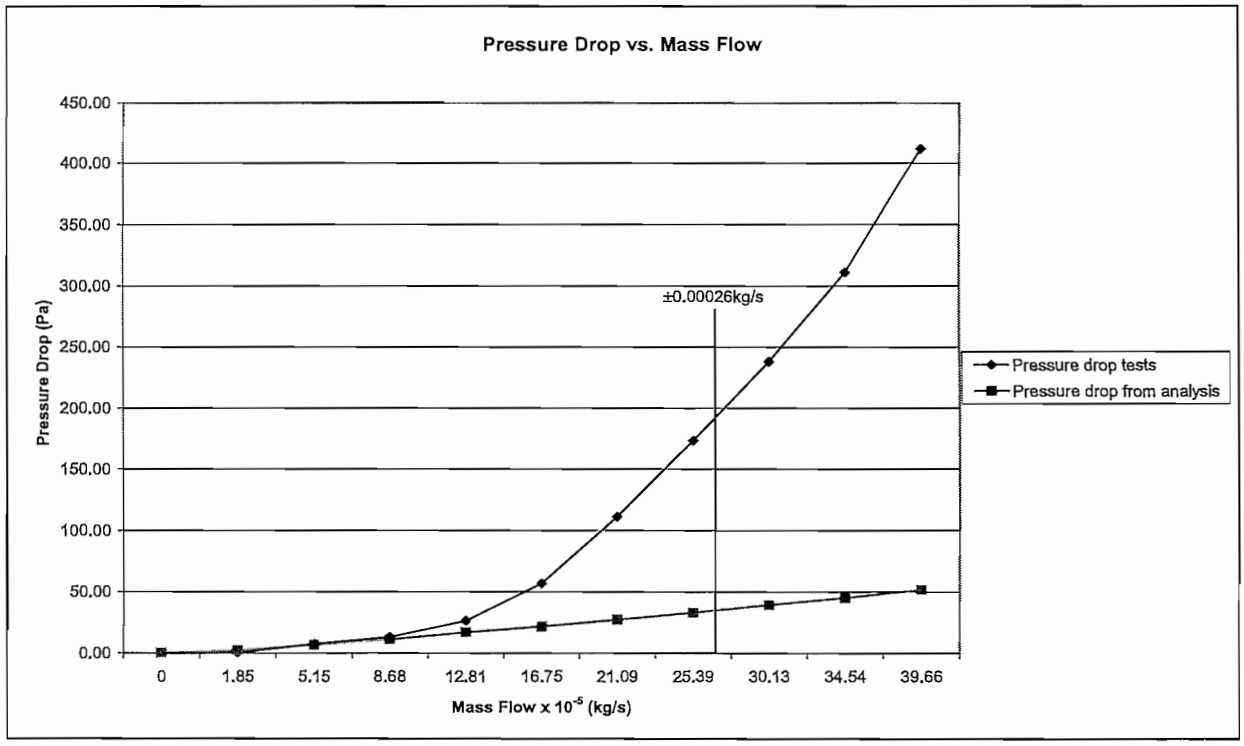

Figure 60: Comparison of the pressure drop test data with that from the analysis

The pressure drop of the tests and that of the analysis correlates well at very low mass flow rates, up to about 8.68×10^{-5}kg/s. For higher mass flows, the pressure drop from the tests becomes larger than the corresponding value from the theoretical model. The pressure drop for the heat transfer test (at a mass flow of 2.26×10^{-4}kg/s, indicated by the vertical line on Figure 60) was about 175Pa while the pressure drop calculated from the model was about 35Pa. This difference may be attributed to the fact that the pressure drop model did not account for flow losses, such as losses through the interfaces connecting the heat exchanger to the rest of the test setup, losses due to unforeseen local turbulences, losses due to leak flows and losses due to fouling of the flow channels. The pressure drop model only accounted for frictional losses in the core region of the heat exchanger. In order to the other losses mentioned, a comprehensive Computational Fluid Dynamics (CFD) model would have had to be set up. The construction of such a detailed model, however, fell outside the scope of this study.

Chapter 6

Conclusions and Recommendations

6.1 Background

High temperature heat management is becoming an increasingly important sector in the energy industry. The efficiency advantages and the versatility of applications of high temperature energy have resulted in this technology becoming one of the industrial targets of the near future. There are, however, still many hurdles in the way of this technology becoming fully feasible. One such a hurdle is the high temperature heat exchanger.

A literature study was made to identify unsolved problems with regards to the use of graphite as a high temperature heat exchanger material and to find out to what extent graphite had been used in heat exchangers in the past. From this it was decided to study the feasibility of manufacturing a printed circuit type heat exchanger from graphite by designing and manufacturing a laboratory scale unit from isotropic graphite. The purpose of this was to identify the challenges associated with manufacturing a PCHE from graphite. Following the manufacturing, the heat exchanger was tested in a controlled environment to study its performance regarding heat transfer and pressure drop. Lastly, a theoretical model of the heat exchanger was used to determine to what extent the results from a theoretical model would correlate with the results from the heat exchanger tests.

6.2 Practical Experiences Gained

A summary of the experience gained during the manufacturing of the heat exchanger is given below:

- In designing the PCHE, it is recommended that the HX plate be symmetrically designed, eliminating the need for two separate designs as well as streamlining the manufacturing process.

- Use of a diamond coated cutting tool is recommended when machining graphite. Even though this tool was somewhat more expensive, it withstood the abrasive wear of the graphite relatively well. In total, eighteen heat exchanger plates were manufactured in this study. The total machining time was about 30h and the same tool was used for all of the machining. It can therefore be concluded that this type of tool is well suited to graphite machining.

- Tool blunting has to be considered in graphite machining. Especially at thin sections, provision has to be made to reduce the pressure exerted on the graphite due to the blunting of the tool. It will be best to change the tool to a new one when it starts to blunt, but lowering the feed rate at thin sections may help to increase the usable life of the tool.

- The importance of clamping the graphite stock material securely to the milling machine cannot be over-emphasized. A vacuum clamp, using a vacuum pump designed for extended operation should be the first choice for high volume manufacturing. However, for the machining of a small number of heat exchanger plates, the corner clamp method proved sufficient.

- Using a larger diameter cutting tool to machine the wider sections, reduced the machine time profoundly.

6.3 Conclusions

From studying the literature, one of the biggest problems facing the use of graphite for heat exchanger construction was found to be its high gas permeability. This study found that the losses in heat transfer effectiveness that was observed from the laboratory scale PCHE might, in part, be attributed to fluid losses to the environment and mixing between the fluid streams due to the porous nature of graphite in the absence of any method to counter permeation (Section 3.4.5). It was also found that the problem of permeability is interconnected with the problem of sealing between consecutive plates of a PCHE, since an effective o-ring seal could not be established on the permeable graphite surface. Therefore, it is recommended that sealing methods like o-ring seals and gaskets only be used if a permeation reducing coating has previously been applied to the graphite surface. However, to establish a robust seal between graphite plates while reducing gas permeation it is recommended that any further studies of this nature make use of diffusion bonding methods used in conjunction with a permeation reducing surface sealant.

From the literature, coatings on the graphite surface were also found to be the most feasible solution to the problem of graphite degradation at high temperatures. A plausible solution proposed by Fergus & Worrell (1995:537) for very high temperatures is a double coating system comprised of an inner coating of boron nitride or carbide and an outer coating of silicon carbide. Also, since the permeation problem as well as the degradation problem seem to be best solved by using coatings on the graphite surface, it may be possible, with further study, to identify a coating that will simultaneously solve both problems.

This study further found that graphite is best shaped using conventional machining techniques like milling. This poses a problem for the manufacturing of PCHEs from graphite, since very small channels (<0.5mm) are usually needed in order to increase the heat transfer coefficient and heat transfer density of PCHEs. End mills in this small size are not readily available and the

machining times for such a manufacturing process would be extremely long. Therefore, in order to render the manufacturing of a graphite PCHE economically and practically viable, further study is needed to identify alternative manufacturing processes that may be applied to this material. Such processes may possibly include laser machining and water jet machining. Since graphite is a very inert material, chemical etching may also be further studied in an effort to identify a chemical that is able to etch graphite.

Heat losses through the surface were found to play a major part in the reduction of the heat transfer effectiveness of a graphite PCHE. Lateral conduction of heat in the material caused a high outer surface temperature leading to large amounts of heat being transferred to the environment instead of the secondary fluid stream. It is therefore vitally important that sufficient insulation be applied to a PCHE constructed from graphite, especially if it will be used as a heater or recuperator. Also, using an anisotropic graphite that has a larger thermal conductivity perpendicular to the graphite layers than parallel to them (Gaies and Faber, 2002), might help to increase the heat transfer between the two fluid streams and decrease the conduction to the surface or the heat exchanger. It is recommended that these possibilities be subjected to further study.

From the above discussions it can be concluded that, if diffusion bonding techniques are utilized, effective coatings are applied and adequate insulation is used, the manufacturing of a PCHE from isotropic graphite would be feasible.

Appendix A

Graphite Material Specifications

Below is a copy of the manufacturer's specifications of the graphite material that was used in this study for the manufacturing of the laboratory scale heat exchanger. The information was found on the Graftech International website at http://www.ucar.com/getattachment/bec97181-4360-45dc-80e6-7d671ca5621e/Grade-ATJ-Isomolded-Graphite.aspx. The date of use was 14 April 2009.

GRAFTech International

ATJ™ Graphite

GrafTech International is a global leader in graphite and carbon products. We enable customer leadership better and faster than our competition, through the creation, innovation and manufacture of carbon and graphite material science based solutions.

Grade ATJ™ Graphite

Grade ATJ™ graphite has been an industry standard for years. It is a fine grain, high strength material that can be machined to precise tolerances and a fine surface finish. ATJ™ graphite has unique thermal shock resistance due to the combination of low thermal expansion, high thermal conductivity, and low elastic modulus.

Typical Applications

- Permanent molds
- Composite tooling
- Continuous casting dies
- Hot pressing molds and punches
- Rocket motor nozzles
- Plungers & rams

Sizes:

Inches	MM
16" x 16" x 65" rectangles	406 x 406 x 1651 mm rectangles
12" x 25" x 80" rectangles	305 x 635 x 2032 mm rectangles
8" - 24" diameter x 72" long rounds	203-610 mm diameter x 1829 long rounds

Grade ATJW™ graphite is a post purified version of ATJ™ graphite for applications requiring very low ash. ATJW™ has the same properties as ATJ™ with an ash content of less than 20ppm.

Typical ATJ™ Graphite Properties at Room Temperature

	ENGLISH	WG	METRIC	WG	SI	WG
Density	lbs/ft³	110	g/cm³	1.76	g/cm³	1.76
Average Particle Size	inches	0.001	mm	0.03	mm	0.03
Specific Resistance	$10^{-4}\Omega$ in.	4.61	μΩm	11.7	μΩm	11.7
Flexural Strength	psi	4500	kg/cm²	317	MPa	31
Young's Modulus	10^6 psi	1.40	kg/mm²	982	GPa	9.7
Tensile Strength	psi	3740	kg/cm²	262	MPa	26
Compressive Strength	psi	9500	kg/cm²	670	MPa	66
Permeability	Darcy	0.002	Darcy	0.002	Darcy	0.002
Hardness	Rockwell "L"	60	Rockwell "L"	60	Rockwell "L"	60
C.T.E. (to 100 °C)	10^{-6}/°F	1.7	10^{-6}/ °C	3.0	10^{-6}/ K	3.0
Thermal Conductivity	BTU-ft/hr ft² °F	67	W/mK	116	W/mK	116
Ash Content	%	.11	%	.11	%	.11

This information is based on data believed to be reliable but GrafTech makes no warranties, express or implied, as to its accuracy and assumes no liability arising out of its use. The data listed falls within the normal range of product properties but should not be used to establish specification limits or used alone as the basis of design. GrafTech's liability is expressly limited to the terms and conditions of sale. ATJ and ATJW are trademarks of GrafTech International Holdings Inc.

121-5026
Rev. 2

101 R. Philpot Plz, Anmoore, WV 26323-0129
Ph: +1-800-845-6805; +1-304-624-1253

La Lecques, 72204 Aguebelonne Cedex, France
Ph: +33 04 79 41 45 00

Via Forno Allione, 2, I-25040 Masonno, Brescia, Italy
Ph: +39 03 64 53 01 31

© 2002 GrafTech International Holdings Inc.

GRAFTech International

www.graftech.com

Appendix B

Programme Code for Mathematical Analysis

This appendix contains the programme code used to analyse the graphite printed circuit heat exchanger. The assumptions used to create this programme are discussed in Section 4.3.

```
"Program for the analysis of the Graphite PCHE"
"Izak de Kock"

"=========================Known Fluid Parameters============================="

    "Cold Side"
    T_c_i = 25 + 273.15 [K]
    P_c_o = 87000 [Pa]                          "Released to Atmosphere"
    m_dot_c = 0.00015 [kg/s]


    "Hot Side"
    T_h_i = 200 + 273.15 [K]
    P_h_o = 87000 [Pa]                          "Released to Atmosphere"
    m_dot_h = 0.00015 [kg/s]

    " Other"
    Nuss = 3.03                                 "See Section 3.4"

"================Geometric and material Parameters (See Section 3.5.1)==============="

    L_ch = 0.179 [m]                            "Channel Length"
    W_ch = 0.00246 [m]                          "Channel Width"
    L_f = 0.001 [m]                             "Fin Length"
    L_w = 0.003 [m]                             "Wall Thickness"
    N_f = 192 [m]                               "Number of Fins/plate"
    N_ch = 9                                    "Number of Channels/plate"
    N_pl = 12                                   "Number of Heat Exchanger Plates"
    P_f = 0.03985                               "Single Fin Perimeter"
    A_f = 0.00003985 [m^2]
    A_f_total = 0.0918 [m^2]                    "Total fin side area"
    A_ff = 0.00053136 [m^2]                     "Total Free Flow Area"
    A_H = 0.1789 [m^2]                          "Heat Transfer Area"
    A_H_cond = 0.008638 [m^2]                   "Heat Transfer Area"
    D_H = 0.00206 [m]                           "Hydraulic Diameter"

    k_graphite = 110 [W/m.K]                    "Graphite Conductivity.  See Appendix A"


"=========================Calculate C_min, C_max and C_r========================="

    C_r = C_min / C_max

    T_c_avg = AVERAGE(T_c_i, T_c_o)
    T_h_avg = AVERAGE(T_h_i, T_h_o)

    c_p_c = Cp(N2,T=(T_c_avg))
    c_p_h = Cp(N2,T=(T_h_avg))

    C_c = m_dot_c* c_p_c
    C_h = m_dot_h* c_p_h

    C_min = min(C_c,C_h)
    C_max = max(C_c,C_h)
```

```
"=====================Convection Heat Transfer Coefficients=================="

    k_c = Conductivity(N2,T=(T_c_avg))
    k_h = Conductivity(N2,T=(T_h_avg))

    h_c = Nuss * (k_c / D_H)
    h_h = Nuss * (k_h / D_H)


"==================================Fin Analysis=========================="

    m_c = SQRT((2 * h_c) / (k_graphite * L_f))
    m_h = ((2 * h_h) / (k_graphite * L_f))^0.5

    eta_f_c = tanh(m_c * L_f) / (m_c * L_f)
    eta_f_h = tanh(m_h * L_f) / (m_h * L_f)

    eta_o_c = 1 - ((A_f / A_H)*(1 - eta_f_c))
    eta_o_h = 1 - ((A_f / A_H)*(1 - eta_f_h))

"================================Wall Resistance========================="

    R_w = L_w / (k_graphite * A_H_cond)


"=========================Overall Heat Transfer Coefficient================="

    1 / UA =  (1 / (eta_o_h * h_h * A_H) ) + R_w + (1 /(eta_o_c * h_c * A_H) )

"================================Number of Transfer Units=================="

    NTU = UA / C_min


"=========================Heat Exchanger Effectiveness======================"

    epsilon = NTU / (1+NTU)


"=========================Maximum Possible Heat Transfer===================="

    Q_dot_Max = C_min * (T_h_i - T_c_i)

"=========================Actual Heat Transfered============================"

    Q_dot = epsilon * Q_dot_Max

"=========================Outlet Temperatures==============================="

    {Q_dot for the cold side = Q_dot for the hot side}

    DELTAT_c = T_c_o - T_c_i
    DELTAT_h = T_h_i - T_h_o

    Q_dot = C_c  * (DELTAT_c)
    Q_dot = C_h * (DELTAT_h)


"================================Pressure Drop=========================="
    P_c_avg = Average(P_c_o,P_c_i)
    P_h_avg = Average(P_h_o,P_h_i)
```

```
rho_c = Density(N2,T=T_c_avg, P = P_c_avg)
rho_h = Density(N2,T=T_h_avg, P = P_h_avg)

V_c = m_dot_c / (rho_c * (A_ff/2))
V_h = m_dot_h / (rho_h * (A_ff/2))

mu_c=Viscosity(N2,T=T_c_avg)
mu_h=Viscosity(N2,T=T_h_avg)

Re_c =  (rho_c * V_c  * D_H) / mu_c
Re_h =  (rho_h * V_h  * D_H) / mu_h

f_c = 57 / Re_c
f_h = 57 / Re_h

DELTAP_c = (f_c * (L_ch / D_H) + 0.5 + 1) * (rho_c * V_c^2) / 2
DELTAP_h = (f_h * (L_ch / D_H) + 0.5 + 1) * (rho_h * V_h^2) / 2

P_c_i = P_c_o + DELTAp_c
P_h_i = P_h_o + DELTAp_h
```

Appendix C

Heat Exchanger Manufacturing Drawings

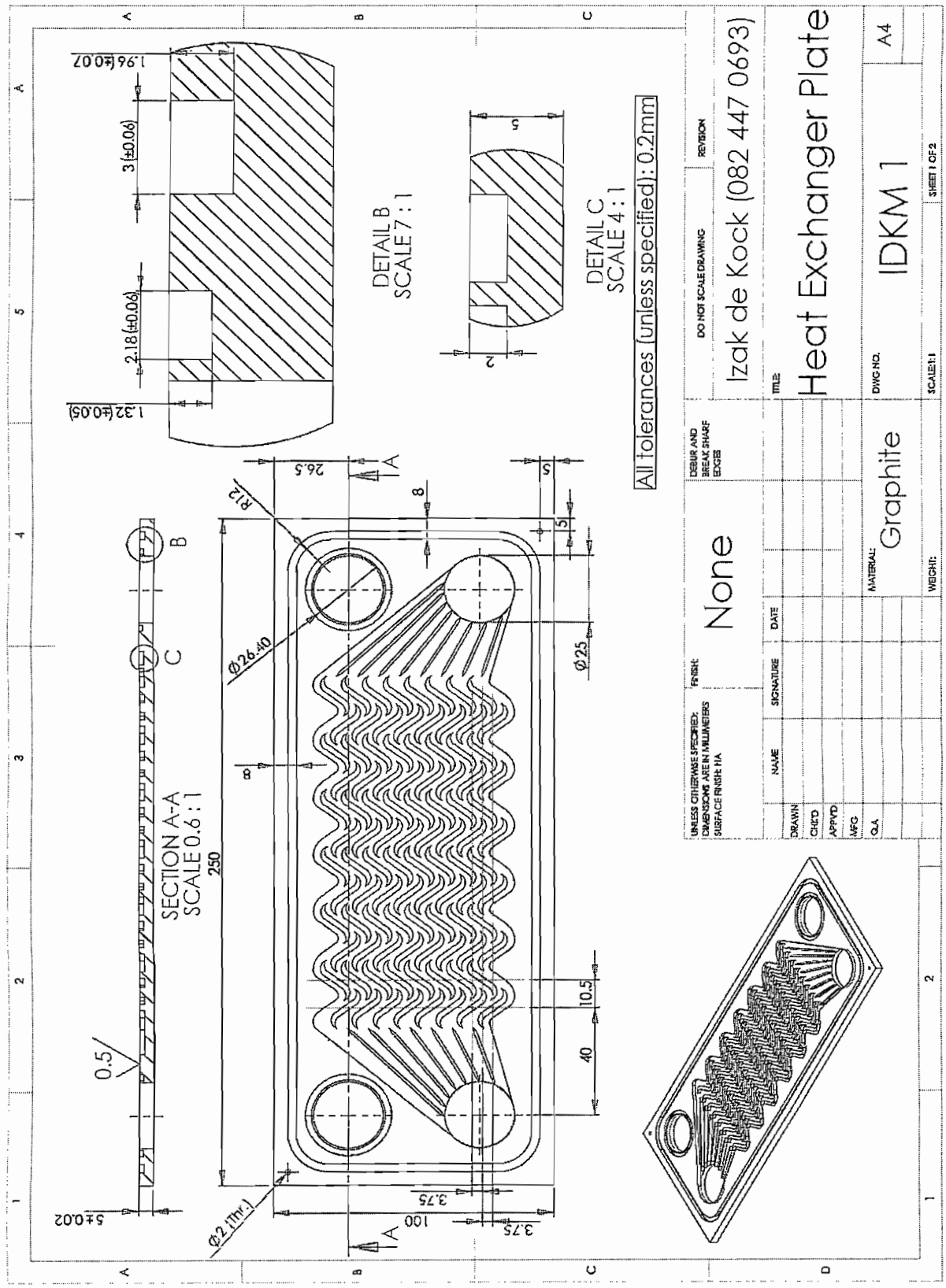
DETAIL B
SCALE 7 : 1
DETAIL C
SCALE 4 : 1
All tolerances (unless specified): 0.2mm
SECTION A-A
SCALE 0.6 : 1
Heat Exchanger Plate
Izak de Kock (082 447 0693)
IDKM 1
Graphite
None
A4
DO NOT SCALE DRAWING
DEBUR AND BREAK SHARP EDGES
UNLESS OTHERWISE SPECIFIED: DIMENSIONS ARE IN MILLIMETERS SURFACE FINISH: tbA
DRAWN
CHKD
APPVD
MFG
QA
NAME
SIGNATURE
DATE
FINISH:
MATERIAL:
WEIGHT:
DWG NO.
SCALE:1:1
SHEET 1 OF 2
REVISION
TITLE:

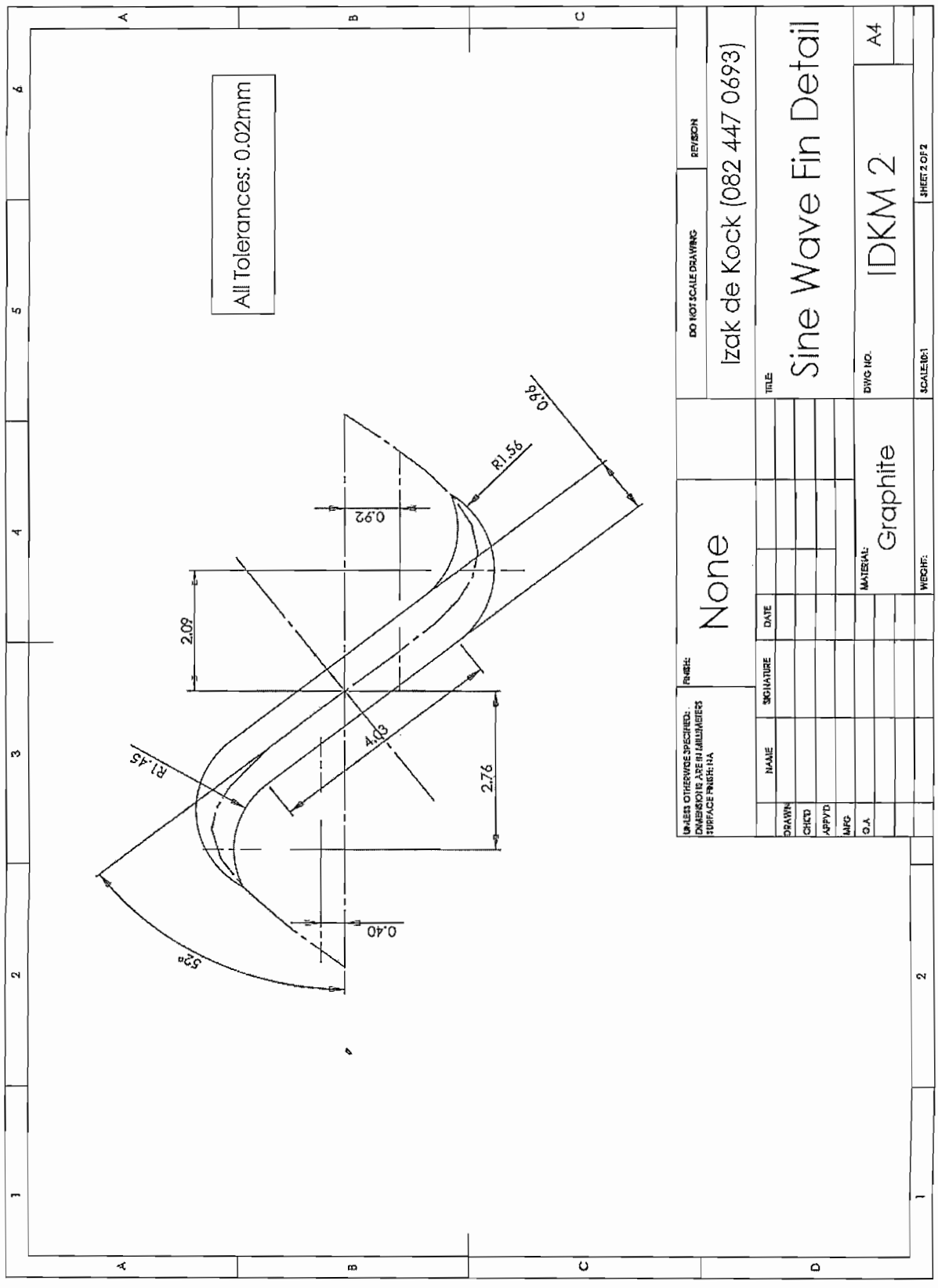
All Tolerances: 0.02mm
R1.56
0.92
2.09
4.03
2.76
R1.45
0.40
52°
0.6°
UNLESS OTHERWISE SPECIFIED:
DIMENSIONS ARE IN MILLIMETERS
SURFACE FINISH: NA
FINISH:
None
NAME
SIGNATURE
DATE
DRAWN
CHK'D
APPV'D
MFG
Q.A
MATERIAL:
Graphite
WEIGHT:
DO NOT SCALE DRAWING
REVISION
Izak de Kock (082 447 0693)
TITLE:
Sine Wave Fin Detail
DWG NO.
IDKM 2
A4
SCALE:10:1
SHEET 2 OF 2

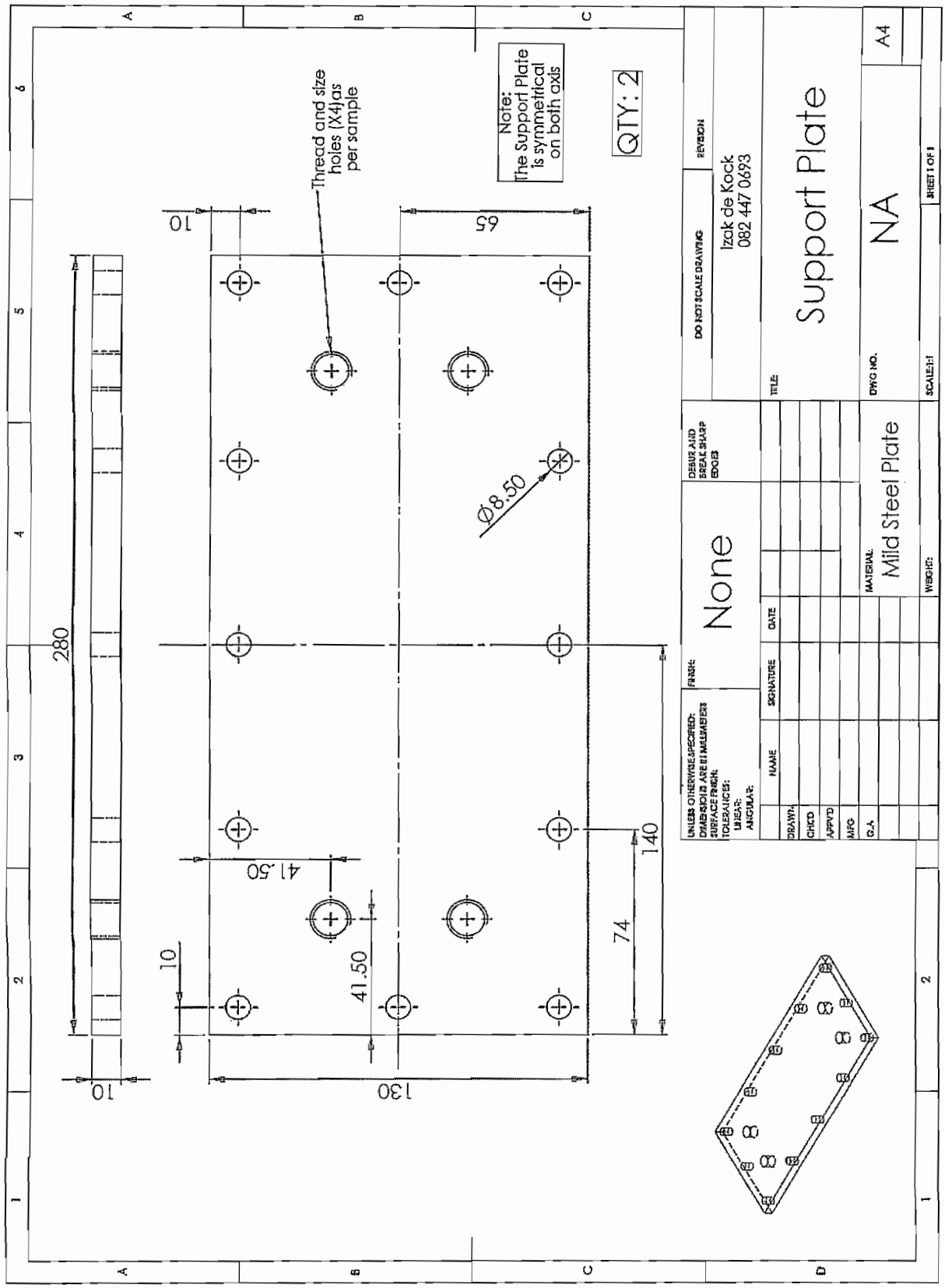
Thread and size holes (X4)as per sample
Note: The Support Plate is symmetrical on both axis
QTY: 2
Ø8.50
280
130
140
74
41.50
10
65
Izak de Kock
082 447 0693
Support Plate
NA
A4
Mild Steel Plate
None

Appendix D

Flow Metre Calibration Curve

The following graph shows the calibration curve for the flow meter used in the feasibility tests. This flow metre was a Fischer & Porter Model 10A6132A/B10 with a tube designation of FP-1/4-25-G-5/81 and a stainless steel ball.

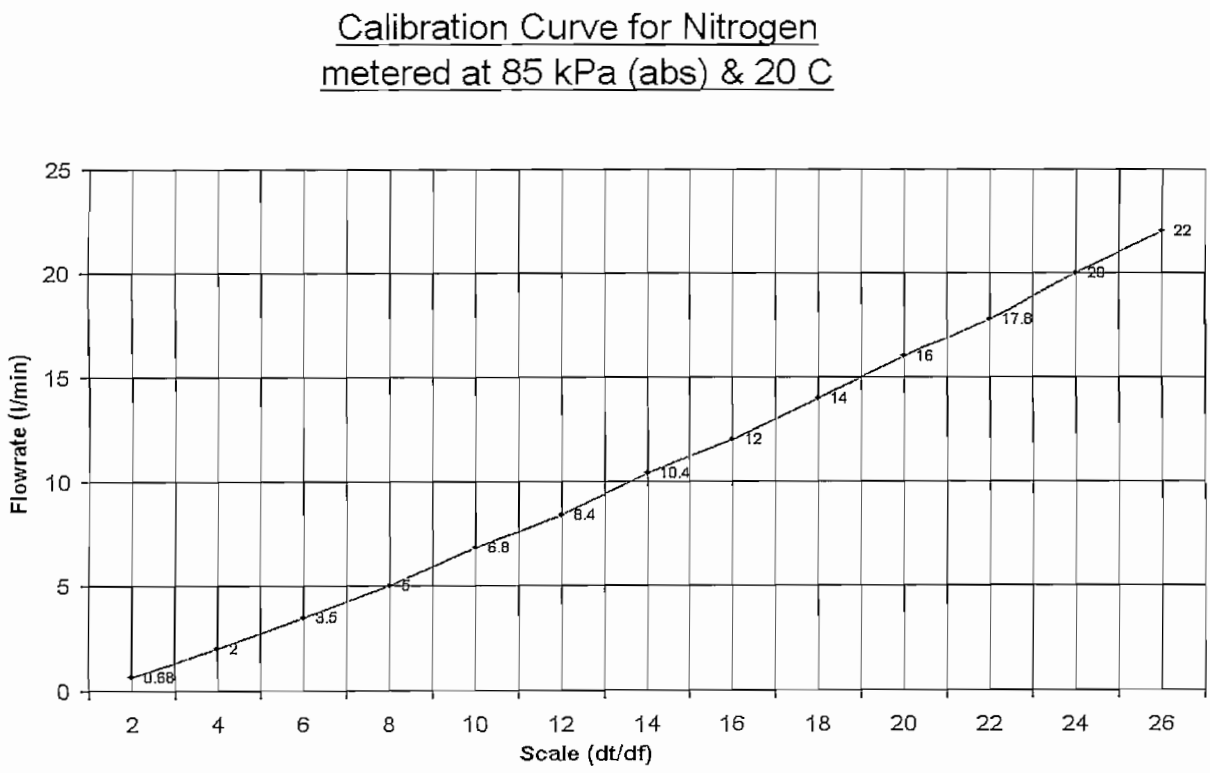

The flow reference for this chart is:

- 1.013 bar (abs)
- 0°C

Bibliography

BUDINSKI, K.G. & BUDINSKI, M.K. 2002. Engineering materials: properties and selection. 7th ed. London : Pearson Education. 424 p.

DUPONT Website. 2009. [Web:] http://www.dupontelastomers.com/products/viton/viton.asp [Date of use: 29 Nov. 2009].

FERGUS, J. & WORRELL, W.L. 1995 Silicon-carbide/boron-containing coatings for the oxidation protection of graphite. *Carbon*, 33(4):537-543.

GAIES, D. & FABER, K.T. 2002. Thermal properties of a pitch-derived graphite foam. *Carbon*, 40(7):1137-1140, June.

HECHANOVA, A.E. 2006. Quarterly Progress Report. (Report delivered as part of the High Temperature Heat Exchanger Project under The UNLV Research Foundation during January 1, 2006 through March 31, 2006) Las Vegas. p. 16-17 (Unpublished)

INCROPERA, F.P. & DEWITT, D.P. 2002. Fundamentals of heat and mass transfer. New York : John Wiley & Sons. 981 p.

KALPAKJIAN, S. & SCHMID, S.R. 2006. Manufacturing engineering and technology. Upper Saddle River, New Jersey : Pearson Hall. 1295 p.

LI, X., KININMONT, D., LE PIERRES, R. & DEWSON, S.J. 2008. Alloy 617 for the high temperature diffusion-bonded compact heat exchangers. (*In* Proceedings of ICAPP '08: Papers read at the 2008 ICAPP conference held in Anaheim, CA USA from 8 to 12 June 2008. Anaheim. p. 282-288)

MCDONALD, C.F. 1996. Compact buffer zone plate-fin IHX--The key component for high-temperature nuclear process heat realization with advanced MHR. *Applied Thermal Engineering*, 16(1):3-32

MCKEE, D.W. 1991. Oxidation protection of carbon materials. (In Thrower, P.A., ed. Chemistry and physics of Carbon, Volume 23. New York : Marcel Dekker, Inc. p. 173-222.)

MOLINA, J.M., RODRIGUEZ-GUERRERO, A., BAHRIANI, M., WEBER, L., NARCISO, J., RODRIGUEZ-REINOSO, F., LOUIS, E. & MORTENSEN, A. 2007. Infiltration of graphite preforms with Al-Si eutectic alloy and mercury. *Scripta materialia, 56:991-994.*

NIEMINEN, I., PARO, J. & KAUPPINEN, V. 1996. High speed milling of advanced materials. Journal of Materials Processing Technology, 56:24-36

PARKER SEALS. 2001. O-ring Handbook. [Web:] http://www.parker.com/literature/ORD 5700 Parker_O-Ring_Handbook.pdf [Date of use: 10 Oct. 2007].

PIERSON, H.O. 1993. Handbook of carbon, graphite, diamond and fullerenes: properties, processing and applications. New Jersey : Noyes Publications. 399 p.

SAITO, K., IIDA, K. & WATANABE, R. 1967. Transaction of the National Research Institute for Metals, 9:267

SCHROETER, R.B., KRATOCHVIL, R. & GOMES, J.dO. 2006. High-speed finishing milling of industrial graphite electrodes. Journal of Materials Processing Technology, 179:128-132

SCHULTE-FISCHEDICK, J., DREIßIGACKER, V. & TAMME, R. 2006. An innocative ceamic high temperature plate-fin heat exchanger for EFCC processes. *Applied Thermal Engineering*, 27(2007):1285-1294

SECO. 2008. Machining Navigator Catalogue. [Web:] http://212.209.32.244/template/start.asp?id=2014 [Date of use: 30 May 2009].

SETTON, R. 2002. Carbon, a fundamental element for research and its applications. (*In* Setton, R., Bernier, P. & Lefrant, S., *eds.* Carbon molecules and materials. New York : Taylor & Francis. p. 6-42.)

SGL GROUP. 2008. Diabon block heat exchangers. [Web:] http://www.sglgroup.com/export/sites/sglcarbon/_common/downloads/products/product-groups/pt/diabon-block-heat-exchangers/PT_e_Blockwaermeaustauscher_2008_01.pdf [Date of use: 3 May 2009].

SGL GROUP. 2008. Diabon Licuflon plate heat exchangers - superior by design. [Web:] http://www.sglgroup.com/export/sites/sglcarbon/_common/downloads/products/product-groups/pt/plate-heat-exchangers-diabon/PT_e_Plattenwaermeaustauscher_07-10.pdf [Date of use: 3 May 2009].

SOGABE, T. & MATSUMOTO, T. 1995. Preparation of glass-impregnated isotropic graphite and its gas permeability. *Journal of the european ceramic society*, 16:395-401

SOGABE, T., KURODA, K. & OKU, T. 1996. Effect of the Ti-addition on gas permeability of the Cu-impregnated high-density isotropic graphite. *Cabon*, 34(9):1154-1156

SOGABE, T., OKADA, O., KURODA, K. & INAGAKI, M. 1996. Improvement in properties and air oxidation resistance of carbon materials by boron oxide impregnation. *Carbon*, 35(1):67-72

SUN, L., HODGKINS, A., MARROW, J., FOK, A.S.L. & MARSDEN, B.J. 2004. An experimental study on the porosity networks in nuclear graphite. (Paper presented at the 2nd Inaternational Topical Meeting on HIGH TEMPERATURE REACTOR TECHNOLOGY held in Beijing, China during 22-24 September 2004.) Beijing. 7p. (Unpublished)

TSUZUKI, N., KATO, Y. & ISHIDUKA, T. 2007. High performance printed circuit heat exchanger. *Applied Thermal Engineering,* 27(2007):1702-1707.

WANG, M., WOO, K., KIM, D., LOU, T. & HUANG, Z. 2004. Study on impregnation of polytetrafluoroethylene in graphite for use as fuel cell collector. *International journal of hydrogen energy*, 30:1027-1030

WEIMING, L. & CHUNG, D.D.L. 2002. Oxidation protection of carbon materials by acid phosphate impregnation. Carbon, 40:1249-1254.

XIAOWEI, L., JEAN-CHARLES, R. & SUYUAN, Y. 2004. Effect of temperature on graphite oxidation behavior. *Nuclear engineering and design*, 227:273-280.

YANG, Y., CHUANG, M. & LIN, S. 2009. Optimization of dry machining parameters for high-purity graphite in end milling process via design of experiments methods. Journal of Materials Processing Technology, 209:4395-4400

ZIRCAR Ceramics 2009. [Web:] http://www.zircarceramics.com [Date of use: 29 Nov. 2009].